DEVELOPMENT OF THE MCNPX DEPLETION CAPABILITY: A MONTE CARLO LINKED DEPLETION METHOD THAT AUTOMATES THE COUPLING BETWEEN MCNPX AND CINDER90 FOR HIGH FIDELITY BURNUP CALCULATIONS

By

MICHAEL LORNE FENSIN

A DISSERTATION PRESENTED TO THE GRADUATE SCHOOL
OF THE UNIVERSITY OF FLORIDA IN PARTIAL FULFILLMENT
OF THE REQUIREMENTS FOR THE DEGREE OF
DOCTOR OF PHILOSOPHY

UNIVERSITY OF FLORIDA

2008

To the spirit of the west endzone crew

ACKNOWLEDGMENTS

This work was initially supported by the Department of Energy, Office of Nuclear Energy, Advanced Fuel Cycle Initiative, AFCI. The AFCI program then evolved into the Global Nuclear Energy Partnership Program, GNEP, which then continued to support this effort. The author would first like to acknowledge his thesis advisor, Dr. Samim Anghaie, from the University of Florida, for his support and guidance through the process of developing an interesting problem, and then seeing the efforts of solving that problem till conclusion. The author would then also like to thank, Dr. Edward Dugan, Dr. Alireza Haghighat, Professor James Tulenko, and Dr. William Vernetson for providing the author with a comprehensive education in reactor physics and fuel depletion analysis. The author would also like to thank Dr. Wesley Bolch, Dr. David Gilland, Dr. Travis Knight, Dr. David Hintenlang, from the University of Florida, for instilling a fulfilling education in the areas of applied radiological engineering. The author would then like to thank Rick Kapernick, Thomas Marcille, Dr. Dave Poston, and Dr. Pratap Sadasivan, from the space reactor design group at Los Alamos National Laboratory, for their financial and mentor support, giving the author a solid foundation in reactor design considerations. The author would also like to thank Dr. Mike Miller, Dr. Peter Santi, Dr. Marytn Swinhoe and Dr. Steve Tobin, from the reactor safeguards group at Los Alamos National Laboratory, for their guidance and suggestions in the methodology development of certain applied capabilities. The author would also like to thank Dr. Holly Trellue, from the reactor design group at Los Alamos National Laboratory for her valued guidance and support from experience in developing a linked depletion capability. Most importantly the author would like to thank Dr. Gregg Mckinney, Dr. Michael James, Dr. Russell Johns, Dr. Joe Durkee, Dr. Joshua Finch, Denise Pelowitz, Dr. Laurie Waters and Dr. Jay Elson, for their patience, support and guidance in implementing the methodology, developing theory, and testing the code's capabilities. Finally, the author would

especially like to thank Dr. John S. Hendricks for his patience and guidance as a superb mentor at Los Alamos National Laboratory.

TABLE OF CONTENTS

page

LIST OF TABLES

LIST OF FIGURES

Abstract of Dissertation Presented to the Graduate School
of the University of Florida in Partial Fulfillment of the
Requirements for the Degree of Doctor of Philosophy

DEVELOPMENT OF THE MCNPX DEPLETION CAPABILITY: A MONTE CARLO LINKED DEPLETION METHOD THAT AUTOMATES THE COUPLING BETWEEN MCNPX AND CINDER90 FOR HIGH FIDELITY BURNUP CALCULATIONS

By

Michael Lorne Fensin

May 2008

Chair: Samim Anghaie
Major: Nuclear Engineering Sciences

Monte Carlo-linked depletion methods have gained recent interest due to the ability to more accurately model complex 3-dimesional geometries and better track the evolution of temporal nuclide inventory by simulating the actual physical process utilizing continuous energy coefficients. The integration of CINDER90 into the MCNPX Monte Carlo radiation transport code provides a high-fidelity completely self-contained Monte-Carlo-linked depletion capability in a well established, widely accepted Monte Carlo radiation transport code that is compatible with most nuclear criticality (KCODE) particle tracking features in MCNPX. MCNPX depletion tracks all necessary reaction rates and follows as many isotopes as cross section data permits in order to achieve a highly accurate temporal nuclide inventory solution.

This work chronicles relevant nuclear history, surveys current methodologies of depletion theory, details the methodology in applied MCNPX and provides benchmark results for three independent OECD/NEA benchmarks. Relevant nuclear history, from the Oklo reactor two billion years ago to the current major United States nuclear fuel cycle development programs, is addressed in order to supply the motivation for the development of this technology. A survey of current reaction rate and temporal nuclide inventory techniques is then provided to offer

justification for the depletion strategy applied within MCNPX. The MCNPX depletion strategy is then dissected and each code feature is detailed chronicling the methodology development from the original linking of MONTEBURNS and MCNP to the most recent public release of the integrated capability (MCNPX 2.6.F). Calculation results of the OECD/ NEA Phase IB benchmark, H. B. Robinson benchmark and OECD/ NEA Phase IVB are then provided. The acceptable results of these calculations offer sufficient confidence in the predictive capability of the MCNPX depletion method. This capability sets up a significant foundation, in a well established and supported radiation transport code, for further development of a Monte Carlo-linked depletion methodology which is essential to the future development of advanced reactor technologies that exceed the limitations of current deterministic based methods.

CHAPTER 1
INTRODUCTION AND BACKGROUND

The purpose of the development the Monte Carlo linked depletion methodology within MCNPX is to provide a high fidelity depletion methodology available within a widely accepted code package that is already the "gold standard" for radiation transport calculations. To understand why development of this methodology is vital to the current nuclear community and why the methodology must be implemented into MCNPX, involves first understanding the history of reactor development from the first natural reactor in Oklo, Gabon, to the current major United States fuel cycle development programs, as well as why the current United States fuel cycle program, the Global Nuclear Energy Partnership (GNEP), is interested in such a technology.

Reactor Development History

The first self-sustaining chain reaction achieved on earth predated the first man made self-sustaining chain reaction by roughly two billion years. The governing process to maintain this self-sustaining reaction required that precisely one neutron from each fission process resulted in another fission event. A delicate balance between processes that resulted in increasing the neutron population, positive reactivity, and processes that resulted in decreasing the neutron population, negative reactivity, was required in order to maintain a self-sustaining reaction. In Oklo, Gabon, considerable heat occurred in several uranium rich deposits when groundwater seeped into the uranium deposits leading to ample moderation that sufficiently increased the probability of fission to allow for a self-sustaining chain reaction.[1] As the uranium rich deposits burned fissile uranium-235, fission products and other transmuted actinides were generated. In some nuclear reactions, fertile actinides consumed radiation resulting in new fissionable actinides that along with uranium-235 contributed to maintaining the sustainability of the chain

reaction. Conversely, the production of fission products and non fissile transmuted actinides, as well as the reduction in moderator density from heat build, contributed to decreasing the probability of fission, ultimately hindering the sustainability of the chain reaction.[2]

Like a gigantic coffee pot percolating away over hundreds of thousands of years, the Oklo reactor would first undergo a fission chain reaction until enough heat and nonfissile nuclides were generated to hinder the self-sustaining chain reaction. The system would then cease to maintain self-sustaining fission events resulting in a cool off in the moderator leading to an increase in the moderator density. This subsequent moderator density increase would correspondingly lead to enough positive reactivity to ultimately restart the chain reaction.

About 2 billion years later, scientists would later discover the fission process and mechanisms in order to fission a nucleus and maintain a self-sustaining reaction. In 1930, W. Bothe and H. Becker found that a highly penetrating radiation was emitted when beryllium, boron or lithium were bombarded by alpha particles from a polonium source.[3] In 1932, Irene Currie and her husband found that protons were produced when striking hydrogen containing substances, such as paraffin, with this newly discovered penetrating radiation. James Chadwick later demonstrated that the evidence from these experiments was compatible with the assumption that this new radiation consisted of an uncharged particle having approximately the same mass of a proton.[3] He named this new particle “neutron”.[3]

In 1934, Enrico Fermi irradiated uranium with neutrons trying to produce the first transuranic element; however, he accidentally achieved the world's first nuclear fission. In 1938, he received the Nobel Prize in Physics, "for his demonstrations of the existence of new radioactive elements produced by neutron irradiation, and for his related discovery of nuclear reactions brought about by slow neutrons”.[3] In 1939, Hans and Strassmann later showed that the

products from neutron bombardment of uranium included elements in the medium mass region, much lighter than the initial uranium nuclide. The presence of these medium mass region nuclides from the bombardment process suggested that the nucleus had split during the reaction, and the fact that the sum of these medium mass nuclides did not add to the sum of the initial parent uranium nuclide suggested that some of the mass in the reaction was converted into energy. L. Meitner and O. Frisch termed this process fission and also calculated the energy released during fission of a U-235 nuclide to be 200 MeV.[3]

Albert Einstein then wrote his famous letter to President Franklin Roosevelt on August 2, 1939 stating "that the element uranium may be turned into a new and important source of energy in the immediate future." That source of energy was to be utilized by the United States to create the first atomic bomb. With theoretical models and simulation, Enrico Fermi later theorized that the neutrons emitted in fission might induce fission reactions concluding that it should be possible to sustain a chain reaction in uranium and that this chain reaction could be made steady state by implementing a balance of fissionable and nonfissionable material. Fermi and Leo Szilard further proposed placing uranium in a matrix of graphite, where graphite was used to slow the fission neutrons to low enough energy in order to increase the probability of fission to maintain a self-sustaining chain reaction. On December 2, 1942, implementing a delicate balance of positive and negative reactivity, based on proper modeling and simulation, the first controlled self-sustaining chain reaction was achieved in a squash court under the University of Chicago's Stagg Field.[3] The later implementation of this discovery was unleashed, on August 6, 1945, when Little Boy exploded over Hiroshima killing over 100,000 people, and on August 9, 1945, when Fat Man exploded over Nagasaki killing 75,000, ultimately ending the war with

Japan. Both atomics bombs were designed using the Monte Carlo modeling and simulation method.

In a later document in 1946, Enrico Fermi published a scheme for outlining the future uses of nuclear energy. In this document he clearly stated that controlled self-sustained fission chain reaction energy may be utilized for power generation for the world by use of a steam cycle or direct energy conversion process.[4] By enriching the amount of U-235 in natural uranium, the uranium could be combined with a water coolant and poison materials in order to make a self-sustaining power reactor system. On December 8, 1953, United States President Dwight D. Eisenhower gave the Atoms for Peace speech to the United Nations and outlined the advantages of commercial power generation. He later tasked the United States Navy with developing the first commercial power station. A proposal by Duquesne Light Company was later accepted for the Shippingport Atomic Power Station, and the first reactor went critical on December 2nd 1957.[5] The Shippingport Atomic Power Station was a type of light water reactor (LWR) called a pressurized water reactor (PWR). Another type of competing LWR design was the boiling water reactor (BWR), which was developed by a combined effort between Argonne National Laboratory and General Electric. The GE Valecitos BWR was the first commercial BWR to be licensed by the United States Atomic Energy Commission.[6]

The PWR concept is characterized as a system in which the coolant is sub-cooled and contains homogeneously dispersed boron poison in order to maintain criticality. The system utilizes an indirect dual-cycle that uses a steam generator to transfer heat from the exiting primary radioactive subcooled reactor coolant to a secondary loop containing nonradioactive steam. This nonradioactive steam is used to spin a turbine that when combined with a generator creates power for hundreds of thousands of homes.[7]

The BWR concept is characterized as a system that has boiling in the reactor core, with the bulk coolant containing no boron, utilizing a direct cycle for power conversion (the demonstration BWR/1 plants utilized a dual cycle). Instead of a secondary loop, this type of system exhausts high quality steam from the top of the reactor through the use of moisture separators and dryers. This radioactive steam is fed directly into the turbines that are also connected to generators used to make power for hundreds of thousands of homes.[7]

The progress of these commercial power systems later led to the development of other competing reactor systems. Due to the advantages in being able to mine large amounts of uranium ore, and due to the thought that a country developing enrichment technology may also be developing weapons technology, the Canadians decided to develop a system that would not rely on enrichment technology. By taking advantage of the scattering and absorption properties of deuterium, the Canadian deuterium uranium reactors (CANDU) were able to generate power with natural U-235 concentrations. Other technologies were also spawned employing a variety of coolants and moderators such as the gas cooled fast reactor (GCFR) and graphite moderated reactors in order to achieve higher operating temperatures and enhanced thermodynamic efficiency. Technologies were also developed to support the breeding of fissile nuclides incorporating various operational characteristics such as the liquid metal fast breeder reactors (LMFBR).[8]

Though all the vast reactor types incorporate many different materials, fuel and coolant forms, geometry combinations and operating strategies, the basic design objectives are still very much the same. The goal is to determine the correct balance of fissile and control material needed in order maintain the self-sustaining chain reaction, operate the system at a prescribed power, for a prescribed amount of time, achieving some type of operating objective while

accounting for reactivity deficits. These reactivity deficits include temperature and isotope buildup effects. The operating objectives range from maximizing capacity factor, to minimizing discharged wasted, to producing irradiation environments, to generating medical isotope material.[9, 10, 11, 12] In order to develop the most optimized and advanced systems for specific operating strategies, designers constantly examine varied types of material and geometry combinations in order to design a system that meets the operating goals at the minimum cost. This process therefore involves simulating a model in order to investigate many varied types of designs, with many design iterations and perturbations, until an optimum configuration is reached.[13] As the model becomes more detailed and gives better understanding of what is actually happening, the designer is able to make a more well-informed decision on how to proceed with designing the system. Furthermore, as the development decisions for nuclear reactor extend beyond running the system at a prescribed power for a prescribed amount time to minimize the nuclear waste and addressing proliferation concerns, a higher fidelity modeling methodology is required in order to make more-informed design decisions.[14, 15]

Advanced Fuel Cycle Initiative

The Advanced Fuel Cycle Initiative (AFCI) was established October 1, 2002, as an evolution of the Advanced Accelerator Applications (AAA) program. The AAA program was a Department of Energy (DOE) program commissioned by Congress in FY2000 to construct a national effort by DOE laboratories, industry, and universities in order to address key significant nuclear issues facing the United States, particularly the advanced fuel cycle technologies, actinide transmutation, and treatment of spent nuclear fuel. The mission of the program was to develop a technology basis for the transmutation of nuclear waste and demonstrate the practicality of the process for use in long-term nuclear waste management.[16] Initially, the focus was on the use of accelerator based systems, hence the program name AAA. In 2002, the

program was evolved into AFCI with the focus changing to chemical separations and transmutation fuel technologies. The idea was to couple reactor use of fuel with transmutation and separation technologies in order to improve the management of nuclear waste through fuel recycle and transmutation.[16]

The mission of the AFCI program was to develop advanced fuel cycle technologies including spent fuel treatment, advanced fuels development, and transmutation technologies for application to current operating commercial nuclear reactors and next-generation reactors with the goal of (1) reducing volume of high-level waste; (2) reducing long-lived and highly radiotoxic elements; (3) reclaiming valuable energy content in spent nuclear fuel.

AFCI was part of an integrated strategy of the DOE office of Nuclear Energy, Science and Technology, which also includes the Nuclear Power 2010 Program, the Generation IV Nuclear Energy Systems Initiative (Generation IV), and the Nuclear Hydrogen Initiative. AFCI was important in reestablishing the viability of civilian nuclear capabilities and facilities in the United States by utilizing services of DOE laboratories, industry, and universities. The development of an advanced high fidelity technology for simulating transmutation and depletion of nuclear fuel fit nicely with the goals of AFCI, thus leading to the initial funding of the MCNPX Monte Carlo linked depletion project.[17] However, in FY2007, AFCI along with the Nuclear Power 2010 Program, the Generation IV Nuclear Energy Systems Initiative (Generation IV), and the Nuclear Hydrogen Initiative evolved into the GNEP program with the objective of developing an Advanced Burner Reactor (ABR) technology in order to transmutate spent nuclear fuel and develop separations technologies in order to maximize the amount of energy extracted from nuclear fuel, minimize nuclear waste, and mitigate concerns regarding proliferation of weapons material from commercial nuclear fuel.[18]

Global Nuclear Energy Partnership

The main goal of GNEP is to advance nuclear power technologies and enhance the nation's nuclear energy capacity while effectively addressing the challenge of nuclear waste disposal and decreasing the risk of nuclear weapons proliferation and.[18] As part of President George W. Bush's Advanced Energy Initiative, GNEP seeks to develop worldwide consensus on enabling expanded use of nuclear power to meet the growing energy demand while ensuring reduced dependence on carbon based energy producing systems.[18] The GNEP campaign recognizes that a plentiful, reliable supply of energy is paramount to sustained economic growth and prosperity, and that nuclear power is the only proven technology that can provide abundant supplies of electricity reliably and without air pollution or emissions of greenhouse gasses. The GNEP campaign has further recognized that the use of this economical, carbon-free technology will reduce the nation's dependence on environment unfriendly energy producing technologies that increase greenhouse gas emissions.[18]

GNEP addresses two key issues: implementing sensitive nuclear technologies in a way that protects global security and determining proper methods of disposing of nuclear waste safely. The proposed new nuclear energy infrastructure would implement a closed nuclear fuel cycle that enhances energy security, while promoting non-proliferation and recycling nuclear fuel to reduce the nation's nuclear waste. This closed fuel cycle requires the development of technologies that enable consumption of long-lived radioactive waste, and recycling of useful fissile isotopes.[9, 19]

The following include the major objectives of the GNEP program:

1. New proliferation-resistant technologies to recycle spent nuclear fuel will be used so that more energy may be recovered and total nuclear waste is reduced.

2. The latest and advanced fuel cycle strategies will be employed in order to reduce the risk of nuclear proliferation worldwide.

3. The growth of prosperity and sustainable development around the world will be encouraged by meeting energy capacity demands through the use of nuclear energy.

4. The nation's dependence on fossil fuels will be reduced encouraging the continual improvement of the environment.

These objectives will be achieved by the following strategies:

1. A new generation of nuclear power plants will be developed in the United States that employ advanced fuel burning strategies in order to minimize actinide wastes.

2. An integrated fuel separations technology and recycling capability will be designed and deployed.

3. An aggressive strategy to manage spent nuclear fuel and nuclear waste in the United States will be determined including permanent geologic storage at Yucca Mountain.

4. A reliable fuel services program will be engineered in which participating nations with secure nuclear technologies would be required to supply and receive fresh and spent nuclear fuel.

5. Cost effective efficient power reactors will be developed and deployed.

6. Nuclear safeguards to enhance the proliferation-resistance and safety of expanded nuclear power will be improved.

In order to achieve the GNEP objectives by implementing the mentioned strategies, a symbiotic fuel cycle strategy must be implemented that utilizes both LWR and fast reactor (FR) technology to maximize the amount of energy extraction from transuranics while minimizing the amount of overall waste buildup. Spent nuclear fuel contains a plethora new actinides due to the transmutation that occurs during the burning of the fuel. These actinides are sources of both long-term radiological hazards, because they dominate the long term ingestion radiotoxicity of the waste, and proliferation hazards, because they are fissionable nuclides.[19] The long lived actinides tend to have much larger half-lives than typical fission products. Therefore the task of actinide burning is of utmost importance to addressing the long term radiological waste problem and mitigating proliferation concern. To burn actinides effectively, the actinides must be

separated from other isotopes that compete for reactions.[20, 21, 22] The GNEP campaign is tasked with developing a separations facility to exact burnable actinides from spent nuclear fuel and separate these actinides from short-lived fission products. The short-lived fission products may be easily stored in a geological repository as these isotopes will decay away to stability in a reasonable amount of time.

Advanced Burner Reactor Campaign

The separated actinides must then be recycled and further incinerated in either an accelerator or reactor. Many types of scenarios have been studied that examine this portioned approach to actinide incineration; however, the transmutation of waste by accelerator option is limited by cost and wasted use of extractable actinide energy. Two basic types of reactors have been considered for further actinide burning. The extracted actinides could be fabricated into mixed oxide (MOX) fuel bundles and placed back into a commercial LWR. The advantage to burning in a commercial thermal spectrum reactor is that commercial reactors are already in operation, and therefore transitioning operating strategies for accepting MOX fuel would seem to be more viable solution than developing an entire new reactor for transmutation.[12, 15, 19, 21] Recycling of plutonium in thermal reactors would also help to reduce total plutonium and seek to mitigate proliferation concern. Developing operating strategies to account for reduced poison worth, from the higher thermal absorption cross section of Pu-239 as compared to the uranium isotopes, and faster reactor response, from the reduced delayed neutron fraction of Pu-239, may be complicated; however, the solutions to these strategies may be engineered and therefore does not limit deployment.[11]

The limit of the effectiveness of multi-recycling of actinides in commercial LWRs is dictated by the amount of higher actinides generated as a function of burnup. In a thermal reactor spectrum, the higher actinides buildup due to lower fission rates (i.e. curium) in those

isotopes and higher capture rates in the thermal spectrum. The fission-to-capture ratio in thermal reactors is not as high as in fast reactors and therefore higher actinides are generated and not fissioned as readily as compared to fast reactors. Therefore more Am, Cm, and Cf are generated as function of burnup in thermal reactors as compared to fast reactors.[19, 22] These isotopes make spent fuel recycle challenging through increased heat generation and spontaneous neutron emission, and further result in both criticality and radiation protection difficulties.

The fast reactor spectrum is more favorable for higher actinide transmutation because the fission to capture ratio is much higher as compared to thermal spectrum reactors.[19] Destruction of long-lived actinides requires excess neutrons. In a fast reactor the difference between neutron production by fission and losses by capture in structural and absorbing materials or leakage from the core is ~0.4 -0.6 neutrons per fission while in a thermal reactor this surplus is well below at 0.1 neutrons per fission.[19] The cross sections in the fast spectrum favor fission rather than capture; however, the fast spectrum cross sections are smaller in magnitude and therefore a larger flux is required to achieve the same destruction yield as in thermal reactors.[15] Since the principal of transmutation consists of recycling actinide wastes in reactor scenarios that favor fission as opposed to capture, development of a fast reactor technology is integral to the objectives of the GNEP campaign in order to maximize energy extraction from fuel and minimize the buildup of long term actinide wastes.

GNEP will develop and demonstrate Advanced Burner Reactors (ABRs) that consume actinide wastes while extracting their usable energy. The objective of developing these fast spectrum reactors will be to destroy actinide wastes in commercial spent nuclear fuel from nuclear power plants, avoiding the need to accommodate material in a geological repository for hundreds of thousands of years while it decays. The reality of this objective is that these ABRs

will not avoid but reduce the burden of current repository demand. Significant prior United States investment in fast reactors, such as Fast Flux Test Facility and the Experimental Breeder Reactor, provides a valuable technology base for supporting future development of ABRs.

Though the development of ABRs requires following the isotopes in exact detail in order understand true transmutation rates of actinide wastes, the initial design process will require thousands of core calculations that integrate neutronic, structural, and thermal hydraulic concerns in order to license the facility. These calculations include varied core operating and shutdown strategies in order to demonstrate that the core may operate at a certain power, for a certain amount of time, and shutdown safely in an accident scenario. Therefore calculations of actinide transmutation rates need not be followed in tremendous detail in order to license the facility so as to hamper the ability to complete the plethora of integrated system calculations. In fact, calculations that capture more detail than what is necessary to license the facility will simply hinder the completion of the design and possibly the building of the facility. If a 2-dimensional diffusion theory code that runs in 5 seconds achieves an adequate result, why waste time running a high fidelity calculation that takes a week (the fallibility in this statement may reside in the fact that without experimental benchmarks to validate the less accurate solution method, one cannot be certain that the approximations applied to that solution method are indeed correct). Therefore high fidelity depletion modeling may not be of interest to the initial design of the ABRs. However, high fidelity depletion modeling is integral to determining adequate source term generation for the development of technologies that will be used to segregate detectable signals into key nuclide signatures to be used for interpreting proliferation concerns.

Reactor Safeguards Campaign

The objective of reactor safeguards is to develop proliferant resistant fuel cycle technologies and programs the help prevent misuse of civilian nuclear facilities for non-peaceful

purposes. Reactor safeguards responsibilities include accounting for special nuclear materials, control of technology and the ability to inspect and verify compliance with international agreements.[23] Under the auspices of the International Atomic Energy Agency reactor safeguards have been an effective deterrent against the spread of nuclear technology and materials. The role of GNEP safeguards is to provide the opportunity to design modern safeguards directly into the planning and building of new nuclear energy systems and fuel cycle facilities. .[23] The GNEP Safeguards campaign will also focused on improving international safeguards including the development of future proliferation-resistant fuel cycle and reactor technologies to be integrated world wide.[23]

The development of safeguards technologies involves improving the way in which diversion of special nuclear material is detected. The source term of the special nuclear material is the actinide wastes generated in nuclear reactors and the soon to be developed ABRs. Therefore the safeguards community is concerned with measuring the content of key specific nuclides within spent fuel leaving the reactor. For the GNEP campaign, the spent nuclear material will take on many different types of combinations depending on the reactor type that generated that specific spent fuel.

The isotope content of key specific nuclides within the spent fuel may be determined by implementing various non-destructive-analysis (NDA) techniques involving the discrimination of a detectable signal into the components of a specific nuclide's radiation signature.[24] The efficiency of the detection equipment to measure the concentration of a specific nuclide is therefore dependent on the ability to segregate the detectable signal into the components that contribute to the specific nuclide's signature and the components that do not contribute.[24] Since the detectable signal may be a conglomeration of many simultaneously contributing radiation

signatures, discrimination of the signal into the key components of a specific nuclide's signature involves knowledge of all the contributions to the signal. From a modeling standpoint, designing more efficient detection equipment involves explicitly following the evolutionary buildup of all isotopes contributing to the detectable signatures. However, in order to accurately account for the temporal evolution of the nuclide inventory of all contributors to the detectable signal of key nuclide signatures, a method that more accurately captures the true system physics of the source term generation becomes paramount.

MCNPX is widely used in the safeguards community for modeling all aspects of reactor safeguards and is considered the "gold standard" in radiation transport modeling. Historically, the MCNPX code lacked the capability to model fuel depletion and therefore could not accurately generate the needed source term for development high fidelity detection equipment. In the past, this source term was either generated by an externally linked technology or by an entirely separate code of which both incorporated varied assumption that ultimately affected calculation accuracy. A technology that calculates a high fidelity time-dependant isotope inventory is essential for determining a sufficient source term use in a very precise calibration and design of high fidelity radiation detection equipment. It is vital that this capability be placed in MCNPX in order to make MCNPX, a tool already implemented by the reactor safeguards and considered a gold standard by the community, a more complete tool for reactor safeguards calculations.

Motivations for a Monte Carlo Depletion Tool in MCNPX

Many deterministic linked tools exist that are capable of modeling fuel depletion for advanced reactor concepts. However, these tools employ a variety of approximations about system physics in order to achieve a quick result.[25-34] For the result to be reliable, costly experimental benchmarking and thorough investigative analysis is required in order to determine

the limits of the modeling technology. Approximations implemented in the calculation of one type of system are not necessarily valid for the calculation of a different system.[32, 34] This issue leads to the necessity to develop and catalogue an assortment of tools employing a diverse range of calculation assumptions.[35] The selection of an adequate modeling tool therefore relies on the ability to predetermine which assumptions are adequate for a particular calculation type and then selecting the design tool employing those assumptions. Therefore, it is possible that false conclusions of system behavior may be drawn from false hypotheses of system physics when incorrect approximations are implemented leading to the inability to make adequate design decisions.

As advanced reactor concepts challenge the accuracy of current modeling technologies, a higher fidelity depletion calculation, which employs few, if any, assumptions of system physics, is crucial to properly model the wide variety of advanced reactor concepts. An optimum modeling tool would not rely upon predetermined knowledge of adequate assumptions that could result in an incorrect calculation; the tool would eliminate system physics assumptions entirely and preserve the true physics behavior. A Monte Carlo linked depletion tool is capable of achieving this goal because true system physics is preserved through the simulation of the actual complete physical process. This makes the Monte Carlo linked depletion method highly robust and capable of analyzing a wide variety of calculations with immense confidence of achieving an accurate result.[36]

A few Monte-Carlo-linked depletion codes exist including ALEPH, BURNCALC, MCODE, MC-REBUS, MCWO, MCB, MCMG-BURN, MOCUP, MONTEBURNS, MVP and RACER.[37-49] Most of these codes are externally linked technologies and implement complicated directory structures to integrate each externally linked code package. This results in increased

memory restrictions that ultimately constrict the maximum size of the calculation model. Some of these efforts are also not supported, and therefore offer little if any code support for the typical user. Some of these efforts use multi-group Monte Carlo and are therefore slave to the calculation assumption of the deterministic methodologies.[49] Most of these codes are also focused on accelerating the calculation by minimizing the amount of isotopes and reactions tracked in order to minimize computational expense at the cost of detail in the simulation thereby loosing fidelity that may be of interest to the user. Since most of these codes are externally linked technologies, in most cases, the codes only work with a minimal amount of functionality of the codes in which they are linked. In order to truly take advantage of the robustness of the Monte Carlo linked depletion method, the technology must be self-contained, eliminate excess top-level processing and calculation size requirements as well as automatically determine and track parameters important to the depletion process.

MCNPX depletion provides a vital modeling framework, within a well established, supported reactor safeguards radiation transport code, for high-fidelity depletion calculations to assist in the development of technologies requiring ample intricate detail in the depletion solution such as the reactor safeguards calculations required for GNEP. Because this capability is fully integrated into the functionality of a well established radiation transport package already utilized by the GNEP safeguards committee, the community now has a tool that meets almost all the functionality required to meet their current modeling needs.

Objective

The goal of this work is to develop a self contained easy-to-use Monte Carlo linked depletion modeling framework within a well established radiation transport package that eliminates calculation size requirements as well as automatically determines and explicitly tracks all the important parameters for computing an accurate depletion solution. This task involves

internally linking the MCNPX steady state-reaction calculator to the CINDER90 number density calculator.[50, 51] MCNPX will be used to calculate steady-state reaction rates and normalization parameters while CINDER90 will be used to calculate the time-dependent isotope buildup/depletion.

The work scope may be bifurcated into two separate processes: code development and code verification and validation. The following ten code development issues will be addressed:

1. A Monte Carlo linked depletion capability that works within the confines of the MCNPX code package will be developed, making sure the depletion capability is compatible with major execution features of MCNPX.

2. The input structure must reside within an MCNPX input deck. The input structure will be simplified yet include ways of user specification for

    a. time steps to report isotope and system data;
    b. power lever and percent of full power level to implement at specific time steps;
    c. burn materials to be depleted;
    d. isotopes to omit;
    e. fission products to track;
    f. nuclide concentrations to manually change for different time steps;
    g. ability to order output according to user specification.

3. The output will contain averaged time-dependent information for

    a. neutron multiplication;
    b. neutrons per fission;
    c. recoverable energy per fission;
    d. burnup;
    e. source neutrons;
    f. isotope concentrations and activity of radioactive isotopes;
    g. sum of isotope concentrations and activity information.

4. For individual burn materials the code output will report

    a. fission power fractions;
    b. burnup;
    c. collision rates;
    d. isotope buildup and activity.

5. The following mechanisms for isotope tracking will include

a. tracking each material specified by the user;
b. selecting fission products to be tracked based on easy-to-implement predefined fission product "Tier" sets;
c. following the concentrations of all the possible daughter reactions from isotopes specified as burn materials;
d. tracking reaction rates of metastable isotopes;
e. manually adjusting burn material concentrations of specific isotopes if necessary.

6. Reaction rates to be computed for use in the depletion process will be determined, and a method will be developed for normalizing the reaction rates based on given and calculated system parameters.

7. A methodology will be implemented for addressing the nonlinearity in the reaction rate utilization in the depletion equation.

8. A method will be engineered for selecting the proper fission yield to be utilized within a specific computation.

9. A capability will be invoked to burn multiple burn materials where individual burn material characteristics may be calculated and reported.

10. A technique will be implemented for accurately capturing the average recoverable capture gamma energy contribution to the true energy per fission event.

Once the methodology is developed the following benchmark studies will be completed:

11. OECD/NEA Burnup Credit Calculational Criticality Benchmark Phase I-B;[52]

12. H. B. Robinson Infinitely Reflected Pressurized Water Reactor Fuel Assembly Calculation;[53]

13. OECD/NEA Burnup Credit Calculational Criticality Benchmark Phase IV-B.[54]

CHAPTER 2
SURVEY OF STATE OF THE ART APPROACHES TO DEPLETION ANALYSIS

During the operation of a nuclear system, the nuclide concentration will change as isotopes consume radiation (neutrons, protons, alphas, betas, etc.) and undergo various nuclear reactions [(n, fission), (n, 2n), (n,p), (n,α) , (n,β), etc.].[2] The temporal change in isotope concentrations results in further changes in scatter, capture, and fission events as isotopes either transmutate or fission into new nuclides possessing different probabilities for these reactions. For example, as U-235 depletes as a result of the fission process, fission products are generated. Because these newly created fission products posses capture reaction probabilities that rival U-235 for neutron capture, the fission products, combined with the depletion of U-235, reduce the propensity of the system to fission and maintain a steady-state chain reaction. In order to maintain a self sustaining steady-state chain reaction, more fuel than is necessary in order to maintain a steady-state chain reaction must be loaded. The introduction of this excess fuel increases the net multiplication capability of the system. To maintain the net neutron multiplication of the system at a steady state, poison material is introduced to absorb the excess neutrons generated from the excess fuel loading. As the fuel depletes and produces absorbing fission products, the controlling material is extracted in order to maintain the delicate reactivity balance needed in order to maintain a self sustaining chain reaction.[9] Therefore it is crucial to monitor the temporal isotopic concentration in the nuclear system because changes in this composition affect the operating strategies that are necessary to maintain a steady-state self-sustaining reaction.

The operating strategies of a nuclear system are affected by the ability to meet limiting values of key operational parameters. These parameters include: flux, power distribution, reactivity, shutdown margin, etc. The limiting values of these parameters are set such that the system be able to operate safely for a prescribed time and meet a prescribed objective. Since

these system parameters therefore limit operational characteristics of the system, it is crucial to compute these values as each value temporally evolves drastically enough to warrant changes in the system operation. The study of the change of these operational parameters with the time-dependent production/ depletion of nuclei is known as depletion analysis.[2]

The Depletion Equation

Solving for the time-dependent change of a specified nuclide involves accounting for all processes that lead to either the creation or destruction of that nuclide. The temporal nuclide density may be described by the Bateman equations.[55] Equation 2-1 states a simplification of a form of the Bateman equations so as to describe the depletion of an individual nuclide:

$$\frac{dN_m(\vec{r},t)}{dt} = -N_m(\vec{r},t)\beta_m + \overline{Y}_m + \sum_{k\neq m} N_k(\vec{r},t)\gamma_{k\to m} \tag{2-1}$$

- $\frac{dN_m}{dt}$ = time dependant change in nuclide m
- $-N_m(t)\beta_m$ = destruction of nuclide m
- $\sum_{k\neq m} N_k(t)\gamma_{k\to m}$ = creation of nuclide m via other nuclides in the system
- $\overline{Y}_m$ = production of nuclide m via an external source

Solving for the time-dependent change of a specified nuclide also involves knowledge of the time-dependent change of each contributing nuclide. Therefore the solution of each nuclides time-dependent change involves solving a set of coupled differential equations.[55] Though solving a set of coupled linear differential equations is a straightforward mathematical process, the coefficients in the coupled depletion equations are nonlinear therefore making the equations unsolvable without approximation. Expanding the destruction coefficient, β_m, and the creation coefficient, $\gamma_{k\to m}$, clarifies the nature of the nonlinearity of equation 2-1:

$$\beta_m = \lambda_m + \sum_r \int \sigma_{m,r}(E)\Phi(r,E,t)dE \tag{2-2a}$$

$$\gamma_{k\to m} = \sum_{m\neq k} L_{km}\lambda_k + \sum_{m\neq k}\sum_r \int Y_{km,r}(E)\sigma_{k,r}(E)\Phi(r,E,t)dE \qquad (2\text{-}2b)$$

- λ_m = destruction of nuclide m by radioactive decay
- $\sum_r \int \sigma_{m,r}(E)\Phi(r,E,t)dE$ = destruction of nuclide m by transmutation reaction
- $\sum_{m\neq k} L_{km}\lambda_k$ = creation of nuclide m by some isotope radioactively decaying to isotope m
- $\sum_{m\neq k}\sum_r \int Y_{km,r}(E)\sigma_{k,r}(E)\Phi(r,E,t)dE$ = creation of isotope m by some isotope transmutating to isotope m via a transmutation reaction, r.

The analysis of the temporal nuclide inventory is complicated by the fact that the temporal nuclide inventory solution is dependent upon the time-dependent flux. Unfortunately, the time-dependent flux is also dependent upon the time-dependent nuclide inventory. To make equation 2-1 linear and solvable, approximations must be made regarding the coefficients. The first approximation assumes that the coefficients be made constant over a time step of interest, tacitly implying that the time-dependent nuclide solution is separable from the spatial transmuation rate calculation. The second approximation assumes that spatial transmutation rates may be calculated using discrete time steps. The transmutation rates for the temporal nuclide inventory calculation are first computed implementing a steady state reaction rate solver. Then those transmutation rates are assumed constant and applied to the temporal nuclide inventory calculation in equation 2-1.

The validity of the approximations is contingent on the fact that the magnitude of the transmutation rate implies that large time durations are needed in order to initiate significant buildup and depletion of nuclides so as to appreciably alter the spatial transmutation rate calculation.[2, 55] The definition of "large time durations" is relative and dependent upon the builup of highly absorbing isotopes during a time duration that lead to a significant change in the transmutation rate. For example, at the initiation of reactor startup Xe-135 and Sm-149 both

contain large absorption cross sections and builup to equilibrium values early in the reactor operating cycle. In reactors containing burnable poisons incorporated into the fuel assembly, the burnout of these highly absorbing isotopes during the fuel cycle also offers a significant change in transmutation rate as the fuel becomes more reactive in the absence of poisons. Taking time steps that exceed the time to equilibrium buildup of these isotopes affects the further trajectory of the depletion solution because the equilibrium buildup of these highly absorbing isotopes does greatly affect the calculation of spatial transmutation rates. This affects the accuracy of the number densities generated from equation 2-1 for that time step which further affects the calculation of transmutation rates for the next time step. As long as the transmutation rates do not significantly change during a time-step, assuming a constant transmutation rate for a given time-step is valid.[56]

Zero-Dimension Depletion Calculation

The depletion equation requires knowledge of reaction rates, decay coefficients and isotope concentrations at a specific time-step in order to solve for the isotope concentrations at the subsequent time-steps. The accuracy in the depletion calculation is highly dependent upon the appropriateness of the coefficients implemented at given time steps in the solution method, and therefore the amount of spatial detail followed in the depletion solution greatly affects calculation accuracy. The depletion equations could be solved on a normalized basis, in which power is specified in a per weight basis and isotopes concentrations are determined on a per weight basis, if the collision rates utilized in equation 2-1 truly emulate the actual collision rates for a given system. Since this type of calculation is solved over a normalized basis, the solution of the coupled depletion equation does not require the coefficients to exhibit spatial dependence. The accuracy and applicability of this solution method resides in the validity of the implemented coefficients for a given analyzed system.[57]

The ORIGEN and CINDER codes, by themselves, are a family of zero spatial dimension depletion codes and therefore the codes have no knowledge of the spatial dependence of the transmutation rates.[51, 58] Dimensions of the analyzed system are approximated by specifying the power in terms of a bases unit (i.e. power/weight). The major assumption that ORIGEN and CINDER make is that the flux is not spatially dependent and may be calculated by equation 2-3: [51, 58]

$$\Phi = \frac{6.242*10^{18}(P)}{\sum_i X_i^f \sigma_i^f R_i} \tag{2-3}$$

- P = System power $[MW]$
- X_i^f = Concentration of the ith fissile nuclide $[g * atom]$
- σ_i^f = Microscopic probability of fission of the ith fissile nuclide $[b]$
- R_i = Recoverable energy per fission event of the ith fissile nuclide $\left[\frac{MeV}{fission}\right]$
- Φ = Total flux $\left[\frac{neutrons}{cm^2 s}\right]$

The calculation of power based on some spatial flux solution is described by equation 2-4:

$$Power = \int_V \Phi(r) Q \Sigma_f dV \tag{2-4}$$

- $\Phi(r)$ = Spatial flux distribution $\left[\frac{neutrons}{cm^2 s}\right]$
- Σ_f = Macroscopic probability of fission $\left[\frac{1}{cm}\right]$
- dV = Differential volume element $\left[cm^3\right]$
- Q = Average recoverable energy per fission for the whole system $\left[\frac{MeV}{fission}\right]$

After determination of flux and system power, the solution methods of the two codes differ in approach. The two most widely used methods for solving the coupled depletion equations involve a simplification of either the matrix exponential method or the Markov linear chain

method. The Markov linear chain method involves uncoupling the coupled depletion equations into a set of partial linear transmutation paths, solving for the partial buildup/depletion of each nuclide within each linear chain, and summing the final buildups of each partial path to determine the final nuclide buildup (CINDER90 method previously explained).[51] This method takes advantage of minimal memory requirements because the computation is broken up into smaller memory manageable sets. The matrix exponential method tries to explicitly solve the depletion equations by casting the solution in terms of a matrix exponential (method used in ORIGEN and other industry based codes that evolved from the ORIGEN methodology).[58, 59] The main objective of both techniques is to try and determine, as accurately as possible, the evolution of the temporal nuclide inventory solution.

Matrix Exponential Method

The underlying concept of the matrix exponential method is that the formulas for solving normal systems of equations with constant coefficients are identical to the formulas for solving first order differential equations with constant coefficients.[60] Equation 2-1 may be recast into the following form

$$\frac{d}{dt} n_m(r,t) = \sum_k B_{mk}(r,t) n_k(r,t) \tag{2-5}$$

where:

$$B_{mk}(r,t) = \begin{cases} L_{km}\lambda_k + \sum_r Y_{km,r}\sigma_{k,r}\Phi(r,t) & for\ m \neq k \\ -\lambda_m - \sum_r \sigma_{m,r}\Phi(r,t) & for\ m = k \end{cases} \tag{2-6}$$

This results in a set of first order homogenous ordinary differential equations with constant coefficients. The solution of this first order differential equation is:[60]

$$N(t) = N(t_0)\exp(Bt) \tag{2-7}$$

where N is a column vector of nuclide densities and B is the matrix of elements calculated of equation 2-6. The function $\exp(Bt)$ is a matrix exponential function, and is therefore calculated from the following expansion:

$$\exp(Bt) = \sum_{m=0}^{\infty} \frac{(Bt)^m}{m!} \tag{2-8}$$

If the size of the matrix is not too large and not too sparse, the main advantage of this method is that the coupled depletion equations may be solved explicitly.[59] However, the depletion equations require knowledge of all transmuted actinides and fission products leading to a large sparse matrix. This large sparse matrix requires an enormous amount memory in order to store all the necessary computations. Also, the sparse matrix contains both very large values and very small eigenvalues depending upon the half-lives of each isotope tracked during the depletion process.[59] Certain isotopes possess half-lives of a fraction of a second while others posses half-lives of a billion years.

The issue of having a large sparse matrix with widely separated eigenvalues leads to problems in the ability to compute the solution and therefore approximations are made in order to generate a stable solvable matrix.[60] Potentially, the size of the matrix can be as large as n^2, where n is the amount of nuclides followed in the set of equations (1700 nuclides for ORIGEN2.2). However, because the matrix is sparse, a recursive relationship may be generated for formulating the matrix exponential function thereby eliminating the massive memory cost associated with storing all the matrix terms of the matrix exponential function. The relationship in ORIGEN2.2 for one nuclide is as follows:

$$x_i(t) = \sum_{n=o}^{\infty} c_i^n \tag{2-9}$$

where c_i^n is generated by use of the following recursive relationship

$$c_i^0 = x_i(0) \tag{2-10a}$$

$$c_i^{n+1} = \frac{t}{n+1}\sum_{j=1}^{N} a_{ij} c_j^n \tag{2-10b}$$

In this solution method a_{ij} is an element in the matrix that is the first-order rate constant for the creation of isotope i from isotope j. This algorithm for solving for the temporal nuclide inventory only requires the storage of a single vector, c_i^n, greatly reducing memory cost.

The main concern computing the summation in equation 2-9 is that it is necessary to ensure precision is not lost as a result of addition and subtraction of nearly equal large numbers. The time step for the calculation may be reduced so as to limit the size of the matrix coefficients; then the resulting matrix may be multiplied by a factor in order to obtain the desired time step.[60] Scaling the matrix calculation would be impractical for a large number of nuclides as many of the nuclides contain very short half-lives. Therefore in order to fix the mentioned numerical issue, ORIGEN2.2 decays analytically all short lived nuclides. A short lived nuclide is defined such that the matrix coefficients for this nuclide, resulting from the large amount of decay, are so large as to result in numerical issues such that the norm of the matrix exceeds the predetermined value of the word length of the computer used for the calculations. This simplification increases the stability of the solution method by eliminating numerical issues. This assumption is, however, only acceptable as long as the isotope does not contain a significant long lived precursor with a large interaction cross section.[60] For short lived daughter isotopes from long lived parent isotopes, the Gauss-Siedel iterative technique is used to accelerate the calculation of these nuclides.

Ultimately, the amounts of isotopes that are tracked explicitly are limited by the maximum memory requirements of the computer utilized to analyze the system. Therefore implementation of the matrix exponential method actually results in only applying a subset of nuclides to the explicit matrix exponential computation, and then employing approximations to follow the rest. The user must then be careful to select a subset of nuclides that best achieves the most correct characterization of the true interaction behavior of the analyzed system, and then the user must implement an adequate approximation to follow the rest of the nuclides. However, further numerical limitation still exists as a result of the amount available precesion resulting from the applied numerical technique. If the user wishes to therefore try to solve the Bateman equations explicitly, the matrix exponential method may be the method of choice; however, if the user determines that a complete set of fission products and actinides is required in order to achieve a reliable answer then the linear Markov chain method is more capable of storing the concentrations of more nuclide sets without the same type of numerical cost.

The CINDER90 Linear Markov Chain Method

The CINDER90 code is a FORTRAN program coupled with an extensive data library used to calculated nuclide inventory.[61] The origin of the CINDER90 code may be traced back to the original development of the CINDER code in 1960 at the Bettis Atomic Power Laboratory (BAPL) in support of thermal reactor simulations. CINDER was utilized by both BAPL and Los Alamos National Lab (LANL) for the design of many reactor-fuel investigations.[61] Many later versions of the CINDER code were developed with improvements in data evaluations, fission yield sets, and enhanced decay information. Initially, CINDER required preset formation of a consistent set of linear chains to describe the creation and transmutation paths of all investigated cases.[61] All versions of CINDER utilized decay and energy integrated reaction rate probabilities along with fission yield information to calculate the temporal nuclide buildup and depletion.

Versions of CINDER preceding CINDER90 were limited to reactor fuel calculations involving fission products (66<atomic weight<172) and actinides (90<atomic number<96).[61]

The development effort of CINDER90 arose from a need by the LANL accelerator community to have a more complete calculator for temporal nuclide inventories.[61] The library of data in CINDER90 was developed to then include isotope decay and interaction probability data for 3456 isotopes including, ~30 fission yield sets, and yield data for 1325 fission products.[51] CINDER90 is also capable of following as many reaction types as data exists within the CINDER90 library file. The CINDER90 computation process involves utilizing linear Markovian chains to determine the time dependent nuclide densities, solving for the independent contributions to nuclide densities in each of a number of linear nuclide chains. Instead of requiring preexisting transmutation path information, in CINDER90 each transmutation of each nuclide defined by available nuclear data is followed until the path reaches a nuclide that is deemed to be insignificant. CINDER90 implements an equation similar to equation 2-1 in order to calculate the time-dependent nuclide densities:

$$\frac{dN_m}{dt} = -N_m(t)\beta_m + \overline{Y}_m + \sum_{k \neq m} N_k(t)\gamma_{k \to m} \tag{2-11}$$

where all terms are the same as equation 2-1 except that $\overline{Y}_m$ is included to represent the average feed rate. Like equation 2-1, equation 2-11 relies on the assumption that the transmutation probabilities are to remain constant for the for the time interval in which a solution is desired.[61]

The set differential equations utilized to solve for temporal nuclide buildup/depletion is coupled since each equation contains time-dependent isotope density information from other nuclides. In CINDER90, this set of coupled equations is reduced to a set of linear differential equations using the Markov method. Linear chains are created for each isotope transmutation

path. The solutions of each linear chain determines a partial nuclide density, N_i. Each calculated partial nuclide density, N_i, computed from a linear chain, is then summed to obtain the total nuclide inventory of nuclide, N_m. The differential equation governing the computation of $\mathrm{N}(t)$ is therefore only coupled to any preceding elements in the sequence leading to the ith element. For the preceding, (i-1) element, all parameters are assumed known. The entire computation is then computed from the simplified equation

$$\frac{d\mathrm{N}_i}{dt} = \overline{Y}_i + \mathrm{N}_{i-1}(t)\gamma_{i-1} - \mathrm{N}_i(t)\beta_i \tag{2-12}$$

where quantities are now indexed by the order in which they appear within a given sequence and γ_{i-1} is the transmutation probability of forming nuclide element N_i. The general solution form of a linear sequence of nuclides coupled by any sequence of absorption or decay, first derived and implemented by the CINDER code, was:

$$\mathrm{N}_n(t) = \sum_{m=1}^{n}\prod_{k=m}^{n-1}\gamma_k \left\{ \overline{Y}_m \left[\frac{1}{\prod_{l=m}^{n}\beta_l} - \sum_{j=m}^{n} \frac{e^{-\beta_j t}}{\prod_{i=m,\neq j}^{n}\left(\beta_i - \beta_j\right)} \right] + \mathrm{N}_m^0 \sum_{j=m}^{n} \frac{e^{-\beta_j t}}{\prod_{i=m,\neq j}^{n}\left(\beta_i - \beta_j\right)} \right\} \tag{2-13}$$

This algorithm therefore depended upon predetermined knowledge of the transmutation path in order to properly include every N_m^0 encountered within a specific path. This method further suffered from large computational cost because the entire transmutation path was to be followed even if the probability was low of incurring further nuclide production of a specific isotope within a chain.[51]

For computational speed enhancement, simplification, and reduction of memory requirements, the CINDER90 code employs a methodology that does not require a predefined set of nuclides employed in a transmutation path. The methodology starts at a base set of nuclides

and follows each path independently. Tests of significance at each step of the transmutation path are set. If the test of significance is failed, then the transmutation path is stopped and further computation of extraneous nuclides is not incurred. This lead to the following simplifications

$$\mathrm{N}_m^0 = 0, m \neq 1 \tag{2-14}$$

$$\overline{Y}_m = 0, m \neq 1 \tag{2-15}$$

ultimately resulting in the following solution for a given linear sequence:[61]

$$\mathrm{N}_n(t) = \prod_{k=1}^{n-1} \gamma_k \left\{ \overline{Y}_m \left[\frac{1}{\prod_{l=1}^{n} \beta_l} - \sum_{j=1}^{n} \frac{e^{-\beta_{jt}}}{\prod_{i=1,\neq j}^{n} \left(\beta_i - \beta_j\right)} \right] + \mathrm{N}_1^0 \sum_{j=1}^{n} \frac{e^{-\beta_{jt}}}{\prod_{i=1,\neq j}^{n} \left(\beta_i - \beta_j\right)} \right\} \tag{2-16}$$

The test for significance in CINDER90 involves calculating the passby quantity, $P_n(t)$. The passby of a nuclide is the time-integrated transmutation of that nuclide for a specified time interval:

$$P_n(t) = \int_0^t \mathrm{N}_n(t) \beta_n dt \tag{2-17}$$

The passby therefore may be thought of as the progeny of nuclide n resulting from transmutation or decay.[61]

The accuracy of CINDER90 is dependent upon the data that is used in the solution of (Eq. 2-11). If the code is used by itself to calculate nuclide inventory, the user would be relying heavily upon the inherent multi-group cross sections, utilized to determine collapsed energy integrated reaction rates, in order to achieve a solution. Since CINDER90 is a zero-dimensional code, similar approximations, as implemented by ORIGEN, would have to be employed in order to determine a flux to be used in the computation of reaction rates. This flux would not incorporate the spatial behavior of the system and therefore lead to inaccurate interaction rate

calculations. This would further propagate into inaccurate temporal nuclide inventory computations. To resolve this issue, CINDER90 must be linked to a steady state reaction rate calculator in order to capture the spatial resolution and possible spectral change of the time-dependent reaction rate behavior.

Necessity for a Linked Approach

In the zero spatial dimension calculation, the flux is no longer spatially dependant and events such as neutron leakage, scatter and absorption are not accurately depicted. The physics of assuming spatial independence of the reaction rates is highly false because the energy dependence of these reactions makes capture and scatter events heavily dependent upon geometric configurations. For example, BWR reactor fuel pins are loaded at various enrichments in combination with gadolinium burnable poisons in order to try and achieve a flat power distribution across the bundle.[62] These bundles are then strategically positioned within the reactor core in order to further maintain a flat power distribution across the reactor core. A flat power distribution is preferential because if the peak to average power in the bundle is too high then fuel centerline melt, creep, and fission gas pressure constraints limit the average power the bundle can be operated, therefore increasing the amount of needed loaded fuel bundles per cycle and ultimately reducing fuel economy. The ability to meet this flat power distribution demand is limited by the reactor asymmetries that force non-periodic boundary conditions on the flux solution. For instance, neutrons, generated in fuel bundles at the core periphery, exhibit more moderation because of the larger interaction with the surrounding water reflector. This asymmetric interaction is further complicated by the fact that the density of the moderator decreases as the moderating fluid heats up and boils as the fluid passes through the reactor core. This reduction in moderation leads to less fission and more capture at the beginning of the operating cycle. The boundary condition for the flux solution is therefore set by the asymmetric

properties of the external reflecting fluid and these imposed boundary conditions lead to a flux gradient across the reactor core.

There exists further complicating asymmetries within the bundle itself. Burnable poisons, large cruciform control blades, water holes, and structural guide tubes within the fuel assembly also further contribute to flux asymmetry within the fuel assembly.[62] The asymmetry in the flux solution further propagates during fuel burnup as capture rates and thermalizations are spatially affected as a function of the asymmetry in isotope concentrations resulting from the asymmetry in prior reaction rates resulting from the asymmetries in the fuel assembly and core structure. Therefore implementing a depletion model for a reactor system without accounting for spatial dependence will lead to discrepancies in the solution as these types of spatial asymmetries in the flux solution lead to further propagation of asymmetry in isotope buildup and depletion.

As isotopes consume radiation, undergo nuclear reaction, and transmutate into new isotopes, the neutron energy spectrum will change due to how the neutrons will interact with the newly created transmuted isotopes.[2] Simply assuming a single energy-integrated cross section set for an entire depletion calculation may not be a valid assumption for systems that undergo significant spectral changes. For example, in a freshly fueled LWR, initially the majority of energy is created by fission of U-235 atoms. As the core burns over time many neutrons are parasitically absorbed by U-238 leading to production of U-239. U-239 quickly decays by beta emission to Np-239 and then to Pu-239 which is highly fissile. At the end of the reactor core life, an immense amount of Pu-239 has been created, absorbed neutrons, fissioned, and contributed to system power. The average thermal absorption cross section for Pu-239 is 1011.3 b which is much higher as compared to U-235 at 680.8 b.[7] The average thermal fission cross section for Pu-239 is 742.5 b which is also much higher as compared to U-235 at 582.2b.[7]

capture cross section is defined as all absorption reactions not leading to fission, and therefore a thermal capture-to-fission ratio may be defined for a specified isotope by equation 2-18:

$$\alpha \approx \frac{\sigma_a - \sigma_f}{\sigma_f} \tag{2-18}$$

Changes in the capture-fission-ratio over time change the amount of neutrons that will be parasitically absorbed as well as created by the fission process. These factors ultimately alter the neutron energy spectrum and thus lead to time-dependant changes in the transmutation rates. The process is also highly geometry dependent because the capture to fission ratios in certain sections of a given system will change at different rates due to the energy flux witnesses in a specific region. Inaccurate capture of these changes ultimately affects the accuracy of the calculation; therefore it is vital for transmutation rates to be recalculated when isotope concentration changes result in significant changes in the energy flux distribution.

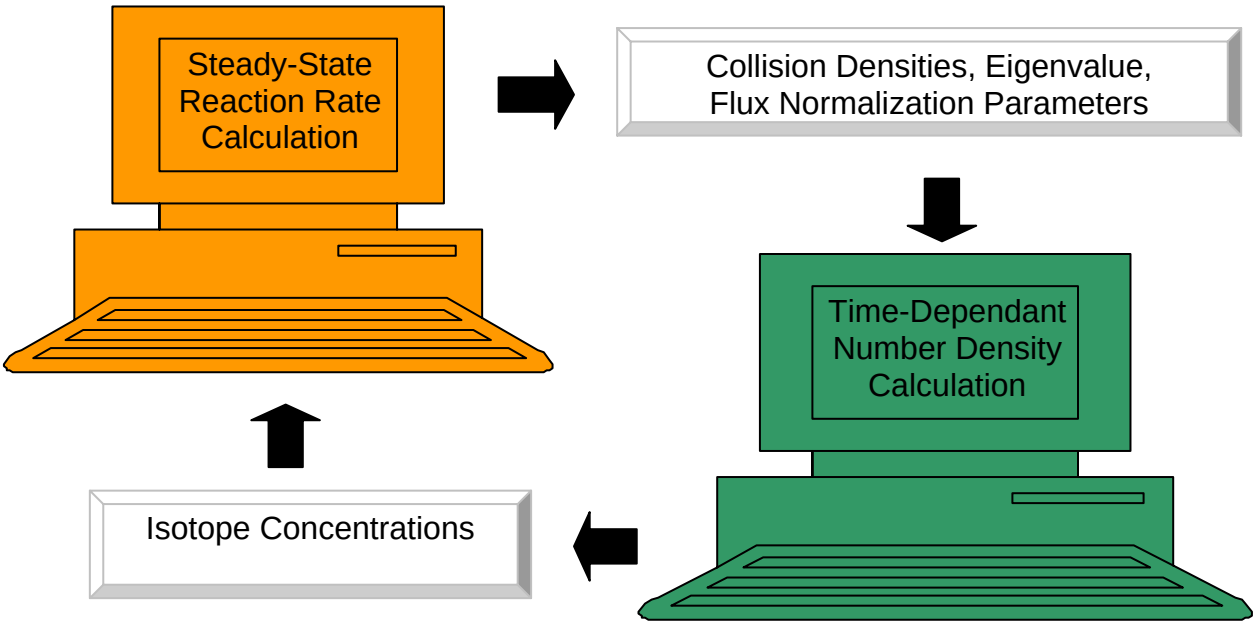

Figure 2-1. Linked Depletion Process.

Since considerable changes in the isotope concentration are required in order to significantly alter the neutron energy spectrum, equation 2-1 may be approximated as separable in space and time. The equation may then be discretized in several time steps where a steady-state recalculation of reaction rates is completed at time intervals where it is assumed that neutron energy spectrum will be altered significantly enough to alter the trajectory of equation 2-1. The procedure for this solution method is outlined in Figure 2-1. The reaction rates utilized in the capture terms of equation 2-1, system eigenvalue, and flux normalization terms are first calculated utilizing a steady-state reaction rate calculator. Those capture reactions are then assumed constant over a specified time step and implemented in a time-dependent number density calculation. The time-dependant number density calculation then calculates a new set of number densities to be utilized in the subsequent steady-state reaction rate calculation. The process repeats itself until the final step.

Methods of Steady State Reaction Rate Calculation

Steady state reaction rates may be calculated by either explicitly solving a form of the Linear Boltzmann Equation (LBE) or determining the average interaction rate behavior of a sample distribution by simulating the actual physical process using the Monte Carlo method.[63, 64, 65] Solving the LBE involves deterministically calculating a continuous spatial reaction rate solution by employing a variety of discretizations and approximations. Accuracy of the calculation is highly dependant upon the validity of the discretization and approximation techniques utilized to represent the system physics.[64] Assumptions must be benchmarked against viable experimental data in order to ensure calculation accuracy. The Monte Carlo method, however, simulates the actual physical process through the random sampling of probabilistic events. The method minimizes approximations applied to system coefficients and relies solely on knowledge of the probability of particle interaction.

Due to the random sampling process, the reaction rates calculated are stochastic and therefore the solutions are probabilistic, in contrast to deterministic, thus having an associated statistical error.[63, 64, 65] Reducing the stochastic error involves modeling larger sample distributions to better account for the average behavior of particle interactions.[66] The need for larger sample sizes to secure adequate calculation precision generally causes the Monte Carlo method to execute slower than a typical deterministic calculation. In certain modeling scenarios, an investigator may wish to analyze a plethora of perturbations to a well understood benchmarked system of which the approximations applied within the deterministic solution method are valid or within the solution tolerance for analyzing the system. The deterministic method is more suited for this type of calculation because the gain in computational performance outweighs the accuracy penalty of which may be within the bounds of the solution tolerance. In other modeling scenarios, an investigator may wish to analyze a system that is not well understood and/or not benchmarked. For this type of calculation, the investigator may wish to compromise computational performance at the expense of enhancing solution accuracy. At the cost of computational performance, the lack of coefficient approximations, exactness in 3-dimensional modeling, and explicitness in angular tracking gives the Monte Carlo method a distinct advantage for this type of modeling scenario. The crux of each modeling technique will be detailed in the subsequent sections.

Deterministic Approach to Reaction Rate Calculations

The deterministic approach to reaction rate calculations involves solving the LBE by using a variety of assumptions to achieve a quick, reliable, spatially continuous reaction rate and neutron multiplication solution. The steady-state LBE is defined as equation 2-19:

$$\hat{\Omega} \bullet \nabla \psi(\vec{r}, \hat{\Omega}, E) + \sigma_t(\vec{r}, E)\psi(\vec{r}, \hat{\Omega}, E) =$$
$$\int d\hat{\Omega}' \int dE' \sigma_s(\vec{r}, \hat{\Omega}' \rightarrow \hat{\Omega}, E' \rightarrow E)\psi(\vec{r}, \hat{\Omega}', E') + \qquad (2\text{-}19)$$
$$\frac{1}{k}\frac{\chi(E)}{4\pi} \int dE' \nu(E')\sigma_f(\vec{r}, E') \int d\Omega' \psi_{g'}(\vec{r}, \hat{\Omega}', E')$$

Generally, this equation is discretized in energy, space, and angle, or an approximation for these dimensions is applied, in order to cast the equation in a deterministic solvable form. [63, 64, 65] The energy variable is discretized into few defined energy groups ultimately segregating equation 2-19 into a set of coupled differential equations, where the coupling of energy groups results from the out-group scatter and fission terms:

$$\hat{\Omega} \bullet \nabla \psi_g(\vec{r}, \hat{\Omega}) + \sigma_{t,g}(\vec{r})\psi_g(\vec{r}, \hat{\Omega}) =$$
$$\sum_{g'=1}^{G} \int d\hat{\Omega}' \sigma_{s,gg'}(\vec{r}, \hat{\Omega}' \rightarrow \hat{\Omega})\psi_{g'}(\vec{r}, \hat{\Omega}') + \frac{1}{k}\chi_g \sum_{g'=1}^{G} \nu\sigma_{f,g'}(\vec{r}) \int d\Omega' \psi_{g'}(\vec{r}, \hat{\Omega}') \qquad (2\text{-}20)$$

The angular dependence of equation 2-20 is accounted for by either discretizing the angular dependence into few angular quadratures, as in the discrete ordinates method, or by assuming isotropic scatter behavior and linear dependence of the angular flux, as in diffusion theory. [63, 64, 65, 67] After angular dependence is accounted for, the examined system geometry must be meshed into a fine grid or cast into a solvable ray tracing system. Reaction rate distributions are calculated within each mesh or along each ray by using assuming homogenized parameters within the mesh or along the ray and implementing the particle fluxes and currents of the neighboring meshes or rays as the boundary conditions for that specific mesh or ray solution. [63, 64, 65]

The mesh shapes or rays should be chosen so that a problem's geometry may be modeled explicitly, and the homogenizations within each of the shapes or rays do not upset the fidelity of the actual calculation. The ideal mesh or ray scheme would include thousands of tiny meshes or

rays so that connect in highly irregular geometries in order to explicitly model a complicated geometry. However, thousands of meshes would require thousands of angular flux at many angular quadratures and many energy groups which would ultimately exceed the memory of any computer. Irregular meshing schemes are available such as in the code Atilla; however, irregular shaped meshing schemes lead to a highly memory intensive bank of complicated algorithms utilized to find a flux solution for each irregular mesh scheme.[68] Assumptions must be employed on acceptable mesh size and shape so as not to violate the allotted computational memory restrictions. Therefore modeling of highly irregular complicated geometries must be approximated by simpler less precise models that may possibly affect the accuracy of the solution method. Ray tracing schemes such as that implemented in the method of characteristics (MOC) are capable of better accounting for complicated geometries by setting up a scheme that solves a solution at the explicit boundaries of a given geometry. The MOC method has been successfully applied for modeling complicated geometries.[69] However, the MOC method, like the discrete ordinates method, relies on approximation schemes to develop proper coefficients (i.e. interaction cross sections) in order to solve the deterministic form of the transport equation.

Within the Evaluated Nuclear Data Files (ENDF), exist infinite-dilute, energy dependant reaction rate probability, cross section, data.[70] This data functions as the coefficients for the transport equation. The data itself are stated at many energy points and therefore is not exactly "continuous" in energy, however since the magnitude of data points existing for a specific reaction is considered in fine enough fidelity to assume a continuous distribution, the data is deemed continuous. The ENDF data therefore represents a continuous function for each reaction type that is dependent upon impingent energy, and used as the coefficients in order to solve the transport equation. Parameters also exist for reconstructing complicated sections of the

coefficient function such as the resonances resulting from the eigenstates of the nucleus. The data are also stated to be infinitely dilute because it is assumed that reaction probabilities do not incur energy and spatial self-shielding. Figure 2-2 shows two separate distributions of flux in the vicinity of a cross section resonance. As compared to a 1/E distribution, the actual flux, Φ(E), will be depressed in the neighborhood of a cross section resonance peak. This effect is termed energy self-shielding since the large interaction probability of the resonance shields the isotope's nuclei from neutrons around the energy E0 leading to a flux depression. If the nuclei of interest is then further contained within a lump of similar nuclei and placed in the pathway of a beam of neutrons with energies in the vicinity of the resonance energy of those nuclei, the majority of neutrons will only interact with nuclei at the surface of the lump. This effect is termed spatial self shielding because the inner nuclei of that lump are spatially shielded by the nuclei at the surface of the lump.[2] In implementing a deterministic solution approach the reaction rate coefficients must be properly adjusted to adequately account for these types of self-shielding in order to properly model the true system physics.

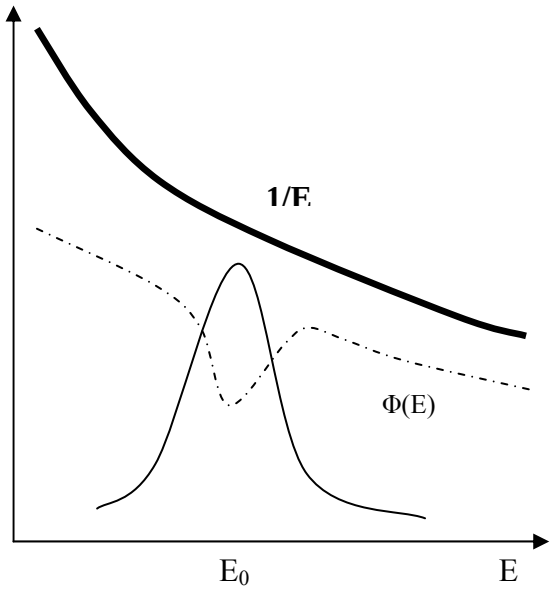

Figure 2-2. Flux depression in the neighborhood of a resonance at E_0.

Casting equation 2-19 into the multi-group form requires that multi-group coefficients be generated. The coefficients are generated based on the premise that the multi-group coefficients be a homogenized term that best represents the average behavior within a specified energy group. To preserve true system physics, the energy group averaged interaction rates are calculated dividing the energy integrated reaction rate, within a specific energy band, by the energy integrated flux within that same energy band as shown in equation 2-21:

$$\sigma(r)_g = \frac{\int_{E_g}^{E_{g-1}} \sigma(r,E)\Phi(r,E)dE}{\int_{E_g}^{E_{g-1}} \Phi(r,E)dE} \tag{2-21}$$

The concern with this approach is that the flux, the variable that is to be to calculated in equation 2-20, is used to calculate the cross section which is then utilized to calculate the flux in equation 2-20 making the process nonlinear. To make the process linear, an approximation is made in which first a homogenous, spatially-infinite, 1-D dimensional calculation is completed with the continuous energy ENDF cross sections. The flux solution from that calculation is then used to generate collapsed group energy self-shielded cross sections for a further multi-group calculation.[63, 64, 65]

Deciding which energy bands to use to compute the group average cross sections will highly affect the ultimate outcome of the further calculations that implement those cross sections. Ideally, a proper group structure, robust enough to be used for a wide class of calculations, would account for every major resonance of every single nuclide. Figure 2-3 displays the absorption cross sections for a few nuclides found in typical reactor calculations. Notice that each isotope contains many different resonances therefore requiring a large amount of groups to capture the true interaction rate behavior of the displayed isotopes. If the rest of the 389 isotopes

containing ENDF data are figured into the calculation, one may then see that an immense amount of energy groups is needed in order to model each resonance. Because the size of the group structure is one of the many parameters that dictate the needed memory allocation to solve a specific problem, in practice, the ideal approach is not viable because it is possible that thousands of energy groups would be necessary in order accurately capture the resonances of each available isotope. Therefore group structures are chosen that utilize as few groups as possible, in order to account for as many resonances as possible, to make the group structure small enough to be practical for an actual calculation.

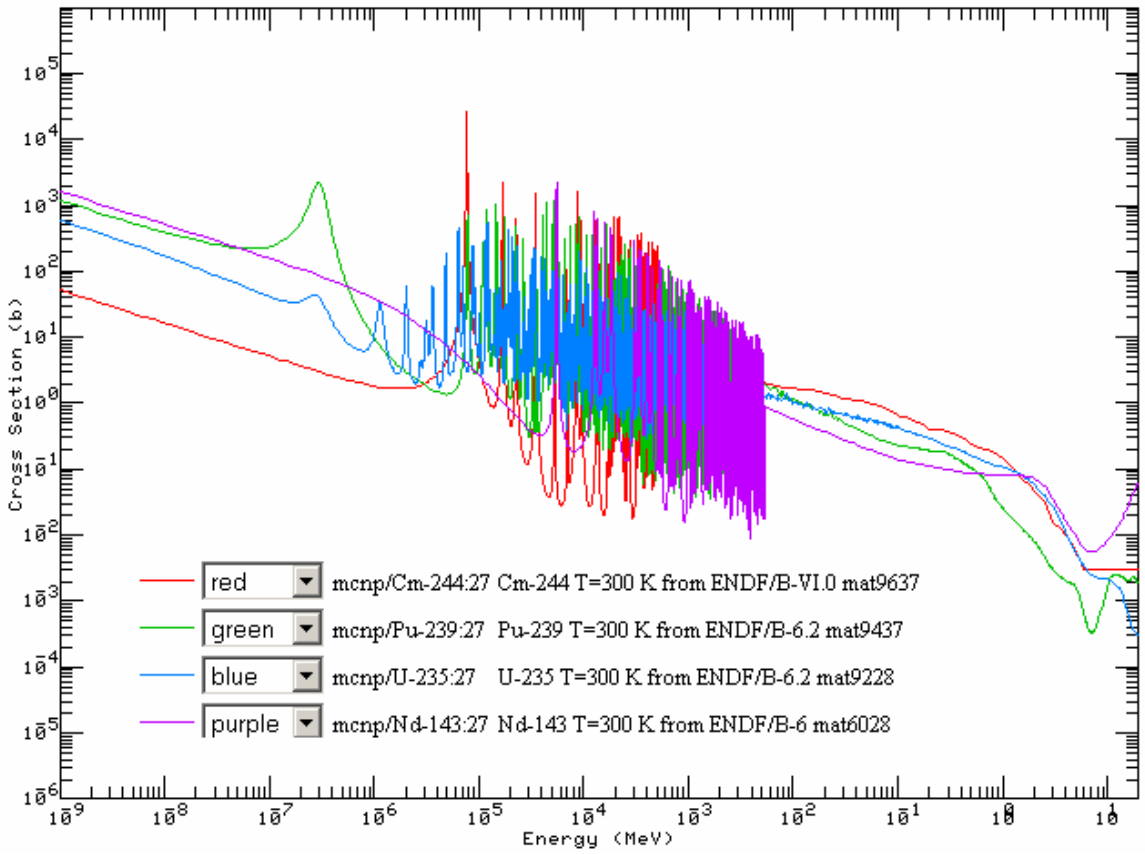

Figure 2-3. Flux depression in the neighborhood of a resonance at E_0.

Accurate group structures may be generated for classes of problems. For example, the nuclear power industry contains accurate multi-group cross section libraries for examining

reactors containing uranium-oxide fuel, with zircaloy clad, surrounded by water, and possibly controlled by born-carbide or hafnium.[25, 26, 30, 32] However, those libraries are not applicable for examining exotic isotope combinations such as uranium-nitride fueled, rhenium cladded and niobium-carbide coated space reactor designs.[71, 72] Furthermore, the nuclear industry is only successful in determining these libraries after years of comparing and tuning cross sections to operational data.

The implementer of a deterministic method is constantly burdened by the choice of appropriate approximations in order to achieve an accurate result. If chosen correctly the implementer will achieve a quick, reliable, non-stochastic, spatially continuous reaction rate and neutron multiplication solution that runs much faster than a Monte Carlo. However, the burden of these choices and the knowledge to make proper determinations of group structure and self-shielding accountability may be out of the experience base of the implementer or may not be possible with current memory restrictions, in which case a more robust tool exhibiting fewer approximations of system physics should be implemented.

Monte Carlo Approach to Reaction Rate Calculations

The Monte Carlo method uses probability theory to model a system stochastically by simulating the actual physical process through the random sampling of events. Like deterministic methods the Monte Carlo method seeks to solve the transport equation to determine the average behavior of the neutron population within a system; however, unlike deterministic methods the Monte Carlo method solves the transport equation in a probabilistic approach. The Monte Carlo method does not require clever simplifications and approximations to determine transport coefficients and model geometry in order to compute solutions of neutron behavior. In certain circumstances, simplifications and approximations employed by deterministic methods alter a calculation so significantly that accuracy of neutron behavioral characteristics is lost.

Since the Monte Carlo method does not rely on these simplifications and approximations of system physics, the method is highly robust and capable of modeling very complex systems.[36, 63]

Combinatorial geometry is used to build models for simulation within the Monte Carlo process.[50] Geometric shapes are represented by the combinations of basic surface types. The geometric shapes created from the combination of these surface types are called "cells". These cells contain homogenized information of isotope concentration and particle interaction behaviors. Most possible shapes/cells incurred in nuclear system design may be modeled as combinations of these basic surface types; therefore making it possible to explicitly model any type of geometry encountered. Particle position is tracked in reference to these cells and surfaces, and the particle track length and interaction behavior are determined from interaction characteristics within each of the encountered cells.[63, 64, 65]

A basic diagram of the Monte Carlo process is displayed in Figure 2-4. Initially, a particle of specified energy and direction enters a cell volume. The distance the particle travels within that cell volume is dependent upon the probability that the particle will have an interaction within the specified volume some distance into the volume. In the one-dimensional case, the probability that the particle interacts within a distance between point "a" and point "b" is determined from the representative probability density function (PDF), f(x), and calculated by equation 2-22:

$$\int_a^b f(x)dx = P\{a \le x \le b\} \tag{2-22}$$

The probability of an event clearly may not be less than 0. If x may be any real value between ∞ and -∞ the distribution may be normalized resulting in equation 2-23:

$$\int_{-\infty}^{\infty} f(x)dx = 1 \tag{2-23}$$

From this equation we can further derive the cumulative probability distribution function (CDF), F(x) in equation 2-24, which will be utilized to ultimately determine the actual length of particle travel:

$$\int_{-\infty}^{x} f(x)dx = F(x) = P\{x' \leq x\} \tag{2-24}$$

In order to then simulate the process of particle travel through the random sampling of events we set the cumulative distribution function equal to a random number, ξ, and invert the equation in order to compute a correlated path length of travel.

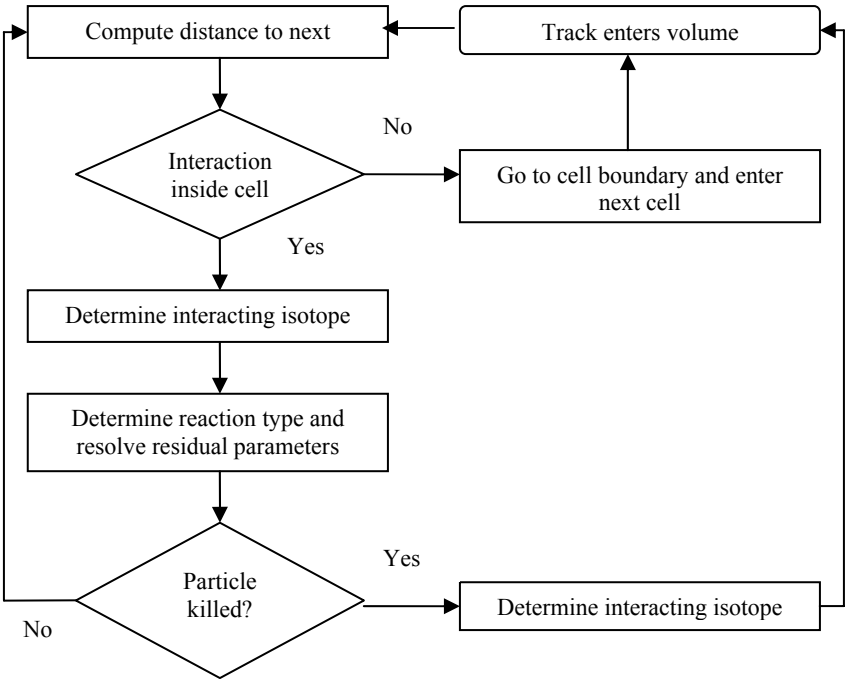

Figure 2-4. Flow diagram for the Monte Carlo particle transport process

If the calculation is in terms of mean free paths and $0 < x < \infty$, the PDF is

$$f(x) = e^{-x} \tag{2-25}$$

and the associated CDF is

$$F(x) = 1 - e^{-x} \tag{2-26}$$

Therefore, inverting the cumulative probability distribution function to solve for the mean free path results in

$$x = -\ln(1-\xi) \tag{2-27}$$

and if we choose ξ to be uniformly distributed between 0 and 1 we can further write

$$x = -\ln(\xi) \tag{2-28}$$

or in terms of track length, l, utilizing the individual isotope number density N_i and microscopic cross section total cross section, $\sigma(E)_{i,t}$

$$l = \frac{-\ln(\xi)}{\sum_i N_i \sigma(E)_{i,t}} \tag{2-29}$$

If a particle then interacts within a cell volume, then the isotope that the particle interacted with must be determined. The probability of a particle at specific energy, E, interacts with isotope *i* is simply the ratio of the number density of *i* multiplied by the total cross section of *i* to the sum of all the isotopes' number densities multiplied their associated total cross sections:

$$p(E)_i = \frac{N_i \sigma(E)_{i,t}}{\sum_i N_i \sigma(E)_{i,t}} \tag{2-30}$$

Then to sample the process from a random event, and assuming ξ to be randomly distributed between 0 and 1, isotope m is selected for interaction only if the following criterion is met:

$$\sum_{i=1}^{k-1} p(E)_i < \xi \sum_{i=1}^{N} p(E)_i \le \sum_{i=1}^{k} p(E)_i \tag{2-31}$$

After the interacting isotope is determined, the type of particle interaction incurred is sampled in a similar manner. First, the probability of incurred a specific reaction, *m*, is computed by [41]:

$$p(E)_{k,m} = \frac{\sigma(E)_{k,m}}{\sum_r \sigma(E)_{k,m}} \tag{2-32}$$

Then to sample the process from a random event, and assuming ξ to be randomly distributed between 0 and 1, isotope m is selected for interaction only if the following criterion is also met:

$$\sum_{i=1}^{m-1} p(E)_{k,i} < \xi \sum_{i=1}^{N} p(E)_{k,i} \leq \sum_{i=1}^{m} p(E)_{k,i} \tag{2-33}$$

After the interaction type is determined then subsequent residual nuclides/particles are determined and resulting energy and angular distributions are calculated.

Particles continue to move within the system until the particle is either absorbed or leaked from the system. A tallying estimator is used in order to retrieve particle information from the system such as reaction rates and fluxes.[63, 64, 65] The most basic Monte Carlo tally estimator is the collision estimator which tallies the amount of a specific collision within a cell volume. In order to calculate the average number of collisions in a volume, V, per unit time the following is used equation:

$$\bar{c} = \tilde{V}\tilde{\sigma}_c\bar{\phi} \tag{2-34}$$

For the Monte Carlo computation the flux may therefore be approximated by:

$$\bar{\phi} = \frac{\bar{c}}{\tilde{V}\tilde{\sigma}_c} \tag{2-35}$$

Where $\bar{\phi}$ is the average flux, $\tilde{\sigma}_c$ is the average macroscopic collision interaction cross section, and $\bar{c}$ is the mean number of collisions in a volume, $\tilde{V}$. If the calculation is normalized to per source particle then the collision estimator may be rewritten as:

$$\hat{\phi} = \frac{1}{\tilde{V}\tilde{\sigma}_c}\frac{1}{N}\sum_i c_i \tag{2-36}$$

A variation of collision estimator is the absorption estimator where the flux is now tallied not at every collision site but at each absorption site:

$$\hat{\phi} = \frac{1}{\widetilde{V}\widetilde{\sigma}_a}\frac{1}{N}\sum_i a_i \tag{2-37}$$

Both the collision and absorption estimators are dependent upon interactions taking place within a volume.[63, 64, 65]

Due to the stochastic nature of the Monte Carlo process, all quantities computed result in a stochastic error (standard error or relative error). The relative error is composed from the sample variance. The actual variance of the population is

$$\sigma^2 = \frac{\sum_{i=1}^{N}(x_i - \mu)^2}{N} \tag{2-39}$$

where μ is the actual population mean. Unfortunately, the actual population mean is almost never known, and therefore the sample mean, $\bar{x}$, is used to determine a sample variance. The x_i's tend to be closer to their average, $\bar{x}$, than to the population average, μ, resulting in estimated values that are too small on average, therefore a n-1 is used in the divisor to account for this underestimating. For a sample distribution, the sample variance of that distribution is calculated by equation 2-38:

$$S^2 = \frac{\sum(x_i - \bar{x})^2}{n-1} \tag{2-38}$$

With further mathematical simplification we derive[73]

$$\frac{\sum(x_i - \bar{x})^2}{n-1} = \frac{\sum(x_i^2 - 2\bar{x}\bullet x_i + \bar{x}^2)}{n-1} = \frac{\sum x_i^2 - 2\bar{x}\sum x_i + \sum \bar{x}^2}{n-1} = \frac{\sum x_i^2 - 2\bar{x}\bullet n x_i + n(\bar{x})^2}{n-1} =$$

$$\frac{\sum x_i^2 - \frac{(\sum x_i)^2}{n}}{n-1} \approx \overline{x^2} - \bar{x}^2 \tag{2-39}$$

The sample variance is referred to having n-1 degrees of freedom. This terminology results from the fact that although the sample variance is based on the n quantities, $(x_1 - \bar{x})$, $(x_2 - \bar{x})$, ..., $(x_n - \bar{x})$, these sum to 0, so specifying the values of any n-1 of the quantities determines the remaining value.[73] The Strong Law of Numbers states that if the true mean is finite then the sample tends to the true mean as the sample size approaches infinity.[66] Furthermore, examining equation 2-38 we see that increasing the sample size, n, decreases the sample variance. The variance of the sample mean is calculated to then be implemented in the calculation of the relative error[74]

$$S_{\bar{x}}^2 = \frac{S^2}{n} \rightarrow R = \frac{S_{\bar{x}}}{\bar{x}} = \frac{\sqrt{\frac{\overline{x^2} - \bar{x}^2}{n}}}{\bar{x}} = \sqrt{\frac{\frac{n^2 \sum x_i^2}{n\left(\sum x_i\right)^2} - 1}{n}} = \sqrt{\frac{\sum x_i^2}{\left(\sum x_i\right)^2} - \frac{1}{n}} \tag{2-40}$$

Because the relative error implements the sample mean variance, increasing the sample size further decreases the relative error of the calculation. A major shortcoming of the collision and absorption estimators is that reliable estimates of the flux, and thus interaction rates, may only be computed if many collisions/absorptions occur within tallied cell volume. For cell volumes containing minimal amount of collisions/ absorptions the relative error for calculated quantities will be high and thus leading to a lack of confidence in the computed quantity.

The track length estimator is another type of Monte Carlo estimator that does not incur the mentioned shortcoming. The track length estimator utilizes the particle's average track length, l, within a specified cell volume to tally flux, and therefore relies of particles passing through a specific cell volume and not if the particle happens to interact within the cell volume. The particle density is equated to the scalar flux by

$$\Phi(\vec{r}, E, t)dVdEdt = vN(\vec{r}, E, t)dVdEdt \tag{2-41}$$

Since a particle with travel a distance vdt during the time increment dt, the scalar flux may be thought of as the total of the path lengths traveled during dt by all particles in the phase space volume of dVdE.[63] The scalar flux may therefore be defined as the total track length traversed by particles within a specified volume

$$\bar{\phi} = \frac{\bar{l}}{\tilde{V}} \tag{2-42}$$

where $\bar{l}$ is the average track length per unit time a particle traverses in volume, $\tilde{V}$. In a Monte Carlo simulation utilizing N particles the track length estimator of the flux may be calculated by:

$$\hat{\phi} = \frac{1}{\tilde{V}} \frac{1}{N} \sum_n l_n \tag{2-43}$$

Because the track length estimator of the flux relies only upon tracks entering a volume, more particles contribute to the calculation of the relative error and therefore computing reaction rates with lower relative error is easier with this flux estimator.[63]

Monte Carlo applied to neutron transport may make two distinct types of calculations: fixed source and criticality. A fixed source calculation involves following a preset amount of particles from a source, given by the user, until the particles are killed. Criticality calculations, however, determine the effective neutron multiplication of a system by constantly changing the geometric source distribution of neutrons for subsequent neutron cycles and following each neutron till it is killed in an inelastic reaction, scattered below the weight threshold, or leaked from the system and then determining if the way in which the neutron was killed resulted in production of new neutrons. Many cycles of source distributions are analyzed in order to converge on a source distribution that is truly representative of the analyzed system so that an accurate characterization of the neutron multiplication may be computed.[50]

For a criticality the total amount of particles examined in the computation may be broken up into the particles distributed per cycle and the total number of cycles examined. Initially the user inputs a guess at the source distribution of particles. These particles then transport and are eventually killed by an inelastic event, scattered below a weight threshold, or leaked from the system. The absorption sites containing fissile nuclides that lead to fission then become the birth sites for the next set of particles in the subsequent cycle. At each absorption site containing a fissile nuclide, the amount of neutrons produced per fission is determined. The amount of neutrons created per source neutron examined represents the multiplication of the system or k_{eff}. If the system is a self sustaining critical system, for each source neutron lost from the system and additional neutron is created for the next cycle. The multiplication of the system is a global parameter and therefore k_{eff} is used to explain the entire global system.

Similar to the mentioned tallying process, three estimators exist for determining criticality. Each estimator involves multiplying the flux estimator by a response function, h, to determine the system multiplication:[74]

$$h = \sum_i \widetilde{\sigma}_{i,n,f}(E)\upsilon_{i,n}(E) \tag{2-44}$$

$\widetilde{\sigma}_{i,n,f}(E)$ is the macroscopic fission cross section of isotope i at energy E, and $\upsilon_i(E)$ is the total number of neutrons per fission of fissile isotope i. The collision and track length estimators are tallied from interactions with each isotope i in all volumes n, by:[74]

$$k_{eff}^{c} = \frac{1}{N}\sum_n c_n \sum_i \frac{\widetilde{\sigma}_{i,n,f}(E)\upsilon_{i,n}(E)}{\widetilde{\sigma}_{i,n,c}(E)} \tag{2-45}$$

$$k_{eff}^{l} = \frac{1}{N}\sum_n l_n \sum_i \widetilde{\sigma}_{i,n,f}(E)\upsilon_{i,n}(E) \tag{2-46}$$

The absorption criticality estimator is computed slightly different form the absorption flux estimator in that only absorptions in fissionable nuclides are tallied

$$k_{eff}^{a} = \frac{1}{N}\sum_{n} c_n \sum_{i} \frac{\widetilde{\sigma}_{i,n,f}(E)\upsilon_{i,n}(E)}{\widetilde{\sigma}_{i,n,a}(E)} \tag{2-47}$$

All three estimators (similar to the flux estimators) rely on large sample sizes and large numbers of hits (i.e. collision/absorptions/number of entering tracks) in order to decrease the relative error of the computation to have high confidence in the accuracy of the computed quantity. Therefore, unfortunately, decreasing the relative error of the calculation is directly correlated with increasing the associated computational cost of increasing the sample size to be followed. Historically, the Monte Carlo method has been used only as a benchmarking technique because of the computational cost associated with large sample sizes. Deterministic codes generally calculate results much faster than Monte Carlo codes. However, as core designers start to examine more advanced technologies that exhibit behavior that violates the validity of the assumptions of the current deterministic methodologies, a method that captures the true systems physics accurately becomes vital in order to effectively characterize system properties.

Current Capabilities and Methods of State of the Art Depletion Codes

Many depletion codes exist in industry and academia for the purpose of determining temporal nuclide inventories and reaction rate distributions.[35] These codes are either externally linked or sequential build technologies that contain a set of constraints used for determining which depletion and transport coefficients to track and calculate. Depending upon the investigated system, more or less detail in the solution method may be invoked in order to achieve an acceptable characterization. The level of acceptable characterization may be dependent on the validity of the benchmarking for the applied method or the actual level of

fidelity necessary to achieve proper knowledge for further design consideration. As many calculations are required in order to license a reactor core, codes utilized by the nuclear power industry for continual fuel cycle design of heavily benchmarked systems may employ many approximations in order to achieve quick reliable results within the timeframe deadline allotted by a particular customer.[9] These assumptions are acceptable based on the premise that the benchmarking of the system covers the design application space in which the code is implemented. On the other hand, codes utilized for the development of radically new system designs, incorporating a wide variety of unique material and geometry combinations that are not heavily benchmarked, may implement a higher fidelity of detail in the solution method employing few if any approximations.

Implementation Architecture

The main focus of most industry-based depletion codes is to support the operation and fuel cycle design of commercial power reactors. Industry-based codes usually focus on streamline manufacturing of heavily benchmarked systems that push the limiting design constraints to maximize returnable profit.[35] These types of systems involve many optimization iterations of common heavily benchmarked technologies. Only broad, generalized parameters are required to meet limiting conditions of operation (i.e. eigenvalue, power density, and linear heat generation rate) for most commercial reactor designs. Therefore, because the calculation tools are heavily benchmarked, the design requirements are broad, and the designer must complete the final design analysis within a short prescribed time period, most of the current licensed industry codes employ deterministic-linked depletion methodologies.[35]

Although various companies, such as Westinghouse, General Electric, Areva, and Studsvick, use slightly different techniques to approximate time-dependent reactor behavior, the overall methodology and processes are quite similar. First, a fine-fidelity deterministic

calculation (using PHOENIX, TGBLA, CASMO-3, etc.) examining many axial and radial slices of the reactor are completed to generate coarser 1- to 4- group-averaged interaction rate parameters for implementation in a coarser calculation of the full-core geometry (using ANC, PANACEA, PRISM, etc.).[35] However, due to the limitations of the deterministic method, these methodologies are only valid within the design space that they have been benchmarked for. Further analysis in group structure and cross section self-shielding is required in order to attempt to apply the tools to more exotic applications. These codes choose to follow a predetermined subset of reaction rates for the transport calculation, and further propagate a subset of fission products to be followed during the depletion calculation. Certain reaction rates may not be of importance to specific reactor designs or may only contribute within the noise of an acceptable solution. Omitting these unnecessary reaction rates results in extra available memory as well as minimizing computation cost. For most industry based codes major fission products such as the Sm and Xe isotopes may be followed explicitly while the buildup of minor reactivity contributors may be grouped into a lumped fission product set.[2, 25, 29, 31, 32] The advantage to fission product lumping is that fewer fission products are followed in the transport process leading to a speedup in computation. The fission product lumps are, however, geometry and spectrum dependant, and therefore though one type of fission product lump may be acceptable for a certain type of system, that same fission product lump may be acceptable for a different system. The combination of the acceptability of the transport method solution (i.e. energy group structure, angular dependence, and geometric approximation), the reaction rates followed, and the fission products tracked limits the application space for most industry based depletion codes.

These codes are usually only valid for the specific systems for which the codes were originally developed. For example, a multi-group code developed for and LWR with certain

group structure, fission products, and reactions followed will not be accurate in determining individual gamma-line signatures of fast reactor fission products for implementation in detector signal segregation. However, that same code is very capable of determining an adequate neutron multiplication and power shape calculation for licensing the reactor for operation.

Academia-based codes generally are developed for finer fidelity design of a robust variety of nuclear systems that are not heavily benchmarked. These codes must implement as few assumptions as possible in order to achieve an accurate result. The types of analysis for these systems involve understanding more precisely the sensitivity of certain parameters within the design making a higher-fidelity methodology, the design tool of choice. In general, deterministic codes developed in academia implement fewer angular approximations [i.e., discrete ordinance transport theory (XSDRNPM) versus diffusion theory], implementing a higher degree of examined dimensions (i.e., 3D versus 2D), and/or using a finer-energy or continuous group structure.[35] Even though higher fidelity deterministic technologies exist to address concerns of angular dependence, by nature of the process, these technologies still suffer from the burden of proper group structure generation and flux self-shielding considerations.

To eliminate dependence from this burden, burnup codes coupling the Monte Carlo reaction rate calculation have received more attention.[36-41,46-48,75] However, due to the long computation times required to execute a detailed high fidelity calculation, these codes have had limiting success in implementation for commercial reactor design processes. To overcome this issue, users would have to consider utilizing longer irradiation steps, with larger spatial zones, following fewer nuclides, and fewer interaction rates per nuclides. An unfortunate example of this issue is exemplified in the MCODE.[39] In the MCODE only isotopes specified by the user are followed in the transmutation process, and only (n,γ) and (n,f) energy integrated reaction

rates are calculated for each nuclide. This simplification neglects key (n,α) reactions as witnessed in the depletion of boron-10. Further acceleration techniques for Monte Carlo may include using multi-group Monte Carlo such as in Keno Va.[76] Multi-group Monte Carlo speeds up the search algorithm when determining and energy dependent cross section at an interaction site because far less energy groups need be queried. However, the limitation of the multi-group approach is ultimately the validity of the group structure to a specific calculation. Implementing approximations to a Monte Carlo linked capability, unfortunately, reduces the robustness of the technology; therefore to take advantage of the explicitness of the Monte Carlo process, computational cost will have to be sacrificed.

All linked depletion methodologies suffer from how the linking process affects the functionality of both codes. For example, MONTEBURNS links MCNPX/5 with ORIGEN2.2 for high fidelity depletion calculations. MCNPX/5 is capable of tracking ~393 isotopes for particle transport and ORIGEN2.2 is capable of tracking 1700 nuclides for transmutation. MONTEBURNS only chooses to follow a small subset of isotopes for particle transport determined by specific reactivity criteria, and is not capable of following multiple isotope transmutations at multiple temperatures.[75] Other features within MCNPX/5 or ORIGEN2.2 are also not compatible with the MONTEBURNS implication as the code was not developed for these purposes. Many other linked technologies suffer from this same deficiency. All linked methodologies suffer the added external input structure necessary to execute the coupling. For example, the SCALE package successfully preserves the functionality of each code by implementing each package as a separate module and using a driver code to execute link each module however, the driver inputs are limited to certain setups and therefore though each code is run as a separate module, the linking input still limits the user to a specific implementation.[77]

Specific features of code mechanics that enable the user larger flexibility might be ignored in the linking process such as: operating in parallel execution and continuing a stopped execution.

All externally linked technologies suffer from the fact that the directory structure of the linked package must be coordinated with the setup of each of the technologies to be linked, and only the functionality of the linked code is supported by the developer of the linking process. For example, ORIGEN is supported by Oak Ridge National Laboratory, MCNP is supported by Los Alamos National Laboratory, and MCWO, a script linking MCNP and ORIGEN, is supported by Idaho National Laboratory; however, MCWO does not support development of ORIGEN or MCNP.[41] Therefore if a user of MCWO finds a particle transport error in MCNP or a transmutation limitation in ORIGEN, developers of MCWO are not responsible or able to support fixes of these independent codes. Codes like the SCALE package benefit from the fact that each code used for calculation is supported by the same organization.[76, 77] Therefore an optimum multi-purpose depletion package is a code system that minimizes approximations in the transport, depletion and linking calculations, supports development of all codes implemented in the solution method and maintains full functionality and benefit of each code used in the calculation.

Nuclide Inventory Limitations/ Calculation Size Considerations

The goal in designing any nuclear system is to determine the minimum amount of incurred cost necessary in order to achieve the power and cycle requirements while still meeting safety margin considerations.[78] To determine these limiting conditions of operation only broad generalized parameters are required (i.e., eigenvalue, power density, linear heat generation rate, and shutdown margin). Hundreds of combinations of loading and control strategies incurring many design iterations are examined in order to meet limiting design criteria. Therefore in order

to reduce the computational modeling expense approximations of larger system behavior must be made.

To model an entire commercial power reactor core explicitly, capturing the exact interaction rate behavior of every single microscopic section of every single material in the system, would be an extremely memory restrictive. Considering that the power distribution varies continuously in the radial and axial directions, reactor designers are forced to make approximations in order to discretize the full depletion model so that it may be solved. Within each discretization, reaction rates for each isotope of interested must be computed and stored for implementation into the time-dependent isotope concentration calculator. For finer discretizations, larger memory requirements and increased computational costs are incurred.[62]

For cases that are not concerned with microscopic phenomenon, instead of trying to simulate an entire system explicitly, detail of a systems behavior may be resolved from examining the large system as composed of average models of explicit sections of the reactor. Many calculations of explicit sections of the larger reactor model are completed and major interaction parameters are collapsed into an average set representing the explicit microscopic section. Then these average sets of parameters are implemented into a courser representation of the full system leading to a final computation that does not require as much explicit detail and therefore reducing memory restriction and enhancing computational incentive.

Currently in the commercial power industry, reactor physics computations are bifurcated into two separate processes. First, a multi-group or stochastic calculation (using MCNP, PHOENIX, TGBLA, CASMO-3, etc.) is completed on a fuel bundle at certain axial zones to generate collapsed interaction parameters. Then those generated collapsed interaction parameters are implemented in a full-core simulator tool (using ANC, PANACEA, PRISM, etc).[35] The

advantage to this process is the speed up in computation; however, the major fault is that the legitimacy of the process now rests upon the validity of the chosen discretizations and averaged parameters that are generated from the finer explicit micro-section calculations, and the fidelity to determine microscopic behavior of interest is now lost in the averaging process.[35]

The most robust, optimum design tool must allow the user the option to examine different sizes of possible geometric averaging techniques as well as the capability to eliminate them entirely. Due to the robust modeling capability of combinatorial geometry, Monte Carlo codes are capable easily modeling both intricate explicit models of the entire system as well as courser representations implementing large blocks of common materials that incur decreased computational expense. Since the Monte Carlo method employs few, if any, assumptions of system physics, collapsed average interaction parameters generated by the code may be secured to be of highest fidelity. This makes utilizing Monte Carlo for either group constant generation or full core modeling the optimum robust linked depletion tool.

CHAPTER 3
METHODOLOGY DEVELOPMENT

A driver program is required in order to structure the execution of coupled algorithms within coupled process. The MCNPX code serves as the driver program for the coupled depletion process. MCNPX was chosen as the driver program because the code is already a large scale multi-purpose particle transport package. The MCNPX code package contains ~1000 subroutines with each subroutine containing hundreds of execution lines. The CINDER90 depletion algorithm is placed within the MCNPX code package, and an interface subroutine sets CINDER90 inputs and retrieves CINDER90 outputs. The other 29 implemented subroutines execute various assignments in order to properly average data, set parameters for implementation in the CINDER90 depletion algorithm, reconstruct atom density information for subsequent particle transport calculations, retrieve input information for problem set up or to construct output. The coupled deletion process involves a Monte Carlo (MCNPX) steady-state reaction rate calculation linked to a deterministic depletion calculation (CINDER90). The whole process resides in roughly 30 subroutines in the MCNPX code (five new subroutines and 25 augmented subroutines). The linking process is displayed in Figure 3-1. MCNPX runs a steady-state calculation to determine the system eigenvalue, 63-group fluxes, collision rates, ν, and Q values. CINDER90 then takes those MCNPX-generated values and carries out the depletion calculation to generate new number densities at the following time step. MCNPX then takes those new number densities and generates another set of fluxes and reaction rates; the process repeats itself until after the final time step.[79] The MCNPX linked depletion architecture requires important decisions regarding isotope tracking philosophy and methods, calculation of depletion equation coefficients, time-dependant cross section averaging techniques, and the implementation architecture.[79] Chapter 3 details the development and implementation of these philosophies

within the MCNPX depletion methodology and offers key important considerations to account for in the development similar technologies.

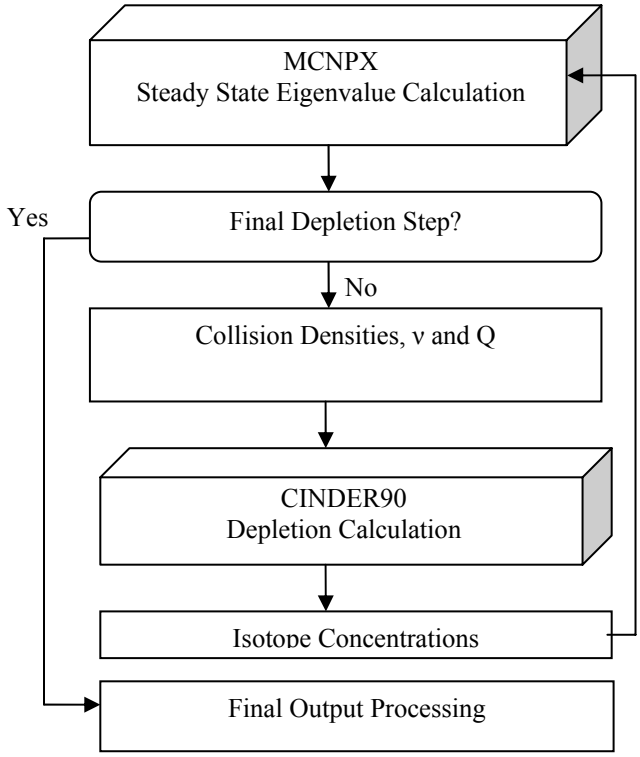

Figure 3-1. Monte-Carlo-linked depletion process model.

Approach to Isotope Tracking

MCNPX depletion burns a system by specified burn material instead of by individual cell location.[78] This technique was employed in order to take advantage of repeated structure geometry simplifications already available in the MCNPX geometry build subroutines that help decrease the size of necessary input in order to burn an entire system.[50] The trade off in taking advantage of this input simplification is that the user must be aware that unique materials are required for each burn cell containing a unique power profile. However, the advantage of this capability eases the burden in modeling complicated geometries.

MCNPX depletion requires that each burn material contain all isotopes to be generated within that material at the beginning of the computation. This therefore requires that the code

determine all fission and activation products upfront as well as particle interaction data to be used in the depletion process. As mentioned previously, the depletion process is bifurcated into two separate processes: steady-state particle transport and isotope transmutation. Particle reaction data for use in the particle transport calculation is available from direct experiment via evaluated data library sets. These evaluated library sets include ENDF, JEF, JENDL, BROND, CENDL, etc. Because most of the evaluated library data sets include reaction information from experiment, ability to execute and retrieve data from experiments limits the amount of isotopes that actually posses evaluated library transport information. For example, generating an experiment to measure interaction rate data from a radioactive isotope with a very short half-life may not be possible and therefore the evaluated nuclear data files will usually not contain transport information for such an isotope. The current ENDF/B VII.0 library only contains actual transport cross sections for 393 isotopes, and therefore, without an analytical or empirical model, a maximum of 393 isotopes may be tracked in particle transport.[80] Unfortunately, the actual transmutation process has the possibility of generating 3400 isotopes. Though there exists measured decay data for most of these nuclides, interaction rate data does not exist. CINDER90 is capable of tracking 3400 isotopes in the transmutation process; however, transmutation rates are required in order to complete the calculation.[61] These transmutation rates will only have spatial dependence if determined from the steady-state reaction rate calculation. However, if continuous energy cross section data does not exist for a specific nuclide, that nuclide cannot be employed in the steady-state reaction rate calculation. For nuclides not containing tabulated transport cross sections in the MCNPX data library, MCNPX does have the capability to use a theoretical model to generate a cross section for that specific isotope; however, this capability was benchmarked for > 150 MeV particle interactions, which is well above the energy regime for

the majority of particle interactions incurring in a reactor, and therefore not a safe technique to be implemented in reactor calculations.[79]

CINDER90 does contain 63-group transmutation rate information for 3400 nuclides.[61] The majority of this data, not derived from evaluated library files, was generated from analytical cross section modeling codes or by expert best estimates. Therefore MCNPX applies a mix and match method for transmutation rates in which if there exists and evaluated library transport cross section for a nuclide for use in MCNPX, then the reaction rate information from that nuclide is calculated directly within MCNPX and sent to CINDER90 as a transmutation coefficient. For all other nuclides, a 63-group spatially dependent flux is calculated within MCNPX and sent to CINDER90 to be match with a 63-group cross section sets available in the CINDER90 data library file, where that cross section set most probably was derived from an analytical model or expert best estimate, to be integrated into a transmutation coefficients for use in the depletion equation.[79] To save computation time and reduce the influx of memory-prohibitive information, MCNPX only tracks those isotopes accounted for from the following processes:

1. Listing the isotope on a material card.
2. Selecting an isotope from a preset fission product tier.
3. Producing the isotope from the Isotope Generator Algorithm.

CINDER90 still tracks all of the daughter/granddaughter/great-granddaughter/etc. decay reactions for 3400 isotopes; therefore, the total isotope concentrations listed in MCNPX are the true concentrations from the full depletion process.

Fission Product Tiers

Executing a successful depletion calculation involves accounting for the reactivity effects of as many fission products as possible. In most cases, a fission event will result in the creation of two-to-three fission products with a total mass that sums to less than the mass of the original

isotope. The creation of the fission product isotopes is probabilistic in nature and follows a distribution. Figure 3-2 displays the fission product distribution for U-235 for thermal and 14 MeV fission reactions. Hundreds of fission product isotope yield combinations are possible for a given fission event from a specific isotope. Each fissionable isotope also contains different yield distributions. Figure 3-3 shows fission product yield distribution for certain pluotonium and uranium isotopes. CINDER90 contains energy dependent fission product yield data for 1325 different fission products.[61]

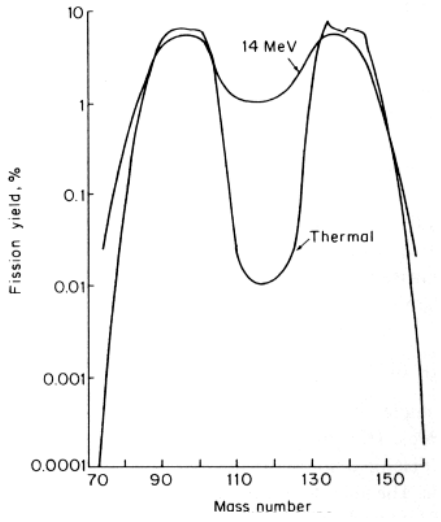

Figure 3-2. Uranium-235 fission product yield distribution.[7]

Due to the nature of the Monte Carlo process, increasing the amount of isotopes tracked in a problem increases the associated computational cost. When a particle interacts within a specified cell volume, a calculation must be run to sample which isotope within that material the particle interacted with. This sampling is dependant upon individual isotope atom density, interaction cross section, and total amount of isotopes within that given cell. Increasing the amount of isotopes, increases the overall associated computational cost. However, not tracking certain fission products within a calculation leads to altered neutron spectrum ultimately leading to inadequate estimation of system reactivity and inaccurate representation of true system

physics. Therefore determining an adequate combination of fission products necessary to sufficiently account for the system physics becomes paramount in achieving an accurate depletion calculation.

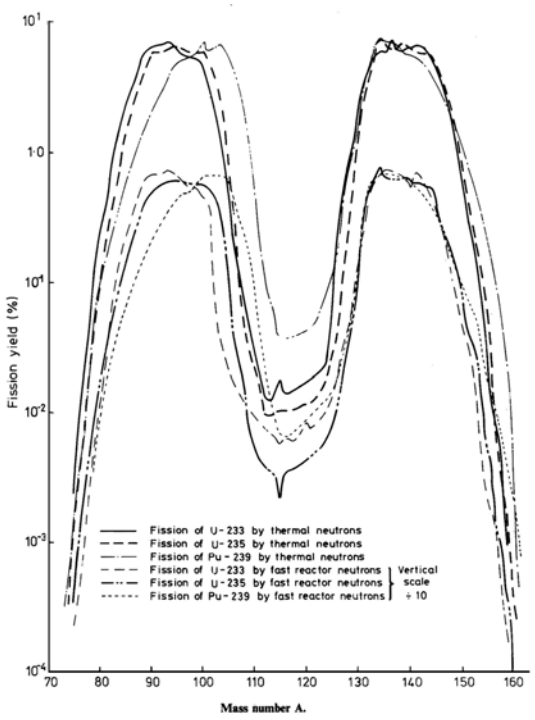

Figure 3-3. Fission Yield Distributions for Various Plutonium and Uranium Isotopes.[81]

Many options exist for determining how the user accounts for the generation of fission products within a calculation. The user could be forced to list, on an input deck, all the fission products that were of interest. This would require that the user had prior knowledge of all the fission products generated during the fission process that contained useful transport cross section information. Inputting every single fission product of interest, in all burn material would be a very cumbersome task. MCNPX offers the user preset fission product "tiers", which are subsets of a preset fission product array. By using preset fission product tier sets, the cumbersome and tedious task of cataloguing every fission product on an input file is eliminated.[82] The user then can omit certain isotopes from the fission product tier if necessary. Three tiers of fission product

content are available. Each tier corresponds only to those isotopes that are used for particle transport in MCNPX and the nuclide densities that are reported in the following output file. In MCNPX 2.6.A the fission product array contained 167 fission products, listed in Figure 3-4, with the following fission product tiers:[79]

1. Tier 1. (default) Zr-93, Mo-95, Tc-99m, Ru-101, Xe-131, Xe-134, Cs-133, Cs-137, Ba-138, Pr-141, Nd-143, Nd-145.9

2. Tier 2. Isotopes contained in the fission product array that are included in the released cross-section library file (XSDIR) for MCNPX.

3. Tier 3. All isotopes contained in the fission product array.

```
32072,32073,32074,32076,33075,34077,34079,34080,34082,35081,
36082,36083,36084,36085,36086,37085,37086,37087,38086,38088,
38089,38090,39089,39090,39091,40090,40091,40092,40093,40094,
40095,40096,41095,41097,42095,42096,42097,42098,42099,42100,
43099,44100,44101,44102,44103,44104,44105,44106,45103,45105,
46104,46105,46106,46107,46108,46110,47109,47111,48110,48111,
48112,48113,48114,48116,49115,50116,50117,50118,50119,50120,
50122,50123,50124,50125,50126,51121,51123,51124,51125,51126,
52122,52124,52125,52126,52128,52130,52132,53127,53129,53130,
53131,53132,53133,53134,53135,54128,54129,54130,54131,54132,
54133,54134,54135,54136,55133,55134,55135,55136,55137,56134,
56136,56137,56138,56140,57139,57140,58140,58141,58142,58143,
58144,59141,59142,59143,59145,60142,60143,60144,60145,60146,
60147,60148,60150,61147,61148,61149,61151,62147,62148,62149,
62150,62151,62152,62153,62154,63151,63152,63153,63154,63155,
63156,63157,64152,64154,64155,64156,64157,64158,64160,65159,
65160,66160,66161,66162,01003,05010,05011
```

Figure 3-4. Original fission product array containing 167 fission products.

Preliminary testing of a typical PWR pin cell calculation utilizing the fission product tiers in MCNPX as compared to the benchmarked MONTEBURNS depletion code suggested that utilizing the maximum amount fission products increased the agreement between the two codes.[81] For preliminary analysis purposes, comparing MCNPX depletion and MONTEBURNS was deemed acceptable for determining "ballpark" estimates of appropriate functionality because MONTEBURNS was also a Monte Carlo linked technology that has been thoroughly benchmarked.[74, 83] Figure 3-5 displays the difference in neutron multiplication versus time and Figure 3-6 and Figure 3-7 display the difference in end-of-life fission product buildup when comparing the varied fission product tiers to the benchmarked MONTEBURNS method.

Analysis with MCNPX 2.6.A suggested that increasing the amount of fission products followed in the calculation, increased the agreement between MCNPX and MONTEBURNS.[82] With the release of ENDF/B VII.0, it was determined that every fission product containing transport cross sections should be included in the fission product array, increasing the array to account for 220 fission products.[84] Each fission product tier continued followed the same criteria as previously implemented. The fission products included in the current 220 fission product array are listed in Figure 3-8.[84]

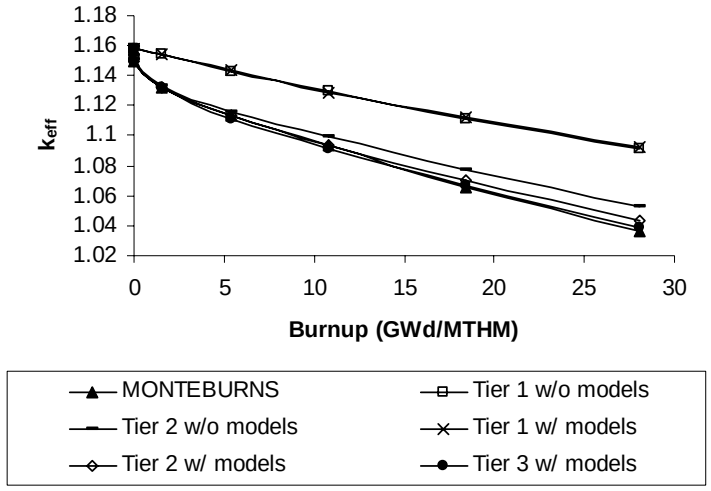

Figure 3-5. Resulting time-dependent neutron multiplication from implementing fission products with and without cross section models in MCNPX as compared to the benchmarked MONTEBURNS method.

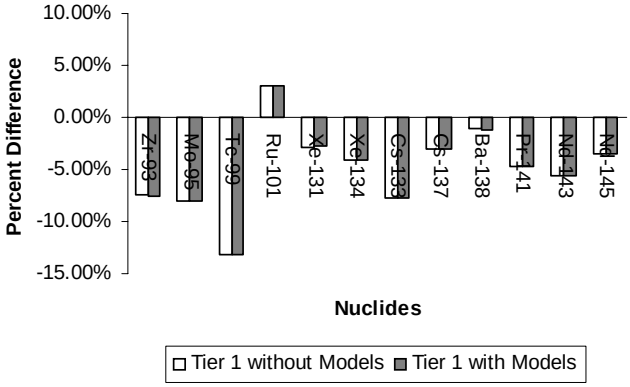

Figure 3-6. Percent difference of certain fission products from MONTEBURNS using MCNPX Tier-1 fission products with and without cross section models.

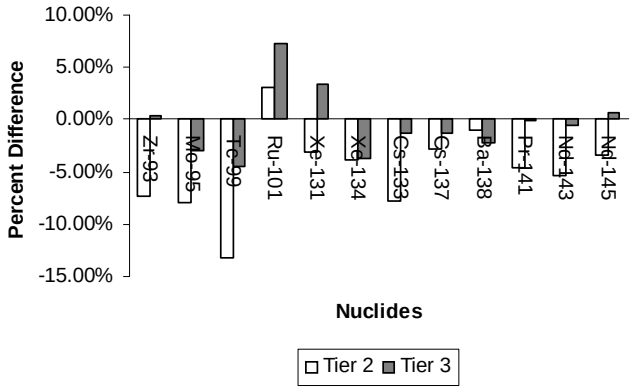

Figure 3-7. Percent difference of certain fission products from MONTEBURNS using MCNPX Tier-2 and Tier-3 fission products with cross-section models.

```
31069,31071,32070,32072,32073,32074,32076,33074,33075,34074,
34076,34077,34078,34079,34080,34082,35079,35081,36078,36080,
36082,36083,36084,36085,36086,37085,37086,37087,38084,38086,
38087,38088,38089,38090,39088,39089,39090,39091,40090,40091,
40092,40093,40094,40095,40096,41093,41094,41095,41097,42092,
42094,42095,42096,42097,42098,42099,42100,43099,44096,44098,
44099,44100,44101,44102,44103,44104,44105,44106,45103,45105,
46102,46104,46105,46106,46107,46108,46110,47107,47109,47111,
48106,48108,48110,48111,48112,48113,48114,48116,49113,49115,
50112,50113,50114,50115,50116,50117,50118,50119,50120,50122,
50123,50124,50125,50126,51121,51123,51124,51125,51126,52120,
52122,52123,52124,52125,52126,52128,52130,52132,53127,53129,
53130,53131,53132,53133,53134,53135,54123,54124,54126,54128,
54129,54130,54131,54132,54133,54134,54135,54136,55133,55134,
55135,55136,55137,56130,56132,56133,56134,56135,56136,56137,
56138,56140,57138,57139,57140,58136,58138,58139,58140,58141,
58142,58143,58144,59141,59142,59143,59145,60142,60143,60144,
60145,60146,60147,60148,60150,61147,61148,61149,61151,62144,
62147,62148,62149,62150,62151,62152,62153,62154,63151,63152,
63153,63154,63155,63156,63157,64152,64153,64154,64155,64156,
64157,64158,64160,65159,65160,66156,66158,66160,66161,66162,
66163,66164,67165,68162,68164,68166,68167,68168,68170,69169
```

Figure 3-8. Enhanced fission product array containing 220 isotopes.

Isotope Generator Algorithm

Storing every decay chain for every possible combination of isotope listed on a burn material card would be extraordinarily memory prohibitive and would greatly slow down the speed of the code. To limit memory consumption and computational cost, only the immediate daughter products from isotopes specified within selected burn materials are tracked in MCNPX for particle transport.[85] These immediate daughter reactions are determined by the Isotope

Generator Algorithm. The algorithm places all possible daughter products, from either reaction or decay, within a burn material card at an atom density of 1E-36.

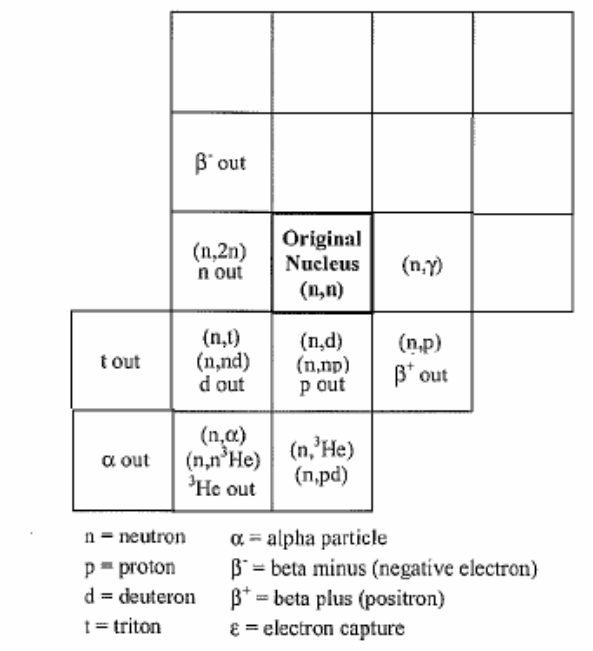

Figure 3-9. Nuclides created from a decay or nuclear reaction process and generated for particle transport by the isotope generator algorithm.[3]

Since the isotopes tracked within the MCNPX steady-state must be determined at the initiation of the entire calculation, specifying the isotope at a super low atom density secures the inclusion of the isotope in the calculation while not incurring an artificial reactivity penalty. Figure 3-9 displays the isotopes generated for a nuclide with $Z > 4$. The location of each generated isotope corresponds to the position of that isotope as it would appear in the Chart of the Nuclides.[3] Each box contains information regarding the interaction or decay process that leads to the creation of that isotope. Blank boxes represent possible decay chain isotopes resulting from multi-interaction processes or from other particle interactions (this is a result of the possible future application of utilizing the code to look at high energy particle interactions in accelerators and solar flares).

Manual Time-Dependent Isotope Concentration Changes

To model real life depletion systems, isotopes may have to added or extracted in order to meet the conditions of the operating strategies. For example, in a PWR, boron must be diluted as fuel is depleted in order to maintain criticality. For another example, in a gaseous fuel or molten salt reactor fission products may need to be extracted continuously in order to maintain system criticality. Certain depletion codes only allow the user to manipulate concentrations of isotopes used to maintain criticality in LWRs such as diluting boron concentration. MCNPX is a general purpose modeling code used to model all types of reactors. For the modeling capability to truly be robust, the user must be able to manually manipulate the concentration of any nuclide during the execution of the depletion process in order to properly model the true system behavior.

MCNPX depletion process allows for the user to manually manipulate the concentration of any isotope within any burned material at any time step. The user invokes this capability by use of the MATMOD keyword on the BURN card (input specification, input structure, cards and keywords are explained in the Input Interface section).[86] The user is able to manipulate the concentration of any isotope by specifying the isotopes atom density, weight density, atom fraction or weight fraction within the burn material volume. The user is also able to able to specify how the concentration will change during the time-dependant cross section averaging process. The capability resides within the burn data retrieval subroutine (burn_mat.F) where new atom fractions and atom densities are set for use in the next particle transport step. The process of manually setting concentrations for isotopes therefore exists post-executing the CINDER90 number density calculation. For particle transport, the MCNPX code requires that isotope concentrations be ultimately be converted to atom fractions to be applied to total material atom densities.

The process for calculating the renormalized atom fractions if the user specifies an isotope to be altered by atom density is as follows:[86]

1. A loop is generated that loops through every isotope used in particle transport.
2. If an isotope is not to be manually altered that isotope's atom density is summed in the s2 variable.
3. If the isotope is to be manually altered that isotope's atom density is summed in the cf variable.
4. The total material atom density is then calculated by
$$\rho_a = s2 + cf \tag{3-1}$$
5. To calculate the individual isotope atom fractions, another loop over all the isotopes is generated, and the individual isotope atom fractions are calculated by
$$AF_k = \frac{\rho_{a,k}}{\rho_a} \text{ where } \rho_a = \sum_k \rho_{a,k} \tag{3-2}$$

The process for calculating the renormalized atom fractions if the user specifies an isotope to be altered by weight density is similar to the previously mentioned process except the code first immediately converts the inputted weight density to an atom density and then the code continues along the same solution path as the previously mentioned process. If the user specifies an isotope to be altered by atom fraction, the following process is utilized: [86]

1. A loop is generated that loops through every isotope used in particle transport.
2. If an isotope is not to be altered that isotope's atom density is summed in the s2 variable.
3. If the isotope is to be altered that isotope's input atom fraction is immediately saved as well as also summed into the fn variable.
4. The total material atom density is then calculated by
$$\rho_a = \frac{s2}{1 - fn} \tag{3-3}$$
5. To calculate the individual isotope atom fractions for an isotope not manually altered, another loop over all the isotopes is generated:

a. If a manually altered isotope is encountered, then the manually given atom fraction is implemented and no calculation is required.

b. For the rest of the isotopes the individual isotope atom fractions are calculated by

$$AF_k = \frac{\rho_{a,k} * (1 - fn)}{s2} \tag{3-4}$$

If the user specifies an isotope to be altered by weight fraction, the following process is similar to the process that implements the altered atom fraction: [86]

1. A loop is generated that loops through every isotope used in particle transport.

2. For an isotope that is to be altered, the following quantities are tracked (sums for this process include only isotopes that are to be altered):

   a. The individual isotope weight percent, w_j, divided by the individual isotope mass, M_j, stored in the x_j variable.

   b. The sum of x_j is stored in the wf variable.

   c. The sum of the w_j's are also tracked and stored in fn variable.

3. If an isotope is not to be altered the following quantities are tracked (sums for this process include only isotopes that are not to be altered):

   a. The sum of the individual isotope masses multiplied by the individual isotope atom densities, $\sum_i M_i * \rho_{a,i}$, are stored in the s3 variable.

   b. The sum of the individual isotope atom densities are then stored in the s2 variable.

4. Another loop over all the isotopes is generated.

5. The following quantity is calculated for each that isotope not to be altered (sums encompass only isotopes not to be altered):

   a. $x_j = \frac{\rho_{a,i} * (1 - fn)}{s3} = \frac{\rho_{a,i} * (1 - fn)}{\sum_i \rho_{a,i} * M_i}$ is stored, where 1-fn represents the weight percent and M_i represents the individual atomic mass for each of the unaltered isotope.

   b. The sum of the x_j variable for unaltered isotopes is then stored in the s4 variable.

6. Another loop over all isotopes is generated

7. The following derivation is used in order to generate the equation for calculating the individual atom fractions for each isotope

$$\left(1-\sum_j w\%_j\right)=\sum_i w\%_i \tag{3-5a}$$

$$\frac{\rho_a = w\%_i * N_A * \rho}{M_i} \tag{3-5b}$$

$$\frac{x_j}{s4+wf}=\frac{\dfrac{\rho_{a,i}*\left(\sum_i w\%_i\right)}{\sum_i \rho_{a,i}*M_i}}{\sum_j \dfrac{w\%_j}{M_j}+\sum_i \dfrac{\rho_{a,i}*\left(\sum_i \dfrac{w\%_i}{M_i}\right)}{\sum_i \rho_{a,i}*M_i}}=\frac{\dfrac{\rho_{a,i}*\left(\sum_i w\%_i\right)}{\sum_i w\%_i*\rho*N_A}}{\sum_k \dfrac{w\%_j}{M_j}+\sum_i \dfrac{\rho_{a,i}*\left(\sum_i w\%_i\right)}{\sum_i w\%_i*\rho*N_A}} \tag{3-5c}$$

$$\frac{x_j}{s4+wf}=\frac{\dfrac{\rho_{a,i}*\left(\sum_i w\%_i\right)}{\rho*N_A*\left(\sum_i w\%_i\right)}}{\sum_k \dfrac{w\%_k}{M_k}+\dfrac{\rho_{a,i}*\left(\sum_i w\%_i\right)}{\rho*N_A*\left(\sum_i w\%_i\right)}}=\frac{\dfrac{w\%_i}{M_i}}{\sum_k \dfrac{w\%_k}{M_k}+\sum_i \dfrac{w\%_i}{M_i}} \tag{3-5d}$$

$$\sum_k \frac{w\%_k}{M_k}+\sum_i \frac{w\%_i}{M_i}\Rightarrow \sum_k \frac{w\%_k}{M_k} \tag{3-5e}$$

$$\frac{\dfrac{w\%_k}{M_k}*N_A*\rho}{\sum_k \dfrac{w\%_k}{M_k}*N_A*\rho}=\frac{\rho_{a,k}}{\rho_a}=AF_k \tag{3-6f}$$

This capability enables manual changing of nuclide concentrations during burnup calculations. For example, boron concentrations are usually specified in parts per million weight concentration while actinide extraction for fuel recycle may be specified in fractions per atom.

The versatility of this capability allows the user flexibility in modeling most types of manual isotope changes that exist under real operating strategies.

Metastable Isotope Tracking

The MCNPX data library requires that isotopes be listed in and referenced by a ZAID format. The ZAID format consists of the following:

- Z = atomic number
- A = atomic mass
- ID = identifier corresponding to the evaluation type (i.e. specific library set, temperature, particle type, etc.)

The following equation is used for calculating the ZAID:

$$ZAID = (Z*1000 + A).ID \tag{3-7}$$

CINDER90 uses the AZS format for listing and referencing isotopes. The AZS format consists of the following:

- Z = atomic number
- A = atomic mass
- S = isomeric state

The AZS format is similar to the ZAID format and calculated using the following equation:

$$AZS = S+10+10*z+10000*A \tag{3-8}$$

Since both formats are required in order to execute both codes, an algorithm is necessary in order to swap formats when accounting for isotopes in each code. Unfortunately, since there did not initially exist a convention for representing isomeric states in ZAID format, transitioning metastable isotope between each code was not trivial. In the past, users created their own naming convention for ZAID format metastable isotopes, and as long as a tabular cross section file was referenced in the XSDIR library file for these types of isotopes, any naming convention could be accepted (i.e. To represent Ag-110m, ZA=47210, Z=47 and A=110+100*(metastable state)). However, because MCNPX is now linked to the CINDER90 code which uses a different

naming convention than MCNPX, an MCNPX standard convention for naming metastable isotopes is now required. Metastable isotopes ZA are represented by using the following equation:

$$A' = (A+300) + (m*100) \qquad \text{where } m=0,1,2,3,4 \qquad (3\text{-}9)$$

For example:

$$\text{Ag-110m} = 47510 \rightarrow 47510 = 47110 + 1^{st} \text{ metastable} \qquad (3\text{-}10)$$

MCNPX uses the following standard naming convention to convert ZAID format to AZS for user in CINDER90, and the conversion takes place within the interface subroutine.[87]

Calculation of Depletion Equation Coefficients

There exists the probability for hundreds of different types of particle reactions within a typical nuclear system. Examining equations 2-1, 2-2a and 2-2b, we can see that increasing the amount of reaction rates tracked per isotope greatly increases the size of the depletion equations for more reaction types contribute to the calculation of the creation and destruction coefficients. Due to the high energy threshold for most of these particle reactions, for the majority of reactor applications, only a base set of reaction actually have a significant probability of contributing to the calculation of the destruction and creation coefficients. Therefore choosing to follow reactions that do not contribute to the calculation restricts the available memory and diminishes computational performance. For the computed reaction rates, the Monte Carlo steady-state calculation computes normalized fluxes and reaction rates per source neutron. The depletion equation requires a total magnitude value for the destruction and creation coefficients. Because the Monte Carlo calculation only calculates these quantities relative to the particle source strength, normalization parameters must be further calculated in order to convert the normalized coefficients into coefficients that are set at the exact magnitude of the analyzed problem. After the normalization parameters have been calculated for each isotope, the code must be able to

properly determine how fission products are yielded from the fission process. The culmination of all of these mentioned procedures compose the important considerations necessary for calculating adequate depletion coefficients for achieving an acceptable solution to the temporal nuclide inventory.

Important Reactions Followed

Each reaction rate tracked per isotope represents memory allocation that further restricts other aspects of an analyzed problem. CINDER90 does contain a 63-group cross section set for all reactions available in the library file. Therefore, CINDER90 theoretically only requires a 63-group flux to match to its 63-group cross section set in order to calculate depletion coefficients. The accuracy of this matching process is therefore highly dependent upon the applicability of the cross section sets to a specific design application as well as being limited by the same approximations applied to typical deterministic calculations. Therefore calculating a continuous energy integrated reaction rate for use in a depletion coefficient for the depletion equation solution better preserves the true system physics represented within the coefficient. Unfortunately, the trade-off in tracking continuous energy integrated coefficients within the Monte Carlo calculation is that each coefficient tracked must be tracked for each isotope which then limits the available memory for other aspects of the calculation. Initially the MCNPX depletion code was set to only track the continuous energy integrated (n,fission) and (n,γ) reaction rates for application in the depletion solution.[17] Previous analysis suggested that the (n,γ) reaction rate was the dominant contributor to the neutron destruction and therefore other capture reaction rates were tracked only by matching a 63-group flux in MCNPX to a 63-group cross section set in CINDER90 in order minimize necessary memory requirements. The code therefore applied a mix and match procedure in which only the dominant contributors to the coefficients were calculated as continuous energy integrated coefficients while the rest of the

reactions were calculated by matching a 63-group flux calculated within the steady-state Monte Carlo to a 63-group cross section set in CINDER90. Recoverable energy per fission and neutrons generated per fission were also tracked and calculated in continuous energy; however, threshold reactions such as (n,3n) and (n,2n) and residual minor capture reactions such as (n,p) and (n,α) were not tracked utilizing continuous energy cross sections. Individual threshold reaction rates were implemented by the 63-group matching approach mentioned previously. The concern of the 63-group matching approach was that the validity of this technique resided in the applicability of the 63-group cross-section set to various designs.

The 63-group cross section set within the CINDER90 code was generated by collapsing a finer cross section set over an initial arbitrary system flux. The arbitrary flux utilized to generate the collapsed 63-group cross section set within CINDER90 generated cross sections that were reliable for calculations only representative of that system flux. Therefore calculations implementing the 63-group cross section set within CINDER90 would be in error if the flux of the examined system differed from the flux utilized to generate the cross section set. Furthermore, if the cross sections themselves were improperly collapsed to be poorly representative of threshold reaction boundaries, the calculation would be further in error. Therefore, MCNPX was augmented to track these threshold reactions properly in continuous energy to eliminate the error in calculation from the multi-group approach.[79, 85]

A numerical benchmark calculation was executed in order to isolate whether MCNPX burnup should track continuous energy reaction rates for (n,2n), (n,3n), (n,p) and (n,α). A hypothetical infinitely reflected pin cell geometry was depleted using MCNPX 2.6.A implementing only (n,γ) and (n,fission) continuous energy reaction rates (OLD MCNPX method) and then compared to MCNPX 2.6.A implementing (n,γ), (n,fission), (n,2n), (n,3n), (n,p) and

(n,α) continuous energy reaction rates (NEW MCNPX method) and MONBTEBURNS. Both of the MCNPX versions used for this test did not employ a time-dependent cross section averaging technique such as the method employed in MONTEBURNS. MONTEBURNS was chosen as a comparator code because of the extensive acceptable benchmarking already completed with this depletion code.[74, 83] It is true that the methods of isotope tracking and reaction rate calculation differ slightly between MCNPX and MONTEBURNS; however, the base solutions should be similar since MONTEBURNS has been extensively benchmarked.

The objective of these comparisons was to determine the magnitude in improvement as a result of employing continuous energy reaction rates for minor capture and threshold reaction events. The analyzed pin cell geometry is displayed in Figure 3-10.

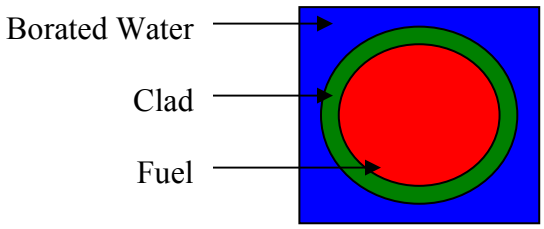

Figure 3-10. Examined infinitely reflected pin cell geometry.

Table 3-1. MOX fuel composition.

ZA value	Atom Density [atoms/cm^3]
8016	4.5854e-2
92235	1.4456e-4
92238	1.9939e-2
94238	1.1467e-4
94239	1.0285e-3
94240	7.9657e-4
94241	3.3997e-4
94242	5.6388e-4

The pin cell geometry consisted of 3 regions: a cylindrical mixed oxide (MOX) fuel region, a zirconium clad region, and a borated water region. The MOX cylindrical fuel dimensions were 365 cm tall and 0.4095 cm in radius, and the clad was 0.0655 cm thick and composed entirely of

natural zirconium. The fuel composition is listed in Table 3-1. The entire fuel pin was encased within a borated water rectangle 365 cm tall with a 1.313-cm length and 1.313-cm width. The borated water composition is listed in Table 3-2.

Table 3-2. Borated water composition.

ZA value	Atom Density [atoms/cm^3]
1001.60c	4.7716e-2
8016.60c	2.3858e-2
5010.60c	3.6346e-6
5011.60c	1.6226e-5

The fuel pin was depleted at a power of 66.956 kWt. This power was approximated to be the individual pin power for a typical 3670 MWth pressurized water reactor assuming ~193 17 X 17 fuel assemblies. The geometry was burned for a total of 730.645 days (2 years). The entire burn time was separated into 6 depletion steps: 0.645 days, 40 days, 100 days, 140 days, 200 days, and 250 days, for a total of 730.654 days. Each steady-state Monte Carlo calculation used 5000 particles per cycle, skipping the first 5 cycles, for 300 cycles. ENDF/BVI.0 cross sections were used for each steady-state calculation. For these calculations, MONTEBURNS used MCNPX 2.5.0 linked to ORIGEN2. Though the depletion steps were unrealistic for achieving an acceptable depletion solution due to the expected significant change in the flux shape and magnitude over such course depletion steps, the comparison of the methods was hypothesized to provide similar results regardless of the implementation as long as the consistency in the approach was preserved. Since both methods employed a linked calculation preserving spatial dependence of the solution, incurring the exact same time steps, both methods were deemed acceptably consistent enough to warrant fair comparison.

Preliminary results comparing the OLD MCNPX method with the MONTEBURNS depletion code displayed discrepancies in certain actinide and fission product buildup. Figure 3-

11 displays the EOL (end of life) percent difference of certain actinides between the OLD MCNPX method and the MONTEBURNS method. The speculated reason for the discrepancies were lack of calculating continuous energy threshold reaction rates (reasons of secondary concern also included limits of the matrix exponential method in ORIGEN2; however, these effects were hypothesized to be of second order effect).

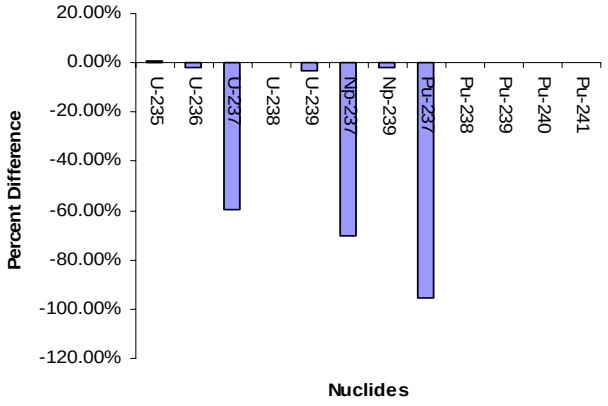

Figure 3-11. Percent difference of certain reference actinides between the OLD MCNPX method and the MONTEBURNS method.

The NEW MCNPX method calculated continuous energy integral reaction rates for (n, fission), (n,γ), (n,2n), (n,3n), (n,p), and (n,α). These integral reaction rates were calculated during the Monte Carlo process and fed to CINDER90 for isotope depletion. This process varied from the OLD MCNPX method in that the majority of significant threshold reaction rates were now calculated in continuous energy and no longer required a 63-group Monte Carlo flux to be matched to a generalized 63-group CINER90 cross-section set.

The integral continuous energy reaction rates were calculated separately for each burn material and tallied at the site of collision. Figure 3-12 displays the improvement in reference actinide calculation. A drastic improvement in actinide generation is realized when using continuous energy reaction rates for threshold reactions. The percent difference in Np-237 drops

from -70.24% to -4.85%, and the percent difference in Pu-237 production drops from -95.69% to -1.02%. Due to accentuation of U-237, Np-237, and Pu-237 differences in Figure 3-11, Figure 3-12 does not capture the improvements in EOL calculation of other important actinides; however, by utilizing the continuous energy reaction rates for threshold and minor capture reactions, 1-2% improvements in actinide predictions are also witnessed in U-236, U-239 and Pu-238.

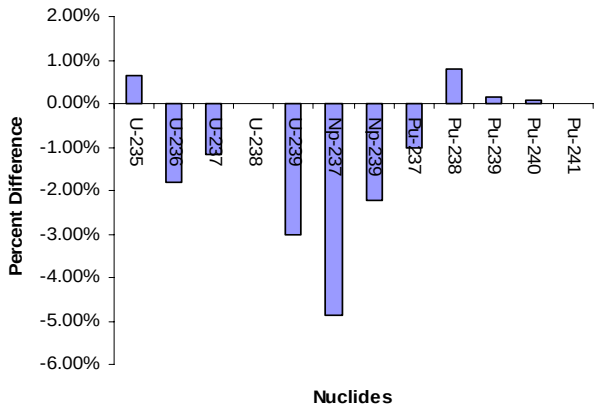

Figure 3-12. Percent difference of certain reference actinides between the NEW MCNPX method and the MONTEBURNS method.

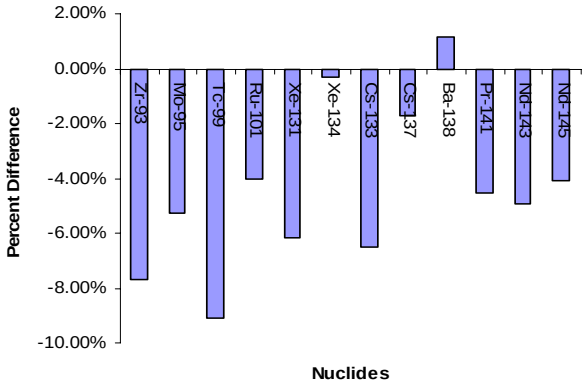

Figure 3-13. Percent difference of certain reference fission products between the NEW MCNPX method and the MONTEBURNS method.

Though tracking continuous energy threshold and minor capture reactions enhanced actinide prediction capabilities, little improvement was witnessed for fission product prediction. The NEW and OLD MCNPX methods for reaction rate tracking witnessed similar discrepancies in fission product buildup. Figure 3-13 displays the difference in EOL fission product prediction when comparing the new MCNPX method to MONTEBURNS. Unfortunately, time-dependent fission product buildup is a major contributor to negative reactivity trajectories, and therefore MCNPX and MONTEBURNS only predicted slightly different time-dependent reactivity. Figure 3-14 displays the difference in time-dependent neutron multiplication between the MCNPX and MONTEBURNS methods. Two major possible reasons existed for the differences in fission product generation between both MCNPX methods and the MONTEBURNS method: fission yield discrepancies and lack of cross section averaging technique.

CINDER90 offers the latest fission yield data available.[61] This data includes fission yield information for 35 fissionable isotopes incurring thermal, fast or high energy neutron reactions. ORIGEN2 contains fewer fission yield data and makes approximations for yield data for fissionable actinides not contained in an ORIGEN library file. Furthermore, not all fission product transmutation paths are followed explicitly in the matrix exponential method in ORIGEN2.[60] Therefore, it was deemed plausible that the fission yields and subsequent transmutation paths used in CINDER90 and ORIGEN2 differed slightly.

The versions of the MCNPX methods examined for this specific study did not implement any type of time-dependent cross section averaging technique. Figure 3-14 displays evidence of this hypothesis. The eigenvalue, k_{eff}, is tracked almost exactly during the short time steps at the beginning of life (BOL) but differs in the longer time steps. Therefore, a predictor corrector methodology was suggested to reduce the difference in isotope transmutation trajectory and

eigenvalue prediction for the two codes (this concept is explained further in the Predictor Corrector Method section). However, because actinide production was improved by tracking continuous energy threshold and minor capture reaction rates, these reaction rates were chosen for inclusion in tracking for further versions of the code.[85]

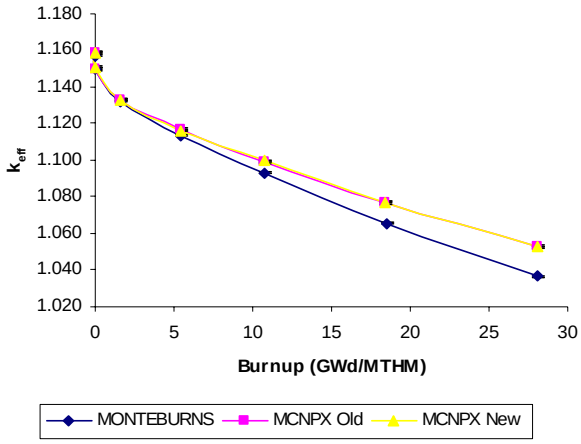

Figure 3-14. Time-dependent eigenvalue calculations.

Flux Normalization

MCNPX calculates reaction rates on a per source basis; however, CINDER90 requires a total magnitude reaction rate to deplete the system appropriately. In order to generate a total magnitude reaction rate, MCNPX must determine the magnitude of the source and multiply this value by the tracked reaction rates per source to calculate the total magnitude of the reaction rates for use in the depletion solution. The source of neutrons in a multiplying system is the total neutron production rate of that system. The total magnitude of the flux may then be calculated by multiplying the flux per source by the production rate as in equation 3-11:

$$\phi_{total} = \phi_{MCNPX} \times Flux\,Multiplier \Rightarrow Flux\,Multiplier = \frac{P \times \nu}{Q_{value}} \qquad (3\text{-}11)$$

- ν = neutrons per fission event
- Q_{value} = recoverable energy per fission event
- P = power level

How these parameters are calculated and what regions of the calculation these parameters are applied complicate the implementation of these parameters as normalization constants.

At each interaction site within a material that contains an actinide, each reaction mentioned in the prior section is tallied along with:

- $(n, \nu * \Sigma_f)$ = neutrons per fission event multiplied by the macroscopic fission cross section for that material per source neutron.
- $(n, Q_{value} * \Sigma_f)$ = recoverable energy per fission event multiplied the macroscopic fission cross section for that material per source neutron.

Calculating neutrons per fission and recoverable energy per fission then involves dividing the above two values by the macroscopic cross section. For a complex system of many different fissionable actinides, in many different burnable regions, the major question, regarding the calculation of the Q_{value} and ν, which now arises, is how to represent the normalization parameters and apply them to the tallied reaction rates. Reaction rates and normalization parameters are tallied within each burn material. If for every specific burnable region of a system, the interaction rates were normalized explicitly by these calculated parameters within that burnable region, it would not be possible to accurately transmute regions that did not contain fissionable actinides. If the region did not contain fissionable actinides, the Q_{value} for that specific region would not exist forcing the normalization multiplier to be undefined.

In order to normalize the reaction rates, the code requires knowledge of the source of neutrons. The source of neutrons is actually a global quantity because neutrons born within one burnable region migrate to other burnable regions for reaction. For example, consider a geometry containing a single cylinder contained within a rectangular fluid of which posses a reflective boundary condition at the boundary of the rectangle. At the center of the cylinder, 100 source histories are started and transported. If 60% of the histories are captured within the

cylinder and 40% leak out and interact in the surrounding material, then 60 neutrons are captured within that cylinder or 0.6 neutrons per source are absorbed. Now let us assume that we now have two cylinders of same dimension as the prior cylinder and separated in a manner so that the pitch between each cylinder mimics the "pseudo" pitch implied from the prior calculation. A rectangular fluid encases both cylinders and that fluid also posses a reflective boundary condition at the boundary of the rectangle. For this new calculation we will still use 100 histories, but start 50 histories in each of the two spheres. Ignoring effects of statistical randomness of particle travel, if the each cylinder employs the same material as the prior example then we would expect that 60% of the neutrons emitted within each cylinder are then captured by each cylinder. Since 50 neutrons are emitted in each cylinder, each cylinder must then capture 30 neutrons. In the first example, some neutrons were emitted from the cylinder into the fluid, hit the fluid boundary, and then were scattered back into the cylinder for interaction. In the second example, the same process happened as well as having neutrons emitted from one cylinder interacting with the other cylinder. Because the source sites of neutrons for neutron interaction within each cylinder may have been located within either cylinder, the neutron source is said to be global to the entire geometry. If we now apply the same thinking to our calculation of flux normalization parameters, these normalization parameters must also be tallied globally. This implementation forces the normalization multiplier to be constant and representative of the entire system. For each specified contributing material, MCNPX first tracks $(\mathrm{n}, \nu * \Sigma_f)$ and $(\mathrm{n}, Q_{value} * \Sigma_f)$ within each specified contributing material, divides by the macroscopic fission cross section within each material, and then volumetrically averages the quantities to generate globally averaged values for neutrons per fission and recoverable energy per fission. These globally averaged values are then combined to create the flux normalization multiplier in equation 3-11. The normalization

multiplier is then said to be the "global production rate" or "source" and multiplied by each reaction rate per source to generate the total magnitude of the reaction rates used as destruction and creation coefficients in the depletion solution. Therefore, it no longer maters if the material that this normalization factor is applied contains actinides or not, for the same averaged normalization constant is applied to reaction rate for each material. The normalization parameters are recalculated and averaged at the end of each time step, so that the multiplier dynamically adjusts to changes in temporal parameters as actinide concentrations are created/depleted.[79]

Table 3-3. Emitted and recoverable energy per fission of U-235.

Form	Emitted Energy (MeV)	Recoverable Energy (MeV)
Fission Fragments	168	168
Fission Product Decay		
Gamma-rays	8	8
Beta-rays	7	7
Neutrinos	12	--
Prompt Gamma Rays	7	7
Fission Neutrons (Kinetic Energy)	5	5
Capture Gamma Rays	--	3-12
Total	207	198-207

The Q_{value} used in the calculation is an estimate of the total recoverable energy per fission event. The total recoverable energy per fission may be described as the sum of many mirco events the lead to the recover of energy from a fission event. Table 3-3 lists the emitted and recoverable energy per fission from each micro fission event for U-235.[7] MCNPX inherently contains an array possessing prompt energy per fission for certain fissionable actinides. Prompt fission release energy is available within the evaluated data libraries, such as ENDF/B and JEFF, for roughly 1/3 of all the actinides. In the ENDF/B based libraries, the breakdown of the data for prompt fission energy release exists within File 1 MT 458.[70] The breakdown of prompt fission

release data includes: prompt kinetic fission energy (EFR), prompt neutron emission energy (ENP), prompt gamma energy (EGP), other delayed energy and neutrino energy contributions.[70] Each actinide available within the prompt fission energy release array in MCNPX, as well as the breakdown of prompt recoverable energy per fission if available, is listed in Table 3-4. The sum of EFR, ENP and EGP for each actinide is the prompt fission release energy for that actinide.

Table 3-4. Prompt fission energy release data available in MCNPX.

Isotope	EFR	ENP	EGP	Total
90232	160.39000	4.41000	7.11000	171.91000
91233	163.50000	5.04000	7.03000	175.57000
92233	168.22000	4.90000	7.72000	180.84000
92234	167.10000	4.85000	7.50000	179.45000
92235	169.13000	4.91600	6.60000	180.64600
92236	167.50000	4.70000	7.30000	179.50000
92237				180.40000
92238	169.80000	4.80400	6.68000	181.28400
92239				180.40000
92240	169.57000	5.21000	6.53000	181.31000
93237	170.60000	5.94000	7.13000	183.67000
94238	173.60000	5.92000	7.13000	186.65000
94239	175.55000	6.07000	6.74100	188.36100
94240	173.70000	6.48000	6.18000	186.36000
94241	175.36000	5.99000	7.64000	188.99000
94242	174.00000	6.76000	5.22000	185.98000
94243				187.48000
95241	176.40000	6.53000	7.90000	190.83000
95242m	182.37000	4.05000	1.17210	187.59210
95243	176.30000	7.53000	6.42000	190.25000
96242	186.22000	5.20000	0.00000	191.42000
96244	178.50000	7.62000	4.37000	190.49000

Values listed are in MeV.

To properly account for all the energy per fission event the inherent prompt values must be adjusted in order to account for delayed energy as well. A constant normalization factor, 1.111, is multiplied by every Q-value calculated in MCNPX in order to account for delayed energy per fission event. This constant normalization factor 1.111 was estimated based on the idea that if multiplied by the prompt energy per fission of a U-235 fission event, the total amount of

recoverable fission, delayed and prompt, would equal 200 MeV.[79] By implementing a constant normalization factor, an approximation is made about the value of the capture gamma energy contributing to the total recoverable energy per fission.

In a large LWR, most of the capture gamma energy is deposited in the heated volume and thus contributes to recoverable energy; however, in a long, thin space reactor a lot of the capture gamma energy leaks out of the system and does not contribute to recoverable energy of the system. Therefore, the capture gamma energy contribution is highly dependent upon system geometry and therefore the normalization constant may or may not estimate the actual Q value properly. Underestimating the Q value leads to an overestimation of the system fluxes and thus, an overestimation of the system collision densities. Because the equation for nuclide depletion is highly dependent on the collision densities as displayed in equation 3-12, increasing the collision density leads to an overestimation of the material burnup.

$$\frac{dN(r,t)}{dt} \approx -\sum_{i}^{E} \phi_i(r,t)\Sigma_i(r,t)N_i(r,t) \tag{3-12}$$

In the current depletion capability, three methods are used to correct this overestimation (input structure will be later explained in the Input Interface section):

1. Adjust the Q value multiplier (B1 value on the BOPT keyword; default = 1.0).
2. Modify the POWER keyword.
3. Alter the system power on the PFRAC keyword.

Unfortunately, the capture gamma contribution to the recoverable energy per fission is burnup dependent. The following equation displays the how the capture gamma energy contribution should be applied to the calculation of total recoverable energy per fission event:

$$Q_{recoverable} = Q_{prompt} + Q_{delayed} + \left(\nu(E) - k_{eff}\right) * Q_{capture\,\gamma} - Q_{neutrino} \tag{3-13}$$

Since neutrons per fission vary as a function of burnup, assuming a critical system is maintained in the calculation, recoverable energy per fission event should also vary as a function of burnup.

In ENDF/B VII.0 only 207 out of 390 isotopes contain capture gamma release data. In some cases, the data contain complete spectra information; however, in many cases the data are incomplete.[80] Without capture gamma photon emission spectra, employing equation 3-13 is impossible because there is no way of determining how and where the emission energy is deposited. The integral energy emission may be calculated from a mass defect calculation. However, transporting a photon possessing the integral energy from the mass defect calculation would not truly represent the physics of the system because the photon would travel farther and deposit energy in different regions of the geometry as compared to the photons generated from the true emission spectra. Nonetheless an initial calculation was completed to determine the average integral capture gamma energy of all isotopes contained within the CINDER90 library file. A mass defect calculation assuming zero energy neutron capture was completed to determine the integral energy from a neutron capture event. The atomic mass data was taken from the Atomic Mass Data Center (AMDC) website.[88] The average integral energy from a capture reaction with isotopes available in the CINDER library file was calculated to be 7.9 MeV per capture. For fission products containing an MCNPX cross section and CINDER90 fission yield information, the average integral energy from neutron capture was calculated to be 6.48 MeV. These calculated values only represent integral quantities based on 0 energy neutron capture. Trying to track the true capture gamma energy deposition was deemed futile in comparison to applying a delayed energy normalization constant because the true gamma ray emission spectra were unknown. The integral energy deposition from the mass defect could be assumed to be deposited locally; however, this assumption would violate the true physics of the system. The implementation of this technique could theoretically at best only improve the calculation of recoverable energy per fission by a few percent and at worst result in a more

inaccurate representation of the recoverable energy per fission as compared to the normalization constant.

The normalization factor was thus chosen as the method for approximating the recoverable energy per fission, and the following recommendations are suggested for trying to better account for capture gamma energy contribution:

1. Photon emission spectra must be generated for all isotopes used in particle transport and these photons should be transported to determine where each photon deposits its energy, and then equation 3-13 may be used to adjust recoverable energy per fission.

2. If the integral mass defect energy is to be employed for determining capture gamma energy contribution, a qualified approximation must be derived for determining how that energy is smeared within the geometry and what percent of that energy escapes the heated volume contributing to system power.

However, since the normalization factor was chosen for implementation, the current recoverable energy approximation will continue to slightly affect the flux normalization constant.

Automatic Fission Yield Selection

Fission products are generated as actinides consume neutrons and undergo fission events. The fission product yield distributions from the fission events are a function of the isotope that the causes fission event as well as the impinging neutron energy at the interaction site. For thermal neutron interactions the fission product yield distributions follows the curves witnessed in Figure 3-2 and Figure 3-3.

For higher energy reactions the fission yield distribution curve flattens and isotopes that did not have a high probability of formation from a thermal reaction now have a higher probability of formation in fast fission events. The differences in the fission products created leads to adverse reactivity conditions; therefore accounting for the proper fission products that are generated during a fission event is vital for calculation of reactivity and further interaction

rate distributions. Currently, the ENDF/B files offer a thermal, fast and high energy fission yield distribution for various fissionable actinides.[80]

Table 3-5. Available actinide fission yield distributions in CINDER90.

Isotope	Thermal	Fast	High Energy	Spontaneous Fission
^{227}Th	x			
^{229}Th	x			
^{232}Th		x	x	
^{231}Pa		x		
^{232}U	x			
^{233}U	x	x	x	
^{234}U		x	x	
^{235}U	x	x	x	
^{236}U		x	x	
^{237}U		x		
^{238}U		x	x	x
^{237}Np	x	x	x	
^{238}Np		x		
^{238}Pu		x		
^{239}Pu	x	x	x	
^{240}Pu	x	x	x	
^{241}Pu	x	x		
^{242}Pu	x	x	x	
^{241}Am	x	x	x	
^{242m}Am	x			
^{243}Am		x		
^{242}Cm		x		
^{243}Cm	x	x		
^{244}Cm		x		x
^{245}Cm	x			
^{246}Cm		x		x
^{248}Cm		x		x
^{249}Cf	x			
^{250}Cf				x
^{251}Cf	x			
^{252}Cf				x
^{253}Es				x
^{254}Es	x			
^{254}Fm				x
^{255}Fm	x			
^{256}Fm				x

The CINDER90 code offers a thermal, fast, high-energy fission yield for each fissile isotope contained in the CINDER90 data file.[61] Table 3-5 displays the actinide containing

fission yield distributions, within certain energy bands, utilized in CINDER90.[61] Since the CINDER90 code is an energy integrated depletion code, and is incapable of determining spectral characteristics, knowledge of the spectral characteristics must be input by the user. Because proper fission yield selection involves predetermined knowledge of the neutron spectrum and because this predetermined knowledge is possibly not known before the system is analyzed, a preliminary calculation may be necessary to determine spectrum information. This preliminary calculation contributes to the computational cost associated with the depletion process.

Selecting the adequate fission yield for a given system is dependent upon selecting the specific yield that best represents the energy band containing the majority of the system's fissions. This selection process therefore depends upon the energy-dependent fission rates. The MCNPX depletion code incorporates an algorithm to determine which energy band contains the largest fission rate and then properly selects the correct fission yield.[85] The MCNPX automatic fission yield selection method is diagramed in Figure 3-15. MCNPX determines which fission yield to use for a specified problem by calculating the integral fission rate for the defined energy boundaries (thermal, fast, and high energy), determining which energy range contains the majority of fissions, and then selecting the appropriate fission yield corresponding to the energy range containing the majority of fissions. The method is versatile in that each individual burn material may implement a separate fission yield if the calculation warrants a separate fission yield for different geometric locations. By using this process, the end user does not have to endure the computational cost associated with a preliminary calculation to determine the proper fission yield to be used for the depletion process. The end user is also given confidence that the fission yield being implemented for a specific problem is in fact the fission yield corresponding to the energy-dependent fission rate of the analyzed system.[85]

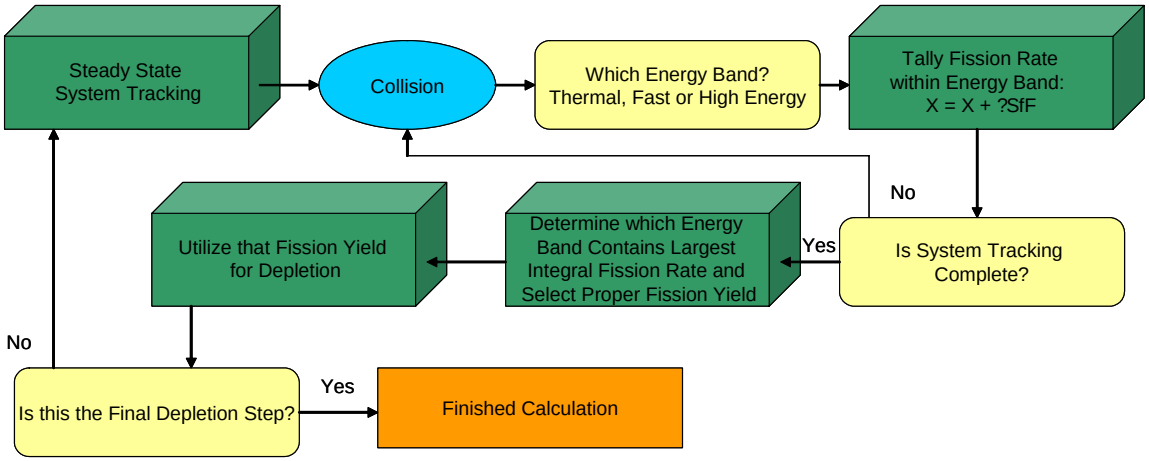

Figure 3-15. Fission yield selection process diagram

Time Dependent Cross Section Averaging Techniques

The depletion equation use interaction rates and nuclide densities to determine the time-dependent nuclide inventory. Reexamining equation 2-1 we see that the depletion equation is only linear if the depletion coefficients are constant; however, in reality the depletion coefficients are also time-dependent. As the nuclide inventory changes over time, as a function of the reaction rates, the interaction rates will also change as a function of time thus making the process of nuclide depletion nonlinear. As discussed in Chapter 2, to make equation 2-1 linear and solvable, the depletion coefficients are assumed constant over a given time step. Because a certain amount of fluence is required in order to change the nuclide concentration significantly enough to further alter the applied reaction rates, the assumption is valid for certain time durations.[2]

Acceptable time durations are related to the equilibrium buildup or depletion of highly absorbing isotopes. How the coefficients are applied within these time durations is paramount to the accuracy of the calculation. Equation 3-14 illustrates how power is proportional to the macroscopic fission cross section multiplied by the flux:

$$Power \sim \Sigma_f \phi \qquad (3\text{-}14)$$

From a first order standpoint, as the fuel burns and the macroscopic fission cross section decreases, the flux must increase in order to maintain constant power. Therefore if the depletion coefficients calculated at t_0(initial time step) are utilized for a depletion to t_a(subsequent time step), the interaction rates implemented into the nuclide inventory calculation will be underestimated in comparison to the average interaction rates; ultimately, leading to an under burning of the system.

Making the depletion coefficients time-dependent in order to account for the true interaction rate behavior makes the depletion equations nonlinear. Therefore if the coefficients must be made constant in order to make the depletion equation solvable, then the average interaction rates must be applied in order to attempt to adequately account for the true interaction behavior. Unfortunately, the true average interaction rates for a given time step cannot be known exactly, for that would involve solving the nonlinear equations exactly which is impossible because the equations are nonlinear. However, a "pseudo" average reaction rate may be calculated by applying appropriate assumptions related to how the interaction rate is expected to behave. Many methods exist for approximating average coefficient behavior in the solution of non-linear equations;[46, 74, 89-91] however, for the method to be useful in a computationally expensive linked Monte Carlo application, the method must implement as few extra Monte Carlo calculations as possible. One general method for approximating this nonlinear behavior without excessive computational expense is the predictor-corrector method.[46, 74, 89, 91, 92] First, an assumption is made about the time-integrated flux (setting it to a constant value) to deplete the system over a time step and calculate a "predicted" value of the number densities, and interaction rates. Values then are "corrected" by depleting the system again over the time step implementing the newly calculated interaction rates. The hope of implementing such a calculation is to deplete

the system using a best representation of the average of the time-dependent parameters. Predictor-corrector methods are defined as any type of routine in which a prediction is made regarding behavior and then a further correction is made if that behavior is deemed to change.

Two cross section averaging techniques were investigated for inclusion in MCNPX. The Cell-2 and MONTEBURNS cross section averaging methods were chosen based on the fact that both codes were highly benchmarked and the methods incurred minimal additional computational cost when applied in Monte Carlo.[74, 91] The Cell-2 method follows a more traditional predictor-corrector approach, and the MONTEBURNS method follows a slightly different approach that still relies upon the same implied assumptions of the traditional predictor-corrector approaches but requires less memory per calculation.

MONTEBURNS Method

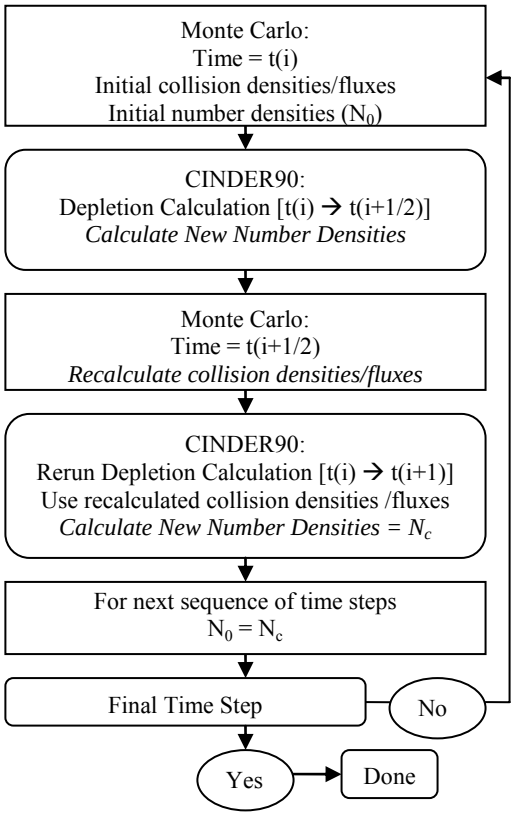

Figure 3-16. MONTEBURNS cross section averaging technique.

The MONTEBURNS cross section averaging procedure is displayed in Figure 3-16.[74] The MONTEBURNS code first makes a predictor calculation of the nuclide inventory to time t(i+1/2), based on interaction rates calculated at time, t(i). The interaction rates then are recalculated using the nuclide inventory at t(i+1/2). It is then assumed that these newly calculated interaction rates are the average interaction rates. Then a calculation is made over the whole time step implementing the newly calculated average interaction rates to generate corrected number densities. The entire process repeats until the final time step.

CELL-2 Method

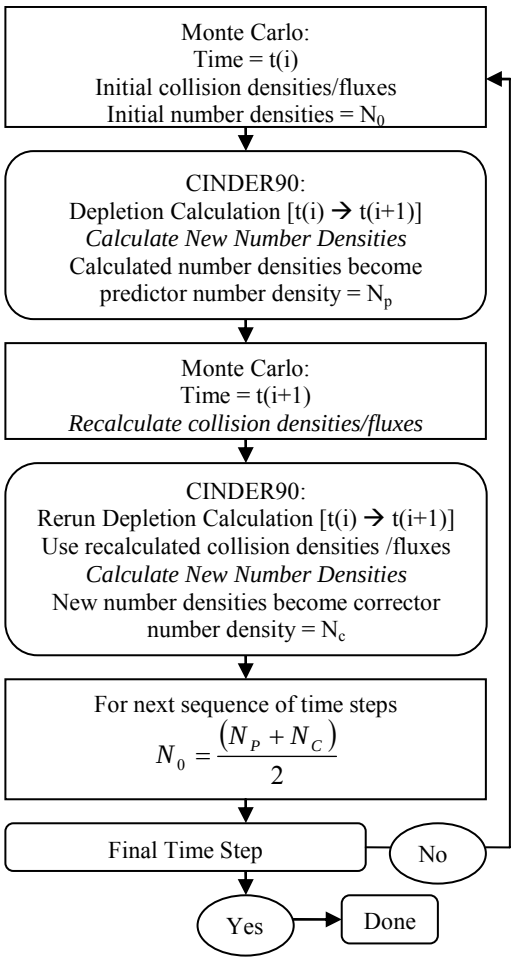

Figure 3-17. CELL-2 Predictor-Corrector method.

The CELL-2 predictor-corrector method is displayed in Figure 3-17.[91] The CELL-2 code first makes a predictor calculation of the nuclide inventory to time, t(i+1), based on interaction rates calculated at time, t(i). The interaction rates then are recalculated using the nuclide inventory at t(i+1), and the system then is redepleted from t(i) to t(i+1) to generate new corrected number densities. Finally, the predicted and corrected number densities are averaged to determine the nuclide inventory at t(i+1). The entire process repeats until the final time step.

Preliminary Analysis

An infinitely reflected pin cell geometry was depleted at a power of 66.956 kWt for 2191 days (6 years), using 5000 particles per cycle for 300 cycles, skipping the first 15 cycles.[92] The three types of calculations examined were

1. MCNPX with no-predictor-corrector method (NoPC);
2. MONTEBURNS predictor-corrector method (PC1);
3. CELL-2 predictor-corrector method (PC2).

An initial test involved only burning for a 371 day period. The 371 day cycle was broken up into 6 steps for testing predictor corrector methods: 0, 0.654, 31, 91, 181, 271, and 371 days. A MCNX calculation without implementing a predictor corrector method was run for 14 time steps: 0, 0.645, 5.7, 16, 31, 46, 61, 76, 91, 136, 181, 271, 321 and 371 days. This case was run as a control case, with the assumption that as the amount time-steps approached infinity the calculation would approach true behavior. Neutron multiplication versus time for the examined cases is displayed in Figure 3-18.

Unfortunately, it appeared that the examined cycle time was not long enough to incur a significant difference from choosing to utilize the predictor corrector method or not, suggesting that the 6 times steps implemented within the 371 day cycle was adequate enough to model reaction rate behavior. A new set of tests were generated examining longer cycle times in order

to truly analyze the benefit of implementing the predictor corrector method. A 2191 day burn (3 cycles of 2 year burns) was split up into various burn steps and analyzed to determine which of the two predictor corrector methods would behave better. NoPC was analyzed using 30, 20, 10, and 5 time steps, whereas PC1 and PC2 were examined using 15, 10, and 5 time steps. Figure 3-19 displays the burn steps implemented to achieve the 2191 day burn.

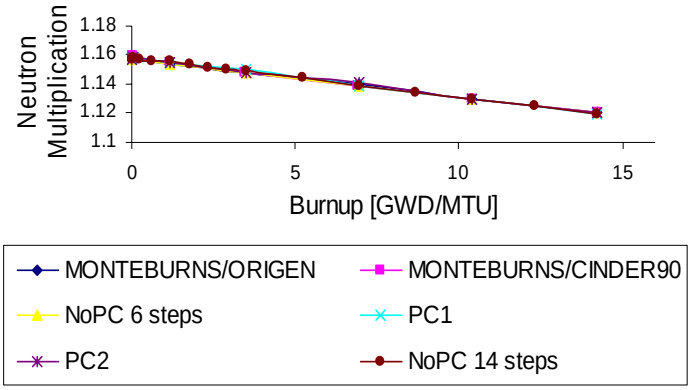

Figure 3-18. Time dependant neutron multiplication for the predictor corrector method tests.

For these cases, the assumption was made that the 30 time step case was assumed to be an infinite set of time steps. Therefore each subsequent case was compared to the 30 step case. Figure 3-20 and Figure 3-21 display the time-dependent neutron multiplication versus burnup for the different predictor corrector cases. Both predictor corrector methods, PC1 and PC2, calculate similar neutron multiplications at each time-step, and the differences in actinide and fission product production and depletion rates were also similar in both methods (>0.4% in EOL production/depletion between both methods).

Figure 3-22 displays the percent difference in neutron multiplication of each case when compared with the NoPC 30-step case. When either the PC1 or PC2 5 step calculation (5 step calculation = 5 predictor steps + 5 corrector steps = 10 total steps) was employed, there was a 3X speedup and less than 1.55 % difference in the EOL k_{eff}. Therefore, for this specific geometry,

the conclusion may be made that both the PC1 and PC2 methods were equally acceptable techniques for reducing the needed number of time steps to achieve an acceptable EOL k_{eff}. Since this result suggested that both methods achieve acceptable answers, and since the MONTEBURNS method employs less memory, because predictor number densities were not saved during the corrector calculation, the MONTEBURNS method was chosen as the method of choice for implementation into MCNPX.[92]

Burnup Steps (GWD/MTU)				
30	20	15	10	5
0.00E+00	**0.00E+00**	**0.00E+00**	**0.00E+00**	**0.00E+00**
2.48E-02	**2.48E-02**	**2.48E-02**	**2.48E-02**	**2.48E-02**
4.09E-01	4.09E-01	4.09E-01	**1.94E+00**	**1.94E+00**
7.93E-01	7.93E-01	1.18E+00	1.15E+01	**2.11E+01**
1.18E+00	1.18E+00	**1.94E+00**	**2.11E+01**	**5.19E+01**
1.56E+00	1.56E+00	6.74E+00	3.07E+01	**8.41E+01**
1.94E+00	**1.94E+00**	1.35E+01	4.13E+01	
2.71E+00	4.82E+00	**2.11E+01**	**5.19E+01**	
3.86E+00	7.70E+00	2.88E+01	6.24E+01	
5.40E+00	1.15E+01	3.65E+01	7.30E+01	
6.94E+00	1.54E+01	4.42E+01	**8.41E+01**	
8.47E+00	**2.11E+01**	**5.19E+01**		
1.00E+01	2.73E+01	5.95E+01		
1.15E+01	3.34E+01	6.72E+01		
1.39E+01	3.96E+01	7.49E+01		
1.62E+01	4.57E+01	**8.41E+01**		
1.85E+01	**5.19E+01**			
2.11E+01	5.95E+01			
2.38E+01	6.72E+01			
2.69E+01	7.49E+01			
3.00E+01	**8.41E+01**			
3.34E+01				
3.73E+01				
4.19E+01				
4.69E+01				
5.19E+01				
5.76E+01				
6.38E+01				
7.03E+01				
7.72E+01				
8.41E+01				

Figure 3-19. Burn steps implemented to achieve 2191 day burn

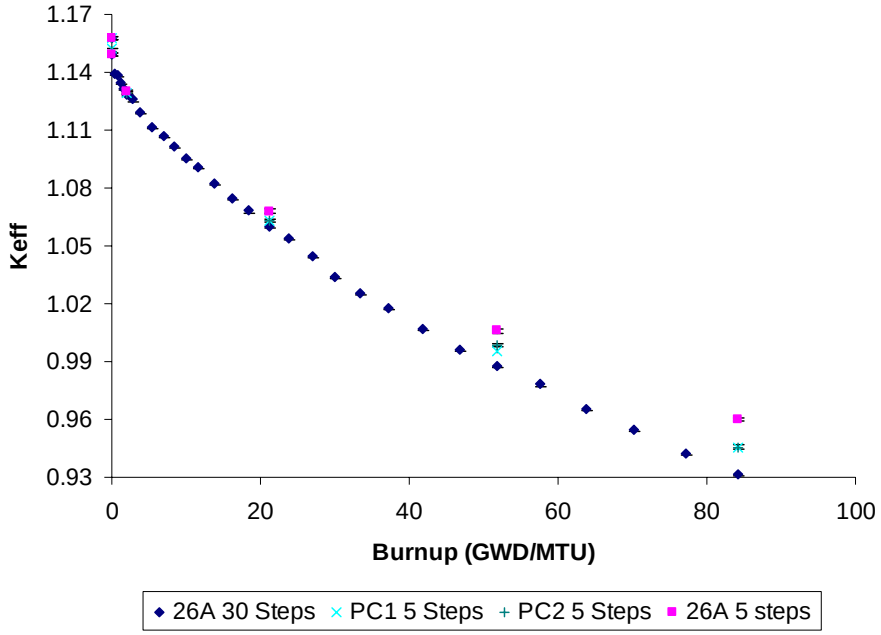

Figure 3-20. Time dependent neutron multiplication utilizing 5 burn steps.

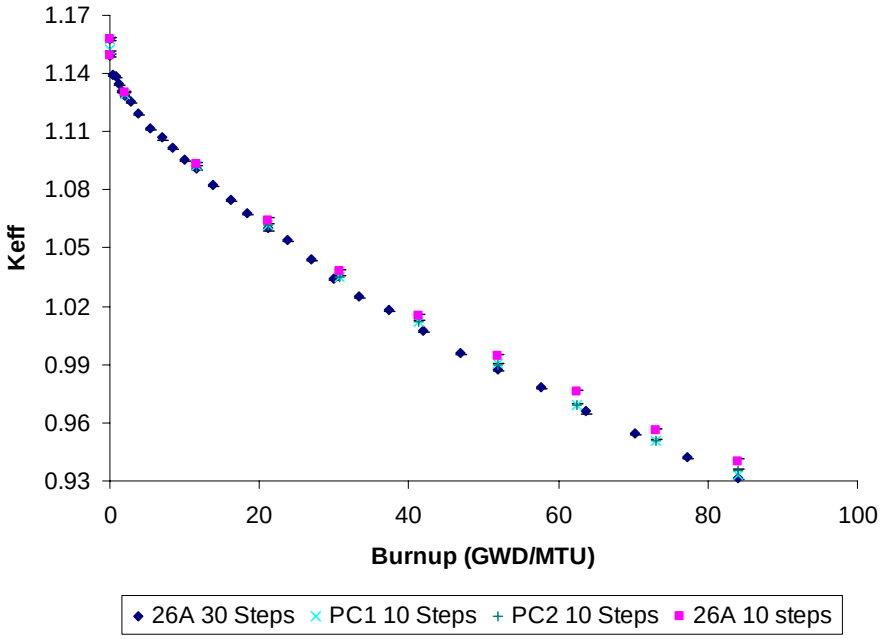

Figure 3-21. Time dependent neutron multiplication utilizing 10 burn steps.

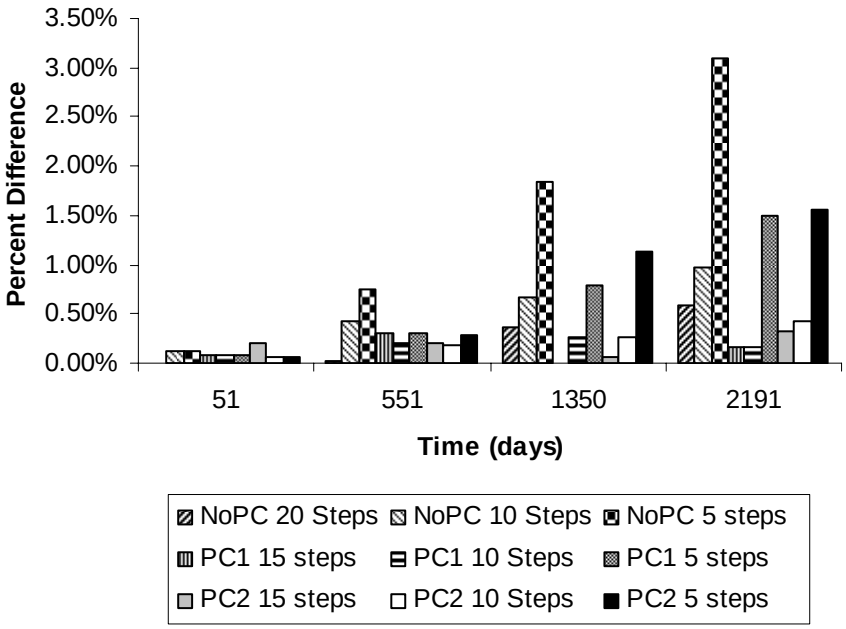

Figure 3-22. Percent Difference in k_{eff} When Compared with the NoPC 30-Step Case

Further Commentary on both Cross Section Averaging Techniques

Both methods tested were not the exact original method employed within both codes. Initially, the CELL-2 method only required a full spectrum calculation for the predictor calculation.[91] The method reuses the predicted number densities to propagate the spectrum calculation at each time step.[91] Corrected number densities are calculated using a similar procedure as detailed in Figure 3-17 except that these new number densities are not implemented in further propagation of the spectra calculation.[91] These corrected number densities only serve to update outputted values of what is to be believed the true number density at that time step. Implementing the CELL-2 method in this way reduces the amount of needed spectra calculations by half the amount. As initially implemented, the MONTEBURNS method only recalculates spectra at the half time steps, and then uses that specta as the assumed average spectra to be implemented over the entire time step. Implementing the MONTEBURNS method in this way also reduces the amount of needed spectra calculations by half the amount.[74] Initially, the

method was tested implementing the corrector spectra based on the premise that the corrector spectra would be required for systems incurring significant concentration change of highly absorbing isotopes. Later evidence from calculations with MCODE supported this premise for BWR lattices containing heavy initial gadolinium loading.[75] This evidence suggested that the predicted spectra and corrected spectra differed significantly enough to warrant a significant enough change in interaction rate to invalidate the applicability of the method for the desired time step. Therefore either smaller time steps were required, therefore limiting the effectiveness of both methods for long time steps, or the corrected number densities were required in order to accurately propagate the temporal nuclide solution. This evidence supports that using the corrected spectra, either from the calculated corrector number densities in the CELL-2 method or from the recalculated spectra at the t0 time steps in the MONTEBURNS methods, improves nuclide predictability. Using the corrected spectra increase the length of acceptable time step to a value beyond which would have been valid if only the predicted spectra were implemented; however, the method still is dependent on the time-step choice. The corrector spectra calculation does represent an extra calculation with extra incurred computational cost. For any depletion system, there may exist an optimum set of time steps in which the extra corrector spectra calculation employed for these time steps does not improve computational cost; however, these optimum time steps are usually unknown prior to calculation. For a general purpose tool, employing the extra corrector spectra calculation gives the user the best change for achieving accuracy in calculation. Because the MCNPX depletion methodology paradigm was to be applied to all types of depletion systems, possibly incurring the limiting cases given from the literature, both methods were tested using the corrected spectra calculation, and the "qausi" MONTEBURNS predictor corrector method was chosen for implementation in MCNPX 2.6.B.[94]

CHAPTER 4
IMPLEMENTATION ARCHITECTURE

The depletion capability is a modular methodology residing within a large scale MCNPX code. As mentioned before, MCNPX is composed of ~1000 subroutines. The depletion process resides in roughly 30 subroutines in the MCNPX code. Five new self-contained subroutines compose the majority of the actual variable averaging, outputting, and interfacing necessary for the depletion methodology while the other 25 augmented subroutines simply allow new variables to be inputted and set within the code package. The objective of confining the major computations to a minimal amount of self-contained subroutines is to make the package modular enough to be portable to earlier or different versions of MCNP. Self containment within minimal subroutines also helps in code augmentation and testing, for if the capability is confined to a small section of the larger code, then finding errors generated by the capability will be centralized to a minimal amount of subroutines employed by the code. If the methodology was not confined and self contained, debugging and coverage analysis would involve looking at larger set of subroutines. Furthermore, without containment to a small set of subroutines, augmentation to the methodology would result in needed coverage analysis for a larger subroutine set of the code increasing the computational cost associated with development and testing.

The MCNPX code requires the user to utilize input files in order to initialize variables for computation. The input file structure includes[50] (1) a title card; (2) cell cards defining a geometry from unions and intersections of surfaces specified on the surface cards (cards explaining certain physics options may also exist within in the cell cards section); (3) surface cards defining base surfaces that are used to define volumes on the cell cards; (3) data cards defining material, source and physics options available for implementation.

For each type of card defining source and physics options, keywords are available that determine how the card is implemented. For example on the SDEF card, the keyword PAR with a particle designator is used for determining the type of particle to be omitted from the source.[50] Since the depletion capability involves many types of options in order to burn a geometry model, the depletion capability was setup in a similar manor as the SDEF card. The development of the input interface and output structure spans MCNPX 2.6.A-F.[79, 84, 86, 87, 94, 95] The input and output features listed below, state the relevant capabilities of the most recent release of MCNPX 2.6.F.[87]

Input Interface

The depletion capability is invoked by using the BURN card. Within the BURN card exists many different types of keyword options. Figure 4-1 displays the input structure for the BURN card. Each input variable is then explained below Figure 4-1.

```
BURN  TIME=T1,T2,T3,...
      PFRAC=F1,F2,F3,...
      POWER=P
      MAT=+/-M1,+/-M2,+/-M3,...
      OMIT=J1,N1,I11,I12,...,J2,N2,I21,I22,...
      AFMIN=A1 A2
      MATVOL= V1, V2, V3, …, Vn
      MATMOD= ...
      BOPT=B1,B2,B3
```

Figure 4-1. Burn card input structure.

The TIME keyword corresponds to the incremental time duration for each depletion step. Each "T_i" listed in this keyword corresponds to a time duration (days) in which the system is burned. The default for this keyword is 1 day. For example:

```
TIME = 10, 100, 15
```

The system is first burned for 10 days, followed by a 100-day burn, followed by a 15-day burn, for a total burn of 125 days.

The PFRAC keyword corresponds to the fractional value of total system power (POWER) in which to burn the system for the equivalent time duration. The PFRAC option only changes the

total magnitude of power used to normalize the flux, and does not account for possible temperature changes in an actual power change. For each T_i value listed on the TIME keyword, a corresponding F_i value listed on the PFRAC keyword must exist. For each T_i value that does not contain a corresponding F_i value, $F_i = 0$ for that time step. The exception is when the PFRAC keyword is not specified at all, and then each $F_i = 1$ for every time step.

The POWER keyword is the total system power level, P, (in megawatts). Because this value corresponds to the total recoverable energy from the system, the value entered on this keyword should correspond to the total recoverable thermal system power. The default for this keyword is 1MW. For example:

```
POWER = 100
```

In this case, the total recoverable thermal system power is assumed to be 100 MW.

The materials to be burned must be listed on the MAT keyword. Each "M_i" entry corresponds to the material number listed in data cards section of the input deck. Figure 4-2 displays an example BURN card and subsequent materials cards referenced by the BURN card as burn materials. In this example, materials m1, m3, and m4 will be burned.

Burnup is calculated for the entire system of materials listed on the MAT keyword, as well as for each individual material listed on the MAT keyword containing a fissile actinide. Negative material numbers signify materials that are not burned, but do contribute to the power normalization by applying the tallied recoverable energy per fission and neutrons per fission of those materials to the total power normalization. Actinide and non-actinide buildup/depletion information for negative MAT numbers is not displayed in the output file because the negative MAT numbered materials are not burned.

```
BURN TIME=100,70
     MAT=1,3,4
     POWER=1.0
     PFRAC=1.0,1.0
     BOPT=1.0 -12 1.0
C Material Cards
m1
      8016.60c 4.5854e-2
     92235.60c 1.4456e-4
     92238.60c 1.9939e-2
     94238.60c 1.1467e-4
     94239.60c 1.0285e-3
     94240.60c 7.9657e-4
     94241.60c 3.3997e-4
     94242.60c 5.6388e-4
m2    2004 -1.0
m3   40000.60c -1.0
m4    1001.60c 4.7716e-2
      8016.60c 2.3858e-2
      5010.60c 3.6346e-6
      5011.60c 1.6226e-5
mt4 lwtr.01t
```

Figure 4-2. BURN card referencing burn materials m1, m3 and m4.

The OMIT keyword allows the user to run a transport calculation without including the transport data from a specified isotope. If an OMIT keyword is used, then the isotope is omitted from the transport calculation and omitted from the output file. Reaction rates are still generated for the isotope by importing a 63-group flux into CINDER90, matching the 63-group flux calculated from MCNPX to a 63-group cross section set inherent within CINDER90, energy integrating the reaction rates, and then producing a total collision rate for each collision type tracked. The OMIT keyword has the has the format

OMIT=$J_1, N_1, I_{11}, I_{12}, \ldots, J_2, N_2, I_{21}, I_{22}, \ldots$

Table 4-1 contains the available options for this keyword.

Table 4-1. OMIT keyword variable tasks.

Input Variable	Variable
J_i	i^{th} material for which to omit nuclides I_{i1}, I_{i2}, etc.
N_i	Number of omitted nuclides listed for the i^{th} material
$I_{i1}, I_{i2}, \ldots$	1st, 2nd, etc., omitted nuclide for the i^{th} material

If J_1=-1, then the omitted nuclide list is applied to all materials and J_2, J_3, etc., are not allowed. There is no default for this option.

The AFMIN keyword allows the user to determine below which mass fraction an isotope will be excluded from the transport calculation. The A1 value of AFMIN keyword signifies the minimum atom fraction for all isotopes in which isotopes below that atom fraction will have their atom fraction set to zero. The default for this option is 1.0E-10. The A2 value sets the decay chain convergence criteria (mentioned in the Benchmarks section). The default for this value is now 1e-10 and was 1e-4 for MCNPX 2.6.E and earlier. Using the new default improves nuclide predictability as the cost of increased computation time.

The B1 value on the BOPT keyword corresponds to the recoverable energy per fission multiplier. The default for this value is 1.0. The user may choose to adjust this value in order to adjust the Q value to better account for the true recoverable energy in the system.

Table 4-2. Options invoked for different B2 values.

Input Value for B2	Output Inventory Ordering
1	High to low, based on mass (default)
2	High to low, based on activity
3	High to low, based on specific activity
4	Increasing zaid

The B2 value on the BOPT keyword corresponds to the selected fission products used in the MCNPX transport process, as well as the format for the nuclide concentrations in the output file. MCNPX reports nuclide concentrations only for isotopes that are listed on the material cards, generated by the isotope generator algorithm, and/or selected from a fission product tier. The B2 value represents the burn table output frequency, ordering, and content flag. Table 4-2 displays the different options invoke for different values of B2. Positive input values cause the output to be printed to the output file only at end of an entire job. Negative input values cause output at the end of each burn step.

Three tiers of fission-product content are available. Each tier corresponds only to those isotopes that are used for particle transport in MCNPX and the nuclide densities, which are reported in the output file. To select a specific tier, add zero (default), 10, or 20 to the magnitude of the B2 input value. Table 4-3 gives a description of the available actinides in each fission product tier.

Table 4-3. Options invoked for different B2 values.

Tier	Fission Product Content
1	Zr-93, Mo-95, Tc-99m, Ru-101, Xe-131, Xe-134, Cs-133, Cs-137, Ba-138, Pr-141, Nd-143, Nd-145 (default).
2	All fission products that posses both CINDER90 yield data and transport cross data that are listed in the default MCNPX library file for MCNPX 2.6.F (XSDIR file).
3	All 220 available fission products listed in Figure 3-8.

The B3 value of the BOPT keyword invokes the models option. Cross-section models are a heritage of the high-energy physics capabilities of MCNPX. The models are benchmarked for a variety of problems for neutron energies >150 MeV. Table 4-4 describes the available options for the B3 value of the BOPT keyword.

Table 4-4. Available options for the B3 value of the BOPT keyword.

B3 value	Available Option
-1	Receive a fatal error if cross section models are used in the problem
0	Zeros out the atom fraction of any isotope using a cross section model (it is preferable to determine which isotopes are needed to be omitted and to place them on the OMIT keyword for the burned material).
1	Use cross section models in the calculation for isotopes not containing tabular interaction rate data.

The MCNPX depletion capability tallies energy integrated reaction rates and normalization constants within each separate burn material using the track length estimator. The track length estimator of the flux is calculated by:

$$\phi = \frac{1}{N}\sum_{n}\left(\frac{(l_n * w_n)}{V}\right) \tag{4-1}$$

Initially, MCNPX was setup to calculate and sum the quantity within the larger parenthesis during each track for each individual burn material and then later divide by the total number of histories. Due to limitations in the repeated structures mapping algorithm in MCNPX, the code cannot always determine the total volume of a plethora of repeated cells. Excessive time is also wasted trying to query and calculate the total volume. For simplicity, in MCNPX 2.6.D, the tallying algorithm in equation 4-1 was altered to

$$\phi = \frac{1}{NV}\sum_{n}\left(l_n * w_n\right) \tag{4-2}$$

Now only the particle track multiplied by the weight is tallied during each track for each individual burn material. Once particle tracking is complete, the track length estimator is now determined by dividing this new quantity by the sum of all volumes for a specific burn material and the total histories. The user may then input the total burn material volume on the MATVOL keyword. This procedure eliminates the dependency of the code to try and determine this total volume when the code may or may not be able to determine this quantity or when the code may require excess computation to map this value. Therefore the user is now free to take advantage of the repeated structure geometry features, such as modeling repeated arrays of fuel pins, while using the burnup capability.[96]

For burnup regions without repeated structures, MCNPX will try to calculate a volume and, if unsuccessful, a fatal error is generated and the user is required to then specify the material volume using a `VOL` card. In the case of cells in a lattice, MCNPX is only capable of successfully accounting for the volumes of materials if each cell is used only once in the lattice. Otherwise, if certain cells are repeated in a lattice, MCNPX is unable to determine the total volume of everywhere the material is repeated. The `MATVOL` keyword is used to account for the volume of materials listed in a repeated structure

MATVOL = V_1, V_2, V_3, …, V_n,

where V_i is the total volume of all cells [cm^3] containing burn material, M_i, on the MAT keyword of the BURN card.

Table 4-5. MATMOD keyword variable values.

Keyword Value	Description
NT	Number of time steps (1 through NT)
TS_{NT}	Time step (1..NT) for which to manually change nuclide concentrations of material $MT_{NT,NM_{NT}}$ Enter "1" for 2nd, etc. (If positive apply concentrations discretely at T_i and $T_{i+1/2}$. If negative apply at T_i, and make linear interpolation between T_i and T_{i+1} to determine the concentration at $T_{i+1/2}$. If TS is negative at T_i and the concentrations of any of the altered isotopes at T_{i+1} is equal to the concentration set at T_i then the concentrations of the altered isotopes will be set to the value at T_i for T_i, $T_{i+1/2}$, T_{i+1}. At $T_{i+3/2}$ the isotopes will undergo a normal depletion and the concentrations will not be set to the value at T_{i+1}.
NM_{NT}	Number of materials at time step "NT" that incur nuclide concentration changes
$MT_{NT,NM_{NT}}$	NMth material number for which to manually change nuclides at time step "NT". Positive value indicates atom/wt. fraction and negative value indicates atom/gram densities.
$K_{NT,NM_{NT}}$	Number of nuclides to manually change for the NMth material
$Z^{K_{NT,NM_{NT}}}_{NT,NM_{NT}}$	1st, 2nd,.. Kth nuclide of the $MT_{NT,NM_{NT}}$ th material at time step "NT" for which a concentration will be specified. List as a ZA value.
$C^{K_{NT,NM_{NT}}}_{NT,NM_{NT}}$	Concentration for the Kth isotope in material $MT_{NT,NM_{NT}}$ at time step "NT". Enter positive values for atom fractions or atom densities, and enter a negative value for wt. fractions or gram densities. See sign of $MT_{NT,NM_{NT}}$ to specify either fraction or density

If the MATVOL keyword is utilized on the BURN card then there must exist a corresponding MATVOL entry for every entry on the MAT keyword of the BURN card. If repeated structures are used without a MATVOL keyword, MCNPX will incorrectly calculate the volume, if possible, assuming that the total volume for the entire burn material is equal to the volume stated on the VOL card and not the accumulated the sum for the amount of times the cell is repeated.

The MATMOD keyword allows for time-dependent manual nuclide concentration changes. The details of the methodology for this feature were explained in the Manual Time-Dependent

Isotope Concentration Changes section. Table 4-5 describes the detail of each value within the MATMOD keyword. The MATMOD keyword uses the following structure for describing a manual concentration change:

$$\begin{aligned}
\texttt{MATMOD} = \texttt{NT}\ \texttt{TS}_1\ \texttt{NM}_1\ \texttt{MT}_{1,1}\ \texttt{K}_{1,1}\ Z^1_{1,1}\ C^1_{1,1}\ Z^2_{1,1}\ C^2_{1,1}\ \ldots Z^{K_{1,1}}_{1,1}\ C^{K_{1,1}}_{1,1} \\
\texttt{MT}_{1,\texttt{NM}_1}\ \texttt{K}_{1,\texttt{NM}_1}\ Z^1_{1,\texttt{NM}_1}\ C^1_{1,\texttt{NM}_1}\ Z^2_{1,\texttt{NM}_1}\ C^2_{1,\texttt{NM}_1}\ \ldots\ Z^{K_{1,\texttt{NM}_1}}_{1,\texttt{NM}_1}\ C^{K_{1,\texttt{NM}_1}}_{1,\texttt{NM}_1} \\
\texttt{TS}_{\texttt{NT}}\ \texttt{NM}_{\texttt{NT}}\ \texttt{MT}_{\texttt{NT},1}\ \texttt{K}_{\texttt{NT},1}\ Z^1_{\texttt{NT},1}\ C^1_{\texttt{NT},1}\ Z^2_{\texttt{NT},1}\ C^2_{\texttt{NT},1}\ \ldots\ Z^{K_{\texttt{NT},1}}_{\texttt{NT},1}\ C^{K_{\texttt{NT},1}}_{\texttt{NT},1} \\
\texttt{MT}_{\texttt{NT},\texttt{NM}_{\texttt{NT}}}\ \texttt{K}_{\texttt{NT},\texttt{NM}_{\texttt{NT}}}\ Z^1_{\texttt{NT},\texttt{NM}_{\texttt{NT}}}\ C^1_{\texttt{NT},\texttt{NM}_{\texttt{NT}}}\ Z^2_{\texttt{NT},\texttt{NM}_{\texttt{NT}}}\ C^2_{\texttt{NT},\texttt{NM}_{\texttt{NT}}}\ \ldots\ Z^{K_{\texttt{NT},\texttt{NM}_{\texttt{NT}}}}_{\texttt{NT},\texttt{NM}_{\texttt{NT}}}\ C^{K_{\texttt{NT},\texttt{NM}_{\texttt{NT}}}}_{\texttt{NT},\texttt{NM}_{\texttt{NT}}}
\end{aligned}$$

When using the MATMOD keyword, if a burn material is set to have a concentration change at T_1, the atom density of that isotope at $T_{1/2}$ is set to the initial value specified at T_0. This is only set for the initial midpoint time step, the rest of the calculation will follow the procedure mentioned above.

Output Structuring

The MCNPX depletion capability offers many varied outputs describing the temporal nuclide inventory process. Initially, the objective of the depletion outputs was to give the user the maximum amount of information necessary in order to make informed system design decisions from understanding important parameters regarding the evolution of the temporal nuclide inventory solution. The depletion outputs may be segregated into five distinct sections. These output sections include collision rates sent to CINDER90 for use as depletion coefficients, generalized global system averaged depletion data, generalized individual material depletion data, individual material nuclide data, and system average nuclide data. Each of the output sections is composed of key important information regarding the temporal nuclide inventory.

Total continuous energy integrated collision rates within a each burn volume are calculated in the particle transport calculation for (n,fission), (n,γ), (n,2n), (n,3n), (n,p) and (n,α). Examining these collision rates is important to understanding how the depletion system operates. The collision rates for each burn material, tracked in particle transport to be sent to CINDER90 for use as depletion coefficients are printed at the end of each steady-state KCODE calculation. The error associated with each collision rate is the error assuming the steady-state calculation is independent from the propagated error resulting from propagated flux and number densitiy error from the burnup calculation. Figure 4-3 displays a cropped example of the format of the collision rate outputs. These outputs help the user to calculate generalized capture-fission ratios, as well as other inelastic reaction ratios, to determine system characteristics.

```
Material #:    1

 no. zaid  (n,gamma)  error  (n,fission) error (n,nu*fission) error (n,fission*Q) error
  1  6012 8.19001E+05 0.5671 0.00000E+00 0.0000  0.00000E+00  0.0000 0.00000E+00  0.0000
  2  6013 2.81939E+08 0.1330 0.00000E+00 0.0000  0.00000E+00  0.0000 0.00000E+00  0.0000
  3  6014 0.00000E+00 0.0000 0.00000E+00 0.0000  0.00000E+00  0.0000 0.00000E+00  0.0000
...
...
 60 96244 8.41178E+13 0.4713 5.60552E+12 0.1094  2.09288E+13  0.1034 1.18632E+15  0.1094
 61 96245 4.07591E+11 0.0850 2.84278E+12 0.0738  1.02719E+13  0.0737 5.68499E+14  0.0738

 no. zaid   (n,2n)    error    (n,3n)    error    (n,alpha)   error     (n,p)     error
  1  6012 0.00000E+00 0.0000 0.00000E+00 0.0000  7.08058E+05  0.6535 0.00000E+00  0.0000
  2  6013 3.16027E+08 0.9128 0.00000E+00 0.0000  0.00000E+00  0.0000 0.00000E+00  0.0000
  3  6014 0.00000E+00 0.0000 0.00000E+00 0.0000  0.00000E+00  0.0000 0.00000E+00  0.0000
...
...
 60 96244 9.03869E+09 0.6024 0.00000E+00 0.0000  0.00000E+00  0.0000 0.00000E+00  0.0000
 61 96245 4.49267E+08 0.4078 0.00000E+00 0.0000  0.00000E+00  0.0000 0.00000E+00  0.0000
...
```

Figure 4-3. Example collision rate outputs.

The burnup summary table contains global system averaged burnup information and is designated “print table 210”. Each time step is listed with the corresponding time duration and actual specified depletion time. The following system averaged quantities are also listed: the power used for the flux normalization, k_{eff}, energy integrated flux, neutrons per fission,

recoverable energy per fission, burnup, and production rate. Figure 4-4 displays an example burnup summary table.

1burnup summary table by material print table 210

neutronics and burnup data

step	duration (days)	time (days)	power (MW)	keff	flux	ave. nu	ave. q	burnup (GWd/MTU)	source (nts/sec)
0	0.000E+00	0.000E+00	1.000E+00	1.54021	7.715E+14	2.452	200.979	0.000E+00	7.616E+16
1	5.000E+01	5.000E+01	1.000E+00	1.50987	7.945E+14	2.473	201.411	7.183E+00	7.664E+16
2	1.000E+01	6.000E+01	0.000E+00	1.51150	0.000E+00	2.474	201.448	7.183E+00	0.000E+00
3	5.000E+02	5.600E+02	2.000E-01	1.43413	1.699E+14	2.510	202.199	2.155E+01	1.550E+16

...

Figure 4-4. Example burnup summary table.

...

Individual Material Burnup

Material #: 1

step	duration (days)	time (days)	power fraction	burnup (GWd/MTU)
0	0.000E+00	0.000E+00	5.015E-01	0.000E+00
1	5.000E+01	5.000E+01	5.016E-01	7.205E+00
2	1.000E+01	6.000E+01	5.002E-01	7.205E+00
3	5.000E+02	5.600E+02	5.002E-01	2.158E+01

Material #: 4

step	duration (days)	time (days)	power fraction	burnup (GWd/MTU)
0	0.000E+00	0.000E+00	4.985E-01	0.000E+00
1	5.000E+01	5.000E+01	4.984E-01	7.161E+00
2	1.000E+01	6.000E+01	4.998E-01	7.161E+00
3	5.000E+02	5.600E+02	4.998E-01	2.152E+01

...

Figure 4-5. Example individual material burnup data.

If multiple materials are burned then there also exists individual material burnup data. Figure 4-5 displays example individual material burnup data. For this example both materials 1 and 4 were burned and therefore individual burn material burnup data is available only for those materials. The available information includes: time step, time duration, actual time, fission power fraction and individual material burnup. The fission power fraction is calculated by

taking the ratio of the fission power in a particular burn material to the sum of all burn materials. The calculated fission power fraction is therefore only related to fissions in burn materials.

$$power\ fraction = \frac{\left(\Phi\Sigma_f VQ\right)_i}{\sum_i \left(\Phi\Sigma_f VQ\right)_i} \tag{4-3}$$

The individual material burnup is calculated by

$$Burnup = Burnup_{i-1} + \frac{POWER * POWER\,Fraction * TIME * PFRAC}{MTHM} \tag{4-4}$$

```
...
nuclide data are sorted by increasing zaid for material   1 volume  3.8457E+02 (cm**3)

 actinide inventory for material   1 at end of step  0, time 0.000E+00 (days), power 1.000E+00 (MW)

  no.  zaid       mass      activity        spec.act.    atom den.     atom fr.      mass fr.
                  (gm)       (Ci)           (Ci/gm)      (a/b-cm)
   1  90231  0.000E+00  0.000E+00  0.000E+00  0.000E+00  0.000E+00  0.000E+00
   2  90232  0.000E+00  0.000E+00  0.000E+00  0.000E+00  0.000E+00  0.000E+00
...
...
   6  92235  3.441E+02  0.000E+00  0.000E+00  2.293E-03   1.000E-01   9.886E-02
...
...
 actinide inventory for material   1 at end of step  1, time 5.000E+01 (days), power 1.000E+00 (MW)

  no.  zaid       mass      activity        spec.act.    atom den.    atom fr.      mass fr.
                  (gm)       (Ci)           (Ci/gm)      (a/b-cm)
   1  9023    1.286E-09   6.837E-04  5.315E+05  8.718E-15  3.832E-13  3.723E-13
   2  90232  2.394E-08   2.625E-15  1.097E-07   1.616E-13  7.100E-12  6.929E-12
...
...
     totals  3.455E+03  2.584E+05  7.479E+01  2.275E-02  1.000E+00  1.000E+00
...
...
 nonactinide inventory for material   1 at end of step  0, time 0.000E+00 (days), power 1.000E+00 (MW)

  no.  zaid       mass      activity        spec.act.    atom den.     atom fr.      mass fr.
                  (gm)       (Ci)           (Ci/gm)      (a/b-cm)
   1   6012  0.000E+00  0.000E+00  0.000E+00  0.000E+00  0.000E+00  0.000E+00
   2   6013  0.000E+00  0.000E+00  0.000E+00  0.000E+00  0.000E+00  0.000E+00
   3   7014  0.000E+00  0.000E+00  0.000E+00  0.000E+00  0.000E+00  0.000E+00
   4   7015  0.000E+00  0.000E+00  0.000E+00  0.000E+00  0.000E+00  0.000E+00
   5   8016  4.684E+02  0.000E+00  0.000E+00  4.585E-02  1.000E+00  1.000E+00
...
```

Figure 4-6. Example cropped actinide output at two separate timesteps and fission product output for one time step.

The time dependant isotope buildup/depletion is listed after the burnup summary information. The isotope buildup/depletion for each individual material is given at each time step. The information is further subdivided into actinide and nonactinide categories. Figure 4-6 displays a cropped exampled of the reported actinide inventory for two separate time steps. At the end of each subdivision is an accumulation total of the isotope information for that subdivision. Atom and weight fractions calculations are based on the fractions of that specific subdivision. After isotope information for each individual material is given, print table 220 lists the sum total information of all actinides and nonactinides from all materials combined for each time step. Figure 4-7 shows a cropped example of print table 220.

1burnup summary table summed over all materials print table 220

nuclides with atom fractions below 1.000E-32 for a material are zeroed and deleted from print tables after t=0

nuclide data are sorted by increasing zaid summed over all materials volume 7.6914E+02 (cm**3)

actinide inventory for sum of materials at end of step 0, time 0.000E+00 (days), power 1.000E+00 (MW)

no.	zaid	mass (gm)	activity (Ci)	spec.act. (Ci/gm)	atom den. (a/b-cm)	atom fr.	mass fr.
1	90231	0.000E+00	0.000E+00	0.000E+00	0.000E+00	0.000E+00	0.000E+00
2	90232	0.000E+00	0.000E+00	0.000E+00	0.000E+00	0.000E+00	0.000E+00
3	90233	0.000E+00	0.000E+00	0.000E+00	0.000E+00	0.000E+00	0.000E+00
4	91233	0.000E+00	0.000E+00	0.000E+00	0.000E+00	0.000E+00	0.000E+00
5	92234	0.000E+00	0.000E+00	0.000E+00	0.000E+00	0.000E+00	0.000E+00
6	92235	6.883E+02	0.000E+00	0.000E+00	4.585E-03	1.000E-01	9.886E-02

...

Figure 4-7. Cropped example of print table 220.

The output is structured so as to give the user maximum amount of information in well organized concise tables. Each concise table is located in the output in the order in which the calculations have been made. For example, the collision rate tables always follow the KCODE information, and the burnup summary tables are then located directly below the collision rate tables (or at the end of the entire output if so invoked by an output option). For a large burnup

example, using many burn materials, the user will generate huge output files as a result of reporting all of the information available in the burnup tables. However, this information is necessary for determining how derivative quantities, such as reaction rates, contribute to the integral solution, such as global time dependant neutron multiplication and isotope analysis.

CHAPTER 5
BENCHMARKS

The Nuclear Energy Agency (NEA) is a specific agency within the Organization for Economic Cooperation and Development (OECD), an intergovernmental organization composed of many industrialized countries, based in Paris, France. The mission of the NEA is to assist its member countries in maintaining and further developing, through international co-operation, the scientific, technological and legal bases required for the safe, environmentally friendly and economical use of nuclear energy for peaceful purposes.[97] The membership consists of 28 countries including: Australia, Austria, Belgium, Canada, Czech Republic, Denmark, Finland, France, Germany, Greece, Hungary, Iceland, Ireland, Italy, Japan, Luxembourg, Mexico, the Netherlands, Norway, Portugal, Republic of Korea, Slovak Republic, Spain, Sweden, Switzerland, Turkey, the United Kingdom and the United States.[97] The NEA is further divided into many working parties and these working parties are composed of expert working groups that are tasked with examining various aspects of the Nuclear Fuel Cycle.[97] Criticality safety aspects of the Nuclear Fuel Cycle are examined by the Working Party on Nuclear Criticality Safety (WPNCS), and understanding the reactivity and isotope prediction capability is the responsibility of the Burnup Credit Criticality Safety expert group. One of the objectives of the Burnup Credit Criticality Safety expert group is to examine burn-up credit as applied to criticality safety in the transportation, storage, and treatment of spent fuel for a wide range of fuel types, including urainium-oxides (UOX) and MOX fuels for PWRs, BWRs, and Vodaa Vodiannee Energititscherski Reactors (VVER). Achieving this objective involves carrying out international comparisons and benchmarks in order to assess the capability of code systems to accurately predict reactivity and temporal nuclide inventories, including both code-to-code and available experimental data comparisons.[97]

In order to asses the validity of the MCNPX depletion method three separate types of OECD/NEA benchmarks were completed. Table 5-1 lists the benchmarks that were used to test the MCNPX depletion capability. In most of the benchmarks, many combinations of operating techniques were investigated. For the purpose of this study, only benchmarks that employ the maximum amount of fission products following all transmuted actinides were investigated. Therefore only a subset of the full amount of cases analyzed in the complete benchmark were examined. However, the analyzed sections of these benchmarks do adequately test the ability of the code to predict real core behavior as a maximum amount of fission products are generated during real reactor behavior. It is important to realize that the specified benchmarks only truly test the codes predictive capability for certain LWR operating strategies. However, before one tries to validate a methodology for more complicated operating scenarios, one must be able to first also correctively predict behavior of well benchmarked LWRs.

Table 5-1. Examined benchmark cases.

Benchmark Case	Geometry Type
OECD/NEA Burnup Credit Phase IB[52]	PWR UO_2 adjusted pin cell calculation
H. B. Robinson[53]	PWR UO_2 assembly calcation
OECD/NEA Burnup Credit Phase IVB[54]	LWR MOX assembly calculation

OECD/NEA Burnup Credit Phase IB Benchmark Specification

The purpose of the OECD/NEA Burnup Credit Calculational Criticality Benchmark Phase IB is to compare computed nuclide concentrations for a simple pin-cell depletion model.[52] Prior radiochemical analysis was completed on a 14 X 14 Combustion Engineering fuel assembly in order to determine nuclide concentrations for use in the benchmark. The simple pin cell model incorporates actual pin dimensions from a Combustion Engineering assembly; however, the fuel pin pitch has been adjusted in order to mimic the fuel-to-moderator ratio exhibited in the full assembly. Further approximations applied to the analyzed geometry included modeling the fuel

pin as an infinitely reflected geometry. An infinitely reflected geometry assumes zero net leakage at the geometry boundary. This type of boundary condition is only incurred within a flat power distribution region of the reactor. Such a region is never incurred on a pin cell level and therefore the approximation of infinitely reflected geometry was expected to affect the final solution outcome.

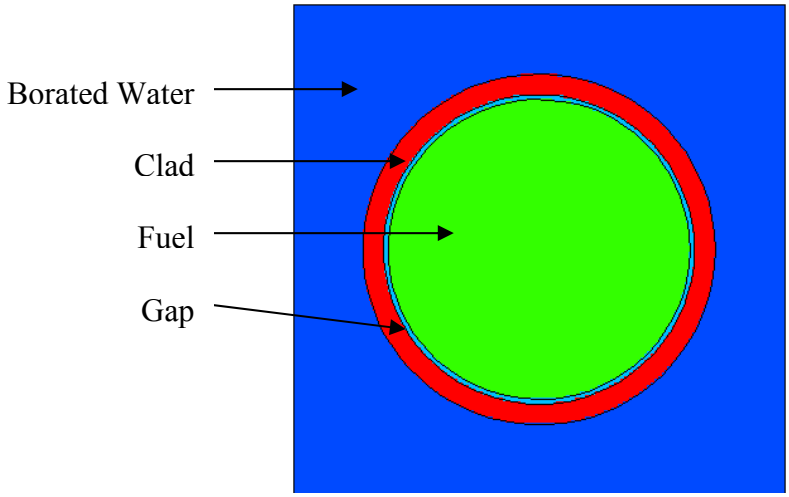

Figure 5-1. Infinitely reflected pin cell geometry.

Table 5-2. Model description for Phase IB Benchmark*.

Parameter	Data
Type fuel pellet	UO_2
Rod pitch	1.5586 cm
Clad outer diameter	1.118 cm
Clad inner diameter	0.986 cm
Fuel diameter	0.9563 cm
Active fuel length	347.2 cm
Effective fuel temperature	841 K
Clad temperature	620 K
Water temperature	558 K

*Data taken from reference.

The pin cell model was divided into four radial regions. The pin geometry is displayed in Figure 5-1 and the fuel pin dimensions are listed in Table 5-2. Temperatures were assumed constant throughout each region. The fuel pin was composed of a tall cylindrical fuel region divided into ten axial regions implementing the same average temperature and volume in each

axial division. Surrounding the fuel region was a cylindrical voided gap region. Enclosing the fuel and gap regions was a cylindrical Zicaloy-2 clad region. Finally encasing the entire geometry was a rectangular borated water box. The fuel, clad, and borated water concentrations are listed in Table 5-3, Table 5-4 and Table 5-5. The compositions are displayed in the same units as listed in the benchmark report.[52] Three different pin burnup cases were analyzed. For each burnup case, four operating cycles were implemented using common burn times, down times and operating concentrations. Table 5-6 details the common operating strategies utilized for each case. Table 5-7 lists the operating powers utilized for each individual case in order to achieve the prescribed burnups.

Table 5-3. Fuel composition for Phase IB Benchmark (density =10.045 g/cm^3).

Nuclide	Number Density (atoms/b-cm)
^{234}U	6.15164E-6
^{235}U	6.89220E-4
^{236}U	3.16265E-6
^{238}U	2.17104E-2
^{12}C	9.13357E-6
^{14}N	1.04072E-5
^{16}O	4.48178E-2

ENDF/B VII.0 temperature dependent cross sections and scattering law data were implemented in the steady state reaction rate calculation. Each steady-state reaction rate calculation was executed using 3000 particles per cycle for 115 cycles skipping the first 5 cycles. Ten starting source locations were equally spaced axially along the fuel pin center. The combination of skipped cycles and source locations was hypothesized to result in an adequately converged fission source distribution, thereby resulting in a further converged reaction rate calculation. The amount time steps, particles per cycle, and cycles were minimized in order to achieve a depletion solution within a minimal amount of time. Running on a linux platform across 25 1.4 GHz Opteron processors, each case ran for ~22 hours.

Table 5-4. Clad composition for Phase IB Benchmark (6.44 g/ cm^3).

Nuclide	Weight Fraction
^{54}Fe	0.0275 %
^{56}Fe	0.4477 %
^{57}Fe	0.0105 %
^{58}Fe	0.0143 %
^{90}Zr	49.0926 %
^{91}Zr	10.8251 %
^{92}Zr	17.8204 %
^{94}Zr	17.3218 %
^{96}Zr	2.8501 %
^{112}Sn	0.0145 %
^{114}Sn	0.0101 %
^{115}Sn	0.0052 %
^{116}Sn	0.2257 %
^{117}Sn	0.1203 %
^{118}Sn	0.3825 %
^{119}Sn	0.1368 %
^{120}Sn	0.5232 %
^{122}Sn	0.0756 %
^{124}Sn	0.0961 %

Table 5-5. Borated water composition for Phase IB Benchmark (0.7569 g/ cm^3).

Nuclide	Number Density (atoms/b-cm)
^{1}H	5.06153E-2
^{16}O	2.53076E-2
^{10}B	2.75612E-6
^{11}B	1.11890E-5

Table 5-6. Operating history data for Phase IB Benchmark.

Operating Cycle	Burn time (days)	Burn Duration (days)	Downtime (days)	Boron Concentration (ppm)
1	306.0	1, 15, 30, 40, 50, 50, 60, 60	71.0	331.0
2	381.7	1.7, 20, 35, 45, 55, 65, 75, 85	83.1	469.7
3	466.0	6, 20, 45, 65, 70, 80, 85, 95	85.0	504.1
4	461.1	6.1, 20, 45, 60, 70, 80, 85, 95	1870.0	492.5

Table 5-7. Operating power (MW) for each case for Phase IB Benchmark.

Operating Cycle	Case A (final burnup = 27.35 GWD/MTU)	Case B (final burnup = 37.12 GWD/MTU)	Case C (final burnup = 44.34 GWD/MTU)
1	0.038068	0.054585	0.068717
2	0.042904	0.059090	0.071786
3	0.037627	0.050434	0.057853
4	0.032172	0.041667	0.048844

OECD/NEA Burnup Credit Phase IB Results

Table 5-8. Initial Phase IB Benchmark results and comparison of Case A (27.35 MWD/MTU).

Isotope	MCNPX Value (mg/g UO_2)	Experiment Value (mg/g UO_2)	% Error*	Range of Values from other Codes
^{234}U	1.408E-1	1.600E-1	-12.00	1.330E-1 to 1.750E-1
^{235}U	7.988	8.470	-5.69	7.445 to 8.661
^{236}U	3.227	3.140	2.77	3.128 to 3.540
^{238}U	8.375E+2	8.425E+2	-0.59	8.637E+2 to 8.415E+2
^{237}Np	2.764E-1	2.680E-1	3.12	2.527E-1 to 3.396E-1
^{238}Pu	9.046E-2	1.012E-1	-10.61	5.721E-2 to 1.083E-1
^{239}Pu	3.790	4.264	-11.12	3.660 to 4.690
^{240}Pu	1.599	1.719	-6.99	1.573 to 8.60
^{241}Pu	6.491E-1	6.812E-1	-4.71	5.310E-1 to 7.335E-1
^{242}Pu	2.952E-1	2.886E-1	2.30	2.000E-1 to 3.192E-1
^{241}Am	2.274E-1	N/A	N/A	2.269E-1 to 2.598E-1
^{243}Am	4.487E-2	N/A	N/A	3.480E-2 to 4.672E-1
^{95}Mo	5.501E-1	N/A	N/A	5.590E-1 to 5.795E-1
^{99}Tc	5.397E-1	N/A	N/A	5.648E-1 to 6.904E-1
^{133}Cs	8.012E-1	8.500E-1	-5.74	6.820E-1 to 8.640E-1
^{135}Cs	3.535E-1	3.600E-1	-1.80	3.728E-1 to 3.959E-1
^{143}Nd	5.752E-1	6.130E-1	-6.16	6.040E-1 to 6.792E-1
^{145}Nd	4.886E-1	5.100E-1	-4.19	4.984E-1 to 5.151E-1
^{147}Sm	1.522E-1	N/A	N/A	1.564E-1 to 1.932E-1
^{149}Sm	1.628E-3	2.900E-3	-43.86	1.626E-3 to 2.900E-3
^{150}Sm	1.762E-1	2.070E-1	-14.86	1.713E-1 to 2.146E-1
^{151}Sm	7.070E-3	N/A	N/A	6.376E-3 to1.413E-2
^{152}Sm	7.940E-2	8.700E-2	-8.74	7.947E-2 to 1.073E-1
^{153}Eu	7.022E-2	7.900E-2	-11.12	6.730E-2 to 8.921E-2
^{155}Gd	2.629E-3	N/A	N/A	1.507E-3 to 5.762E-3

*(Calculated/Measured-1)*100

The Burnup Credit Phase IB benchmark contains data from a variety of calculation tools, as well as experimental results from radiochemical analysis of the 14 X 14 Combustion Engineering fuel assembly, for certain key actinides and fission products. The initial MCNPX calculated nuclide concentrations for all three benchmark cases are displayed in Table 5-8, Table 5-9 and Table 5-10. For each nuclide the following quantities are listed: MCNPX calculated value, experimentally determined value, percent error between MCNPX calculated value and experimental value and range of calculated values from other various methodologies presented in the benchmark.

Table 5-9. Initial Phase IB Benchmark results and comparison of Case B (37.12 MWD/MTU).

Isotope	MCNPX Value (mg/g UO_2)	Experiment Value (mg/g UO_2)	% Error*	Range of Values from other Codes
^{234}U	1.148E-01	1.400E-01	-17.96	1.080E-1 to 1.570E-01
^{235}U	4.587	5.170	-11.28	4.022 to 5.510
^{236}U	3.641	3.530	3.15	3.526 to 3.930
^{238}U	8.303E+02	8.327E+02	-0.28	8.292E+02 to 8.360E+02
^{237}Np	3.980E-01	3.560E-01	11.79	3.619E-01 to 4.919E-01
^{238}Pu	1.727E-01	1.893E-01	-8.77	1.144E-01 to 2.069E-01
^{239}Pu	3.849	4.357	-11.66	3.710 to 4.877
^{240}Pu	2.057	2.239	-8.14	1.996 to 2.347
^{241}Pu	8.379E-01	9.028E-01	-7.19	7.510E-01 to 9.846E-01
^{242}Pu	5.916E-01	5.761E-01	2.69	4.200E-01 to 6.347E-01
^{241}Am	2.853E-01	N/A	N/A	2.880E-01 to 3.418E-01
^{243}Am	1.181E-01	N/A	N/A	9.637E-02 to 1.391E-01
^{95}Mo	7.066E-01	N/A	N/A	7.214E-01 to 7.545E-01
^{99}Tc	6.898E-01	N/A	N/A	7.327E-01 to 8.372E-01
^{133}Cs	1.022	1.090	-6.24	8.784E-01 to 1.117
^{135}Cs	3.793E-01	4.000E-01	-5.17	3.967E-01 to 4.317E-01
^{143}Nd	6.523E-01	7.160E-01	-8.90	7.013E-01 to 8.254E-01
^{145}Nd	6.112E-01	6.530E-01	-6.41	6.326E-01 to 6.600E-01
^{147}Sm	1.607E-01	N/A	N/A	1.659E-01 to 2.201E-01
^{149}Sm	1.653E-03	3.000E-03	-44.91	1.736E-03 to 3.092E-03
^{150}Sm	2.311E-01	2.710E-01	-14.72	2.297E-01 to 3.152E-01
^{151}Sm	7.397E-03	N/A	N/A	7.990E-03 to 1.571E-02
^{152}Sm	9.521E-02	1.040E-01	-8.45	9.761E-02 to 1.416E-01
^{153}Eu	9.940E-02	1.090E-01	-8.81	9.960E-02 to 9.960E-02
^{155}Gd	4.076E-03	N/A	N/A	2.538E-03 to 1.028E-02

*(Calculated/Measured-1)*100

Table 5-10. Initial Phase IB Benchmark results and comparison of Case C (44.34 MWD/MTU).

Isotope	MCNPX Value (mg/g UO_2)	Experiment Value (mg/g UO_2)	% Error*	Range of Values from other Codes
^{234}U	9.896E-02	1.200E-01	-17.53	9.030E-02 to 1.440E-01
^{235}U	2.897	3.540	-18.18	2.389 to 3.716
^{236}U	3.772	3.690	2.21	3.641 to 4.030
^{238}U	8.243E+02	8.249E+02	-0.07	8.234E+02 to 8.316E+02
^{237}Np	4.794E-01	4.680E-01	2.44	4.327E-01 to 5.934E-01
^{238}Pu	2.399E-01	2.688E-01	-10.76	1.656E-01 to 2.810E-01
^{239}Pu	3.832	4.357	-12.04	3.659 to 4.902
^{240}Pu	2.292	2.543	-9.86	2.180 to 2.661
^{241}Pu	9.229E-01	1.020	-9.52	8.560E-01 to 1.111
^{242}Pu	8.479E-01	8.401E-01	0.93	5.960E-01 to 9.103E-01
^{241}Am	3.071E-01	N/A	N/A	3.102E-01 to 3.785E-01
^{243}Am	1.924E-01	N/A	N/A	1.634E-01 to 2.316E-01
^{95}Mo	8.100E-01	N/A	N/A	8.092E-01 to 8.742E-01
^{99}Tc	7.852E-01	N/A	N/A	8.449E-01 to 9.861E-01
^{133}Cs	1.160	1.240	-6.45	9.723E-01 to 1.286
^{135}Cs	3.958E-01	4.300E-01	-7.94	3.977E-01 to 4.605E-01
^{143}Nd	6.746E-01	7.630E-01	-11.58	7.397E-01 to 8.839E-01
^{145}Nd	6.858E-01	7.440E-01	-7.82	7.170E-01 to 7.560E-01
^{147}Sm	1.598E-01	N/A	N/A	1.655E-01 to 2.302E-01
^{149}Sm	1.686E-03	4.700E-03	-64.13	1.842E-03 to 3.286E-03
^{150}Sm	2.690E-01	3.610E-01	-25.49	2.725E-01 to 3.980E-01
^{151}Sm	7.585E-03	N/A	N/A	8.102E-03 to 1.682E-02
^{152}Sm	1.038E-01	1.210E-01	-14.25	1.077E-01 to 1.587E-01
^{153}Eu	1.173E-01	1.480E-01	-20.75	1.210E-01 to 1.596E-01
^{155}Gd	5.046E-03	N/A	N/A	3.379E-03 to 1.318E-02

*(Calculated/Measured-1)*100

MCNPX initially had poor nuclide prediction. The predictive capability also seemed to get worse at higher burnups. MCNPX was able to calculate actinide prediction within the range of other depletion codes; however, the actinide predictions were not close to the measured values and the percent error between measured and calculated values increased with increasing burnup. MCNPX fission product predictions were outside of the range values predicted by other depletion codes, and the fission product predictions were also not close to the measured values. The percent error between measured and calculated fission product values also increased with increasing burnup. Because the MCNPX results were poorer at higher burnups, it was

hypothesized that the burnup per time step might affect the accuracy of the result. Limitation of the burnup per time step is function of both significant changes in reaction rate over a time step, and limitations in the actual depletion algorithm. It is true that common time steps were used for each burnup case, and therefore the burnup step durations were unequal for all three cases. Therefore for the higher burnup cases it is possible that the time step duration was too long and too much burnup occurred ultimately invalidating the assumption that significant change in flux had not occurred. However, since the predictive capability was so poor compared to a deterministic solver, the hypothesis that the CINDER90 algorithm may be faulted was tested.

CINDER90 uses a Linear Markov Chain method in order to solve the depletion equations. CINDER90 solves for nuclide densities by following a series of equations along the transmutation chain.[61, 50] The following procedure is used:

1. Linear chains are created for each isotope transmutation path.
2. The solutions of each linear chain determines a partial nuclide density
3. Each calculated partial nuclide density, computed from a linear chain, is then summed to obtain the total nuclide inventory of nuclide.

The differential equation governing the computation of the ith nuclide is therefore only coupled to preceding contributing nuclides leading to the creation of the ith nuclide. However, in order to stop the propagation of a chain, the code determines if significant progeny will be created; and if the current nuclide does not produce significant progeny the calculation of the chain ceases. A series of checks exist within CINDER90 to determine if progeny will be created, passby calculation, and these checks posses limiting checking values for determining significance. For example, the magnitude of the nuclide density of a given isotope and the integral of the creation coefficient must both be above a certain value or the code ceases the transmutation chain. This would appear to affect short half-live nuclides in secular equilibrium and all resulting nuclides

within that transmutation chain. Preliminary investigation suggested that the order of such checks and the magnitude of the limiting checking values determined how accurately the code determined if significant progeny existed thereby ultimately affecting the solution outcome.

Table 5-11. MCNPXc Phase IB Benchmark results and comparison of Case A (27.35 MWD/MTU).

Isotope	MCNPX Value (mg/g UO_2)	Experiment Value (mg/g UO_2)	% Error*	Range of Values from other Codes
^{234}U	1.422E-01	1.600E-1	-11.13	1.330E-1 to 1.750E-1
^{235}U	8.339	8.470	-1.54	7.445 to 8.661
^{236}U	3.173	3.140	1.06	3.128 to 3.540
^{238}U	8.375E+02	8.425E+2	-0.59	8.637E+2 to 8.415E+2
^{237}Np	2.794E-01	2.680E-1	4.25	2.527E-1 to 3.396E-1
^{238}Pu	9.445E-02	1.012E-1	-6.67	5.721E-2 to 1.083E-1
^{239}Pu	3.891	4.264	-8.74	3.660 to 4.690
^{240}Pu	1.640	1.719	-4.60	1.573 to 8.60
^{241}Pu	6.615E-01	6.812E-1	-2.90	5.310E-1 to 7.335E-1
^{242}Pu	3.069E-01	2.886E-1	6.36	2.000E-1 to 3.192E-1
^{241}Am	2.320E-01	N/A	N/A	2.269E-1 to 2.598E-1
^{243}Am	4.886E-02	N/A	N/A	3.480E-2 to 4.672E-1
^{95}Mo	5.661E-01	N/A	N/A	5.590E-1 to 5.795E-1
^{99}Tc	5.661E-01	N/A	N/A	5.648E-1 to 6.904E-1
^{133}Cs	8.259E-01	8.500E-1	-2.83	6.820E-1 to 8.640E-1
^{135}Cs	3.620E-01	3.600E-1	0.54	3.728E-1 to 3.959E-1
^{143}Nd	5.840E-01	6.130E-1	-4.73	6.040E-1 to 6.792E-1
^{145}Nd	4.894E-01	5.100E-1	-4.04	4.984E-1 to 5.151E-1
^{147}Sm	1.518E-01	N/A	N/A	1.564E-1 to 1.932E-1
^{149}Sm	1.679E-03	2.900E-3	-42.10	1.626E-3 to 2.900E-3
^{150}Sm	1.854E-01	2.070E-1	-10.44	1.713E-1 to 2.146E-1
^{151}Sm	7.401E-03	N/A	N/A	6.376E-3 to1.413E-2
^{152}Sm	8.124E-02	8.700E-2	-6.62	7.947E-2 to 1.073E-1
^{153}Eu	7.257E-02	7.900E-2	-8.13	6.730E-2 to 8.921E-2
^{155}Gd	2.724E-03	N/A	N/A	1.507E-3 to 5.762E-3

*(Calculated/Measured-1)*100

A further investigation was completed to set the limiting checking value for density contribution of a specific nuclide to 1E-10 from the default 1E-4 value in order to determine if this change actually affected the ultimate depletion outcome. Table 5-11, Table 5-12 and Table 5-13 display the results augmenting this limiting checking value (MCNPXc). All of the same

conditions applied in the initial calculations were also applied for the MCNPXc cases. The results from the MCNPXc cases show significant improvement in actinide and fission product prediction.

Table 5-12. MCNPXc Phase IB Benchmark results and comparison of Case B (37.12 MWD/MTU).

Isotope	MCNPXc Value (mg/g UO_2)	Experiment Value (mg/g UO_2)	% Error*	Rang of Values from other Codes
^{234}U	1.164E-01	1.400E-01	-16.88	1.080E-1 to 1.570E-01
^{235}U	4.822	5.170	-6.73	4.022 to 5.510
^{236}U	3.619	3.530	2.51	3.526 to 3.930
^{238}U	8.303E+02	8.327E+02	-0.28	8.292E+02 to 8.360E+02
^{237}Np	4.032E-01	3.560E-01	13.26	3.619E-01 to 4.919E-01
^{238}Pu	1.750E-01	1.893E-01	-7.55	1.144E-01 to 2.069E-01
^{239}Pu	3.987	4.357	-8.50	3.710 to 4.877
^{240}Pu	2.120	2.239	-5.31	1.996 to 2.347
^{241}Pu	8.699E-01	9.028E-01	-3.65	7.510E-01 to 9.846E-01
^{242}Pu	5.936E-01	5.761E-01	3.04	4.200E-01 to 6.347E-01
^{241}Am	2.976E-01	N/A	N/A	2.880E-01 to 3.418E-01
^{243}Am	1.186E-01	N/A	N/A	9.637E-02 to 1.391E-01
^{95}Mo	7.293E-01	N/A	N/A	7.214E-01 to 7.545E-01
^{99}Tc	7.277E-01	N/A	N/A	7.327E-01 to 8.372E-01
^{133}Cs	1.060	1.090	-6.24	8.784E-01 to 1.117
^{135}Cs	3.930E-01	4.000E-01	-5.17	3.967E-01 to 4.317E-01
^{143}Nd	6.750E-01	7.160E-01	-8.90	7.013E-01 to 8.254E-01
^{145}Nd	6.172E-01	6.530E-01	-6.41	6.326E-01 to 6.600E-01
^{147}Sm	1.632E-01	N/A	N/A	1.659E-01 to 2.201E-01
^{149}Sm	1.711E-03	3.000E-03	-44.91	1.736E-03 to 3.092E-03
^{150}Sm	2.521E-01	2.710E-01	-14.72	2.297E-01 to 3.152E-01
^{151}Sm	7.924E-03	N/A	N/A	7.990E-03 to 1.571E-02
^{152}Sm	9.892E-02	1.040E-01	-8.45	9.761E-02 to 1.416E-01
^{153}Eu	1.035E-01	1.090E-01	-8.81	9.960E-02 to 9.960E-02
^{155}Gd	4.251E-03	N/A	N/A	2.538E-03 to 1.028E-02

*(Calculated/Measured-1)*100

For the most part, the results calculated by MCNPXc fell within the range of values calculated by the other depletion codes. These calculated values, however, did not exactly match the measured experiment values. There are many possible explanations for the discrepancies in calculated results as compared to the experimental data. The reasons include: (1) nuclear data;

(2) treatment of normalization parameters; (3) inadequacy of time steps; (4) statistical variance (5) differences in neutron spectra; (6) spatial reactivity effects of the modeled geometry.

Table 5-13. MCNPXc Phase IB Benchmark results and comparison of Case C (44.34 MWD/MTU).

Isotope	MCNPXc Value (mg/g UO_2)	Experiment Value (mg/g UO_2)	% Error*	Rang of Values from other Codes
^{234}U	1.006E-01	1.200E-01	-16.14	9.030E-02 to 1.440E-01
^{235}U	3.131	3.540	-11.54	2.389 to 3.716
^{236}U	3.758	3.690	1.84	3.641 to 4.030
^{238}U	8.247E+02	8.249E+02	-0.02	8.234E+02 to 8.316E+02
^{237}Np	4.854E-01	4.680E-01	3.72	4.327E-01 to 5.934E-01
^{238}Pu	2.434E-01	2.688E-01	-9.47	1.656E-01 to 2.810E-01
^{239}Pu	3.970	4.357	-8.89	3.659 to 4.902
^{240}Pu	2.362	2.543	-7.13	2.180 to 2.661
^{241}Pu	9.633E-01	1.020	-5.56	8.560E-01 to 1.111
^{242}Pu	8.463E-01	8.401E-01	0.74	5.960E-01 to 9.103E-01
^{241}Am	3.222E-01	N/A	N/A	3.102E-01 to 3.785E-01
^{243}Am	1.919E-01	N/A	N/A	1.634E-01 to 2.316E-01
^{95}Mo	8.359E-01	N/A	N/A	8.092E-01 to 8.742E-01
^{99}Tc	8.303E-01	N/A	N/A	8.449E-01 to 9.861E-01
^{133}Cs	1.206	1.240	-2.71	9.723E-01 to 1.286
^{135}Cs	4.104E-01	4.300E-01	-4.56	3.977E-01 to 4.605E-01
^{143}Nd	7.038E-01	7.630E-01	-7.76	7.397E-01 to 8.839E-01
^{145}Nd	6.930E-01	7.440E-01	-6.85	7.170E-01 to 7.560E-01
^{147}Sm	1.635E-01	N/A	N/A	1.655E-01 to 2.302E-01
^{149}Sm	1.751E-03	4.700E-03	-62.75	1.842E-03 to 3.286E-03
^{150}Sm	2.975E-01	3.610E-01	-17.59	2.725E-01 to 3.980E-01
^{151}Sm	8.239E-03	N/A	N/A	8.102E-03 to 1.682E-02
^{152}Sm	1.084E-01	1.210E-01	-10.39	1.077E-01 to 1.587E-01
^{153}Eu	1.228E-01	1.480E-01	-17.00	1.210E-01 to 1.596E-01
^{155}Gd	5.289E-03	N/A	N/A	3.379E-03 to 1.318E-02

*(Calculated/Measured-1)*100

Nuclear Data

The MCNPX benchmark calculations used ENDF/B VII.0 temperature dependent cross section data for steady-state particle transport. The range of values calculated from other depletion codes used either ENDF/B IV.0 or V.0 which was the data available at the time of the benchmark. Possible discrepancies in the implemented transport data may result in calculation

error. CINDER90 uses ENDF/B VI.0 fission yield data. This data may differ from the fission yield available in ENDF/B V.0 or IV.0 resulting in further error in calculation. CINDER90 also contains transmutation cross sections for 3400 nuclides. Over 3000 of those nuclides do not contain available ENDF data. Therefore cross section determination codes were used to calculate the data implemented in CINDER90. The CINDER90 data may also differ from what is used by other codes leading to further error in calculation when comparing to other tools.

Treatment of Normalization Parameters

MCNPX currently does not account for the true recoverable energy per fission. An approximation is made in order to try and determine the delayed energy contribution. The delayed energy contribution is unfortunately system dependent. For this modeled system, however, the geometry modeled was not the actual experimental geometry and therefore accounting for the true recoverable energy per fission in the adjusted geometry would not be possible. Therefore the assumptions made about delayed energy contribution were deemed acceptable for lack of a better approximation but known to affect the final solution outcome.

Inadequate Time Steps

The same time steps were used for each examined case. Therefore a larger amount of burnup was witnessed per time step for the higher burnup cases. It is possible that the time steps used for the benchmark were not short enough in order to account for significant change in neutron spectrum. Adequate time step selection is usually a trial and error process of accounting for significant changes in the neutron spectrum as a result of the asymptotic buildup of highly absorbing isotopes. Therefore choosing time-steps that are too large will not properly account for significant changes in neutron spectrum ultimately resulting in calculation error.

Statistical Variance

By using the Monte Carlo method and simulating the actual physical process, the calculated reaction rates, used as coefficients for the depletion solution, possessed an associated statistical error. This error propagates through the linked solution process. Therefore the coefficients generated for each time step possessed a propagated statistical error. For rarely sampled interactions, this error can be very large ultimately affecting the transmutation vector for nuclides resulting from those interactions. Furthermore, the cross sections themselves also posses a measured error associated with each value. The combination of the measured error incurred from determining the cross section values and the stochastic error from the modeling process ultimately influences the accuracy of the calculated results.

Differences in Neutron Spectra

The Combustion Engineering 14 X 14 fuel assembly that was used for the experimental benchmark was burned with a critical spectrum. The modeled geometry, however, possessed a spectrum that was either supercritical, for the beginning time steps, or subcritical, for the latter time steps. Unfortunately, true system operating parameters were not given. For example, to maintain criticality in a PWR, the boron concentration in the water coolant is constantly diluted in order to subsidize the negative reactivity deficit incurred from burning fuel. For the benchmark cases, boron concentration was assumed constant over the entire cycle. Therefore the neutron spectrum of the modeled geometry could not possibly be made critical.

Simply adjusting the boron concentration to maintain criticality in a pin cell model would also result in further error. Criticality is maintained in a system by balancing the leakage and absorption. For example, the critical spectrum in a modeled geometry is preserved by accounting for the leakage of neighboring geometries while operating the system with the true operating conditions. Unfortunately, when modeling a subsection of a larger geometry, the

leakage into that subsection may not be known and must be approximated. Approximating a pin cell calculation with reflective boundary conditions is a false representation of the boundary conditions witnessed in a typical reactor. The only way to truly burn the fuel bundle at critical is to model the entire system. This benchmark did not give specification for modeling the entire system and therefore errors should be expected in comparing results with experiment.

Spatial Reactivity Effects of the Modeled Geometry

The modeled geometry was an infinitely reflected pin cell with adjusted fuel-to-moderator ratio in order to try and mimic the same nuclide buildup as a 14 X14 Combustion Engineering fuel assembly. An infinitely reflected boundary condition is only appropriate for scenarios in which the boundary posses a true zero net leakage. For a certain section of a larger geometry, approximating a zero net leakage boundary condition is acceptable if the section of the geometry resides in a region possessing a flat flux or power distribution. For example, a fuel assembly that sits in a region of the reactor where the fuel assembly is surrounded by similar fuel assemblies exhibiting a similar power distribution. Unfortunately, this condition is never truly realized on a pin cell level. A radial power distribution exists across the fuel assembly and therefore each pin within the bundle burns at a different rate. By only modeling a single fuel pin to represent the entire fuel assembly, the spatial reactivity effects are ignored that would otherwise be witnessed in the full fuel assembly. This disregard of spatial reactivity effects ultimately affects the accuracy of the solution outcome. Because only a pin cell is modeled, comparisons between the calculated results and radiochemical analysis data taken from the full assembly analysis are expected to be error.

Further MONTEBURNS Comparisons

MONTEBURNS calculations for the OECD/NEA Burnup Credit Calculational Criticality Benchmark Phase IB had been completed as part of a prior thesis.[75] Due to computational

limitations at the time of those calculations, a coarser representation of the benchmark was modeled. The model implemented for that work used a single 360 cm tall fuel zone, ENDF V cross sections, and single time steps for operating durations (the exact model description implemented is explained in the reference). The model also lacked many of the fission products captured by the MCNPX depletion methodology (setting the MONTEBURNS transmutation importance fraction to 0.001). In the thesis, values were only calculated for cases A and B, and these values were within the range of values demonstrated by other codes and MCNPX.

In order to better compare the MONTEBURNS methodology and MCNPX, a series of MONTEBURNS 2.0 calculations were rerun using the same fidelity model as implemented for the MCNPX depletion calculations. ENDF VII.0 temperature dependent cross sections were implemented. The same kcode parameters, time steps, power levels, and manually set material concentrations used in the MCNPX calculations were also used for the MONTEBURNS 2.0 calculations. For these MONTEBURNS calculations, the importance fraction was set to 1e-10 in order to account for more of the fission and activation products. MONTEBURNS 2.0 was incapable of burning the borated water region and resetting the boron concentrations at each step. MONTEBURNS 2.0 was also incapable of modeling the same isotope at multiple temperatures; therefore all fission products that aligned with cladding nuclides used the same temperature dependent cross sections for the cladding temperature. These two issues are easily handled in MCNPX, however, not treated in MONTEBURNS 2.0, and therefore differences were expected as a result of these discrepancies. MONTEBURNS results are compared with MCNPXc results and experimental values, for cases A and B, in Table 5-14 and Table 5-15.

The higher fidelity MONEBURNS calculations for this benchmark are in larger error than the MCNPXc calculations. The reasons for the gross error in ^{238}Pu is mostly due to the ^{242m}Am

and ^{242}Am cross section mixup. The large over prediction of nuclides is not well determined. Increasing the amount of fission products tracked within MONTEBURNS 2.0 causes a competition for capture and therefore reduces actinide burning and transmutation. However, the prior thesis results show a large under prediction of nuclide concentration while the new results show a large over prediction. These discrepancies may be related to the treatment of incomplete cross sections, or limitations of the MONTEBURNS 2.0 tally routines, or limitations of the ORIGEN2.2 algorithm.

Table 5-14. MONTEBURNS* Phase IB Benchmark results and comparison of Case A (27.35 MWD/MTU).

Isotope	Experiment Value (mg/g UO_2)	% Error MONTEBURNS OLD**	% Error MONTEBURNS NEW**	% Error MCNPXc**
^{234}U	1.422E-01	-2.45	2.77	-11.13
^{235}U	8.339	-4.32	9.06	-1.54
^{236}U	3.173	2.09	3.07	1.06
^{238}U	8.375E+02	-0.5	0.31	-0.59
^{237}Np	2.794E-01	6.65	6.11	4.25
^{238}Pu	9.445E-02	-6.12	25.03	-6.67
^{239}Pu	3.891	-7.50	7.34	-8.74
^{240}Pu	1.640	-2.00	10.29	-4.60
^{241}Pu	6.615E-01	-2.72	9.77	-2.90
^{242}Pu	3.069E-01	6.65	12.07	6.36
^{133}Cs	8.259E-01	1.91	-6.92%	-2.83
^{135}Cs	3.620E-01	4.46	-1.40%	0.54
^{143}Nd	5.840E-01	-0.36	-5.51%	-4.73
^{150}Sm	1.854E-01	-13.22	-14.51%	-10.44
^{152}Sm	8.124E-02	-1.35	-6.39%	-6.62
^{153}Eu	7.257E-02	5.11	-5.71%	-8.13

*MONTEBURNS OLD = MONTEBURNS from prior thesis; [75]
MONTEBURNS NEW =MOTNEBURNS 2.0 with higher fidelity model
***(Calculated/Measured-1)*100

The results do show major cause for concern, because a higher fidelity model should show better results. It seems that modeling more of the available fission products actually hurt the calculation; however, further testing is required in order to determine the root cause of the miscalculation. New MONTEBURNS versions have been developed since MONTEBURNS 2.0

and therefore further testing will be required in order to determine the origin of this cause and whether or not the cause is problem dependent.

Table 5-15. MONTEBURNS* Phase IB Benchmark results and comparison of Case A (37.38 MWD/MTU).

Isotope	Experiment Value (mg/g UO_2)	% Error MONTEBURNS OLD**	% Error MONTEBURNS NEW**	% Error MCNPXc**
^{234}U	1.164E-01	-5.05	-11	-16.88
^{235}U	4.822	-9.66	-31.71	-6.73
^{236}U	3.619	2.68	-11.43	2.51
^{238}U	8.303E+02	-0.28	1.25	-0.28
^{237}Np	4.032E-01	14.38	-36.40	13.26
^{238}Pu	1.750E-01	-3.84	-44.37	-7.55
^{239}Pu	3.987	-7.46	3.95	-8.50
^{240}Pu	2.120	-2.47	-18.18	-5.31
^{241}Pu	8.699E-01	-4.05	-21.07	-3.65
^{242}Pu	5.936E-01	7.41	-77.15	3.04
^{133}Cs	1.060	2.55	20.93	-6.24
^{135}Cs	3.930E-01	4.79	7.42	-5.17
^{143}Nd	6.750E-01	-0.76	11.81	-8.90
^{150}Sm	2.521E-01	-8.96	-30	-14.72
^{152}Sm	9.892E-02	-0.20	27	-8.45
^{153}Eu	1.035E-01	13.17	-30	-8.81

*MONTEBURNS OLD = MONTEBURNS from prior thesis; [75]
MONTEBURNS NEW =MOTNEBURNS 2.0 with higher fidelity model
***(Calculated/Measured-1)*100

H. B. Robinson Benchmark Specification

The Burnup Credit Criticality Safety expert group offers the Spent Fuel Isotopic Composition database containing measured nuclide composition data for 14 LWRs in order to help validate burn-up codes.[97] The H. B. Robinson benchmark is one of the 14 available LWR benchmarks. Post irradiation examination measurements exist for select fuel pins within one 15 X 15 Westinghouse fuel assembly from the H. B. Robinson Unit 2 reactor.[53] For a specific fuel pin within the assembly, radiochemical analysis was completed at several axial levels corresponding to several different burnups. The benchmark was chosen for this study because full assembly geometry specification was available, and the full modeled assembly was

considered to be in a core location assumed to possess a reasonably "flat enough" power distribution to assume zero net leakage at the physical boundary of the assembly. Because zero net leakage was assumed at the assembly boundary, it was also further assumed that the assembly could be modeled as infinitely reflected at the geometry boundary. Because leakage from assembly to assembly is affected by the ultimate core boundaries, power shaping and poison positioning, this assumption is not exactly true. However, the assumption was deemed acceptable enough to model the assembly because the power distribution across the assembly region was assumed "flat enough".

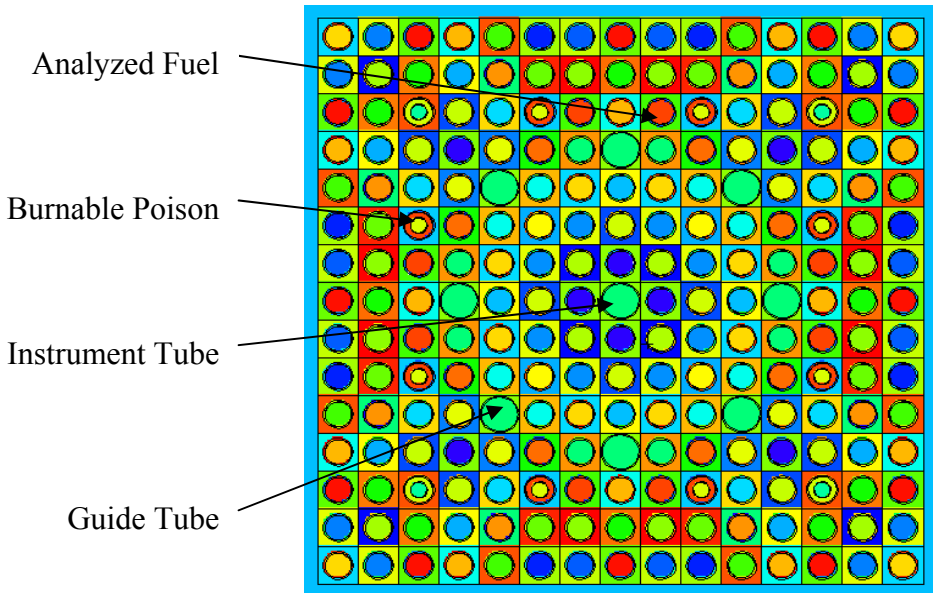

Figure 5-2. Infinitely reflected pin cell geometry.

Oak Ridge National Laboratory had also completed a verification study of the SCALE package using this benchmark. This verification study offered knowledge of how to setup the benchmark for direct comparison with the SCALE package. The Oak Ridge National Laboratory report, ORNL/TM-12667.28, was therefore used to determine the benchmark setup.[53] The H. B. Robinson Fuel assembly was modeled using eighth bundle symmetry, and took advantage of repeated structure modeling available since MCNPX 2.6.D. The exact modeled geometry is

displayed in Figure 5-2. Table 5-16 displays the modeled assembly design data for the benchmark. The material compositions for the fuel, clad, guide tube, and burnable poison rod materials are specified in the Oak Ridge National Laboratory report, ORNL/TM-12667.28.[53]

Table 5-16. Fuel assembly design data for H. B. Robinson Benchmark*.

Parameter	Data
Assembly general data	
Designer	Westinghouse
Lattice	15 × 15
Number of fuel rods	204
Number of guide tubes	8
Number of burnable poison rods	12
Number of instrument tubes	1
Assembly pitch	21.50 cm
Assembly fuel	443.7 kg U
Fuel rod data	
Type of fuel pellet	UO_2
Enrichment: wt % ^{235}U	2.561
wt % ^{234}U	0.023
wt % ^{236}U	0.013
Pellet density	9.44 g/cm^3
Rod Pitch	1.43 cm
Rod OD	1.0719 cm
Rod ID	0.9484 cm
Pellet diameter	0.9242 cm
Active fuel length	365.76 cm
Clad temperature	595 K
Clad material	Zircaloy-4
Guide tube data	
Inner radius	0.6502 cm
Outer radius	0.6934 cm
Material	Zircaloy-4
Instrument tube data	
Inner radius	0.6502 cm
Outer radius	0.6934 cm
Material	Zircaloy-4
Burnable poison rod data	
Air OD	0.5677 cm
SS304 OD	0.6007 cm
Air OD	0.6172 cm
Borosilicate glass OD	1.0058 cm
Air OD	1.0173 cm
SS304 OD	1.1151 cm

*Data taken from reference[53]

Each steady-state Monte Carlo calculation was completed running 4000 histories per cycle for 155 cycles skipping the first 25 cycles. Initial source particles were started in each of the fissile fuel locations. Though the geometry was modeled in 3-dimensions, only 1 axial region was utilized; therefore the model does not account for axial variation of the power distribution as a function of burnup. However, each fuel pin, within an eighth assembly symmetric section, used a separate burn material in order to account for radial variation of the interaction rates. Four different cases, corresponding to four axial locations, experiencing four separate burnups, were examined as part of the benchmark. Cases A-D represents the different burnup cases from the benchmark: (1) Case A = 16.02 GWD/MTU; (2) Case B = 23.8 GWD/MTU; (3) Case C = 28.47 GWD/MTU; (4) Case D = 31.66 GWD/MTU. The measured burnup given for case A did not correspond to the final time interval specified in the Oak Ridge National Laboratory Report. For the Case A calculation, the final operating interval was changed from 156 days to 165 days in order to correspond to the expected burnup exhibited in the assembly.[54] Table 5-17 and Table 5-18 display the operating intervals, time steps used for each interval, corresponding down times, and cycle dependent soluble boron concentrations for Case A-D.

Table 5-17. Operating data for H. B. Robinson fuel assembly.

Cycle	1	2	3	4
Operating Interval (days)	243.5	243.5	156	156
Interval Time Step Durations (days)	1, 15, 20, 30, 37, 44, 46	1, 15, 20, 30, 37, 44, 46	1, 15, 20, 30, 40, 50	1, 15, 20, 30, 40, 50*
Downtime (days)	40	64	39	--**
Average Soluble Boron Concentration (ppm)	625.5	247.5	652.5	247.5

* This value was set to 59 for Case A.
** This value was set either to 3936 for Cases A-B or 3637 for Cases C-D.

Table 5-18. Operating data for H. B. Robinson fuel assembly

Case	Total Burnup (GWD/MTU)	Moderator Temperature (K)	Moderator Density (g/cm^3)	Fuel Temperature (K)
A	16.02	559	0.7544	743
B	23.81	559	0.7538	830
C	28.47	576	0.7208	883
D	31.66	576	0.7135	923

H. B. Robinson Benchmark Results

The results of the benchmark were compared to the results from SCALE as specified in ORNL/TM-12667.[53] The SCALE sequence used in the calculations was SAS2H/ORIGEN-S analysis sequence and 27-group cross-section library (27BURNUPLIB) of SCALE-4.[53] Two sets of analysis were completed. The first set used the original MCNPX, and the next set used the modified MCNPXc. The results of the benchmark using MCNPX are displayed in Table 5-19, and the results of the benchmark using MCNPXc are displayed in Table 5-20.

Table 5-19. The H. B. Robinson Benchmark results* using MCNPX compared with SCALE.

	Case A 16.02 GWD/MTU		Case B 23.8 GWD/MTU		Case C 28.47 GWD/MTU		Case D 31.66 GWD/MTU	
Isotope	MCNPX	SCALE	MCNPX	SCALE	MCNPX	SCALE	MCNPX	SCALE
^{235}U	0.18	0.60	-3.11	1.40	-11.8	-4.90	-9.66	0.10
^{236}U	-1.62	-1.5	-1.05	-2.20	3.72	2.20	1.18	-0.50
^{238}U	-0.12	0.10	-0.60	-0.60	0.47	0.50	-0.73	-0.20
^{237}Np	-10.57	1.50	-8.09	0.90	-14.72	-6.50	-10.69	-0.40
^{238}Pu	-6.35	7.00	-6.41	7.70	-9.22	5.30	-8.66	8.20
^{239}Pu	-3.19	-1.5	-4.75	-4.20	-5.42	-4.90	-6.52	-3.70
^{240}Pu	-1.23	5.90	-1.45	6.00	-11.03	0.50	-8.79	5.4
^{241}Pu	-8.23	6.00	-6.30	5.50	2.43	14.30	3.08	11.10
^{99}Tc	7.74	12.40	4.20	8.60	9.58	14.60	5.53	11.70
^{137}Cs	-3.10	0.20	-3.10	-0.80	-0.38	3.90	-3.09	1.2

*Percent difference from measured experimental results [(Calculated/Measured -1)*100].

The results displayed in 5-18 exhibits the same trend in burnup and predictive capability as the MCNPX results for the OECD/NEA Burnup Credit Phase IB. As burnup increases, nuclide predictive capability gets worse and the calculated values seem not as close to the actual

measured calculation. For example, the calculation percent difference from experiment for most actinides for Cases A-B was <8%; however, at higher burnups, Cases C-D, the calculation percent difference from experiment grew to 14%. Though the SCALE values and the MCNPX values seemed relatively close in magnitude, further calculations were also completed using MCNPXc to see the magnitude of improvement. In Table 5-19, the results show significant improvement in actinide prediction for uranium and plutonium isotopes when utilizing MCNPXc.

Table 5-20. The H. B. Robinson Benchmark results* using MCNPXc compared with SCALE.

	Case A		Case B		Case C		Case D	
	16.02 GWD/MTU		23.8 GWD/MTU		28.47 GWD/MTU		31.66 GWD/MTU	
Isotope	MCNPXc	SCALE	MCNPXc	SCALE	MCNPXc	SCALE	MCNPXc	SCALE
^{235}U	0.47	0.60	-0.58	1.40	-8.19	-4.90	-5.35	0.10
^{236}U	-1.81	-1.5	-1.90	-2.20	2.77	2.20	0.57	-0.50
^{238}U	0.12	0.10	-0.54	-0.60	0.53	0.50	-0.73	-0.20
^{237}Np	-6.63	1.50	-7.31	0.90	-11.21	-6.50	-7.41	-0.40
^{238}Pu	-4.125	7.00	-3.86	7.70	-3.29	5.30	-1.89	8.20
^{239}Pu	-0.005	-1.5	-0.37	-4.20	-0.38	-4.90	-0.52	-3.70
^{240}Pu	4.013	5.90	0.59	6.00	-6.94	0.50	-3.66	5.4
^{241}Pu	2.4	6.00	2.82	5.50	1.88	14.30	1.36	11.10
^{99}Tc	10.815	12.40	6.76	8.60	12.13	14.60	8.49	11.70
^{137}Cs	-1.152	0.20	-1.88	-0.80	0.67	3.90	-1.81	1.2

*Percent difference from measured experimental results [(Calculated/Measured -1)*100].

The possible reasons for error in the calculation are similar to those mentioned in the OECD/NEA Burnup Credit Phase IB benchmark. Errors in nuclear data, treatment of normalization parameters, statistical variance in reaction rates, and not modeling a critical spectrum all contribute to errors in the calculation. It is important to note that the same time step durations were also used for each of the cases. Therefore each case was modeled using different size burnup steps. The coefficients for the depletion calculation were therefore updated over longer burnup steps for the higher burnup cases. Therefore these results also suggest that the longer burnup step durations used for the higher burnup cases may have been too large to assume

that significant change in the flux had not occurred over the time step. As mentioned previously, selecting adequate time steps depends upon the buildup and depletion of highly absorbing isotopes that affect the neutron spectrum in the material. Therefore, as is displayed in the results, the prior statement may be further translated to mean that adequate time selection is not just related to resident time but also related to the combination of resident time and operating power over that time, or burnup. However, for Cases A-B, the percent difference in actinide prediction from measured experiment is <4% except for Np-237 which is superior to the SCALE calculation. These results therefore suggest that MCNPX is very capable of modeling full assembly behavior and accurately predicting nuclide buildup as long as adequate burnup step durations are maintained.

Another important source of error to consider is that the measured data also possess error as a function of the precision and accuracy of the measurement process. Unfortunately, the measurement error for this benchmark does not exist. The Spent Fuel Isotopic Composition database posted on the NEA website also does not contain measurement error for any of the 14 available experimental benchmarks.[97] Most of the reports used to generate the database do contain the methods of radiochemical analysis applied to extract the experimental data; however, these reports do not contain a quantification of the error associated in obtaining the measured data. This problem of not listing experimental error therefore must be addressed in future benchmarks in order to understand the validity of calculated results when compared to the measured data.

OECD/NEA Burnup Credit Phase IVB Benchmark Specification

Both the OECD/NEA Burnup Credit Phase IB benchmark and H. B. Robinson benchmark modeled typical PWR uranium dioxide fuel operating conditions. In order to prove the versatility of the of the MCNPX depletion methodology for different types of reactors, another

operating scenario, besides a typical PWR uranium dioxide fuel operating strategy, was investigated. The OECD/NEA Burnup Credit Phase IVB benchmark offers a suite of benchmark calculations for mixed oxide fuel (MOX).[54] MOX assembly modeling is important to a closed reactor fuel cycle because the recycled assembly will contain a combination of uranium and plutonium (and possibly other actinides) at BOL for the recycled assembly.[9] Calculations of the OECD/NEA Burnup Credit Phase IVB benchmark have been completed with many different depletion codes, and therefore an adequate comparison database is available for the benchmark.[54]

Table 5-21. Fuel assembly design data for OECD/NEA Burnup Credit Phase IVB Benchmark.

Parameter	Data
Assembly general data	
Lattice	17× 17
Number of fuel rods	264
Number of guide tubes	24
Number of instrument tubes	1
Fuel rod data	
Type of fuel pellet	MOX
Rod pitch	1.26 cm
Clad thickness	0.065 cm (no gap between fuel and clad)
Pellet diameter	0.410 cm
Active fuel length	365.76 cm
Fuel temperature	900 K
Clad temperature	620 K
Clad material	Zircaloy-2
Guide and Instrument tube data	
Inner radius	0.571 cm
Outer radius	0.613 cm
Material	Zircaloy-2

Modeling a single infinitely reflected MOX fuel assembly does not adequately represent the true reactor operating conditions of the assembly. Many neutronic characteristics of the MOX assembly limit the assembly's placement to certain patterns within certain sections of the reactor core. The higher absorption cross sectiond of the plutonium isotopes, limits the negative reactivity worth of control material, such as dissolved boron or control blades, in the presence of the MOX assembly. The high fission cross section of Pu-239 and large initial loading of Pu-239

produces large fission peaks; therefore to accommodate this affect and flatten the power peak, MOX assemblies are placed away from water gap regions.[9] Finally, the fact that Pu-239 possesses a smaller delayed neutron fraction ($\beta = 0.0021$) and shorter neutron lifetime ($l = 27\mu s$), than U-235 ($\beta=0.0065$, $l = 47\mu s$), thus limiting controllability of kinetic response, limits the amount of MOX assemblies placed in the reactor core.[9] Countries already implementing the MOX fuel cycle, such as France, limit the amount of MOX loading to no more than 30%, and never load MOX assemblies surrounded by other MOX assemblies.[9] However, since the H. B. Robinson benchmark only offered code-to-code comparison with SCALE, the author decided to use the OECD/NEA Burnup Credit Phase IVB benchmark as a comparison tool, knowing that modeling a infinitely reflected MOX assembly would not model true reactor behavior, because the benchmark offered data from a variety of codes for adequate code-to-code comparison for MOX assembly modeling strategy.

Table 5-22. Initial MOX fuel composition for Case A for Phase IVB Benchmark.

	Values Expressed in (atoms/b-cm)		
Nuclide	High Enrichment	Medium Enrichment	Low Enrichment
^{234}U	2.57E-07	2.64E-07	2.68E-07
^{235}U	5.38E-05	5.53E-05	5.60E-05
^{238}U	2.12E-02	2.18E-02	2.21E-02
^{238}Pu	5.17E-05	3.61E-05	2.85E-05
^{239}Pu	1.13E-03	7.87E-04	6.20E-04
^{240}Pu	5.35E-04	3.74E-04	2.95E-04
^{241}Pu	1.94E-04	1.36E-04	1.07E-04
^{242}Pu	1.46E-04	1.02E-04	8.06E-05
^{16}O	4.66E-02	4.66E-02	4.65E-02

Two types of infinitely reflected 17 X 17 MOX fuel assemblies were modeled. Each modeled case assembly was composed of MOX fuel pellets encased in Zircaloy-2 clad fuel pins along with Zircaloy-2 guide tubes. The geometry specifications for both cases are given in Table 5-21. The Case A model included a MOX assembly possessing plutonium nuclide concentrations consistent with typical concentrations expected from a first recycle PWR

assembly. The Case B model included a MOX assembly possessing plutonium nuclide concentrations consistent with typical concentrations expected from weapons disposition material.

Table 5-23. Initial MOX fuel composition for Case B for Phase IVB Benchmark.

	Values Expressed in (atoms/b-cm)		
Nuclide	High Enrichment	Medium Enrichment	Low Enrichment
^{234}U	2.69E-07	2.73E-07	2.75E-07
^{235}U	5.63E-05	5.71E-05	5.74E-05
^{238}U	2.22E-02	2.25E-02	2.26E-02
^{238}Pu	5.09E-07	3.56E-07	2.81E-07
^{239}Pu	9.49E-04	6.64E-04	5.23E-04
^{240}Pu	6.06E-05	4.24E-05	3.34E-05
^{241}Pu	3.02E-06	2.11E-06	1.66E-06
^{242}Pu	5.01E-07	3.50E-07	2.76E-07
^{16}O	4.65E-02	4.65E-02	4.65E-02

For each case, three types of plutonium concentration loadings were used for the fuel pins within each case. Table 5-22 lists the fuel compositions for Case A, and Table 5-23 lists the fuel composition for Case B. Table 5-24 lists the borated water composition and Table 5-25 lists the Zircaloy-2 composition used for the fuel clad and guide tubes. Figure 5-3 displays the distribution of the different fuel pins throughout the fuel assembly for both cases. Each steady-state reaction rate case was completed using 4000 particles per cycle skipping the first 25 cycles for 155 cycles. Initial source locations were placed within each fissile cell location. Case A was burned at 17.896 MW, and Case B was burned at 17.862 MW. The operating data for the assembly is listed in Table 5-26.

Table 5-24. Borated water composition for Phase IVB Benchmark (660ppm boron, density 0.7245 g/cm^3).

Nuclide	Number Density (atoms/b-cm)
^{1}H	4.8414E-02
^{16}O	2.4213E-02
^{10}B	4.7896E-06
^{11}B	1.9424E-05

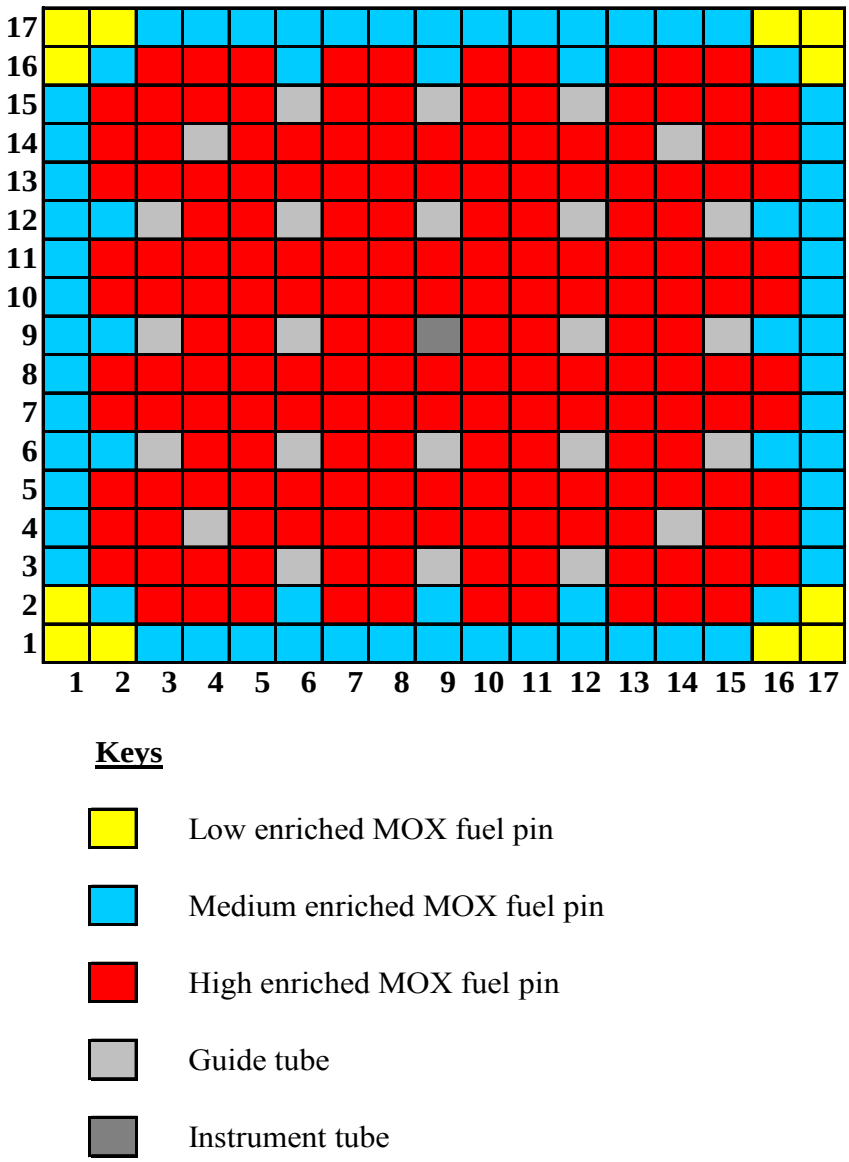

Figure 5-3. MOX fuel enrichment map for Phase IVB Benchmark.

Table 5-25. Zicaloy-2 composition used for clad and guide tube material for Phase IVB Benchmark (density 5.8736 g/cm^3).

Nuclide	(Atoms/b-cm)
^{50}Sn	2.9656E-06
^{52}Sn	5.7189E-05
^{53}Sn	6.4848E-06
^{54}Sn	1.6142E-06
^{54}Fe	7.8122E-06
^{56}Fe	1.2245E-04
^{57}Fe	2.8278E-06
^{58}Fe	3.7633E-07
^{90}Zr	1.9889E-02
^{91}Zr	4.3373E-03
^{92}Zr	6.6297E-03
^{94}Zr	6.7186E-03
^{96}Zr	1.0824E-03

Table 5-26. Operating data for Phase IVB Benchmark.

Cycle	1	2	3
Operating Interval (days)	420	420	420
Interval Time Step Durations (days)	1, 15, 20, 30, 50, 60, 60, 60, 60, 64	1, 15, 20, 30, 50, 60, 60, 60, 60, 64	1, 15, 20, 30, 50, 60, 60, 60, 60, 64
Downtime (days)	30	30	0, 1826.25

OECD/NEA Burnup Credit Phase IVB Benchmark Results

The OECD/NEA Burnup Credit Phase IVB benchmark offers cycle by cycle nuclide buildup and depletion information for a plethora of actinides and fission products. Table 5-27, Table 5-28, Table 5-29 and Table 5-30 present the MCNPX EOC 1, 2, 3 and after 5 years of cooling results for Case A as compared to the range of values achieved from other depletion codes in the benchmark. Table 5-31, Table 5-32, Table 5-33 and Table 5-34 present the MCNPX EOC 1, 2, 3 and after 5 years of cooling results for Case B as compared to the range of values achieved from other depletion codes in the benchmark. Due to the success in nuclide prediction of MCNPXc, each of these cases were run using MCNPXc.

Table 5-27. EOC 1 results for Case A of the Phase IVB Benchmark.

Nuclide	MCNPX (atoms/b-cm)	Range of Values from Other Depletion Codes (atoms/b-cm)
^{234}U	5.8483E-07	2.1279E-07 to 5.8216E-07
^{235}U	4.3753E-05	4.3720E-05 to 4.3925E-05
^{236}U	2.6406E-06	2.4858E-06 to 2.6190E-06
^{238}U	2.1134E-02	2.1155E-02 to 2.1163E-02
^{238}Pu	4.1533E-05	4.0713E-05 to 4.1630E-05
^{239}Pu	8.0377E-04	7.9700E-04 to 8.1275E-04
^{240}Pu	4.7370E-04	4.7109E-04 to 4.8300E-04
^{241}Pu	2.1855E-04	2.1520E-04 to 2.2011E-04
^{242}Pu	1.6393E-04	1.3389E-04 to 1.3785E-04
^{237}Np	1.6176E-06	1.0400E-07 to 1.6560E-06
^{241}Am	9.4895E-06	8.4140E-06 to 8.8762E-06
^{243}Am	1.8069E-05	1.5613E-05 to 1.8260E-05
^{242}Cm	9.5381E-07	8.7154E-07 to 9.8523E-07
^{243}Cm	1.3915E-08	1.1641E-08 to 1.4560E-08
^{244}Cm	5.3807E-06	2.6688E-06 to 3.9610E-06
^{245}Cm	2.8581E-07	1.2915E-07 to 1.9877E-07
^{95}Mo	1.2829E-05	1.1690E-05 to 1.7651E-05
^{99}Tc	2.1958E-05	2.1756E-05 to 2.3060E-05
^{101}Ru	2.2331E-05	2.1640E-05 to 2.3054E-05
^{103}Rh	2.0106E-06	1.9630E-05 to 2.2642E-05
^{109}Ag	5.0294E-06	4.6603E-06 to 5.9460E-06
^{133}Cs	2.4605E-05	2.3463E-05 to 2.4597E-05
^{143}Nd	1.5949E-05	1.5350E-05 to 1.6594E-05
^{145}Nd	1.1238E-05	1.1183E-05 to 1.1518E-05
^{147}Sm	8.0947E-07	7.8960E-07 to 8.2700E-07
^{149}Sm	4.2895E-07	3.7767E-07 to 4.3945E-07
^{150}Sm	4.7391E-06	4.7807E-06 to 5.1050E-06
^{151}Sm	1.3397E-06	1.3420E-06 to 1.5281E-06
^{152}Sm	2.7837E-06	2.7790E-06 to 3.1530E-06
^{153}Eu	2.0936E-06	2.0380E-06 to 2.2411E-06
^{155}Gd	8.6977E-09	4.3940E-09 to 1.6769E-08

Table 5-28. EOC 2 results for Case A of the Phase IVB Benchmark.

Nuclide	MCNPX (atoms/b-cm)	Range of Values from Other Depletion Codes (atoms/b-cm)
^{234}U	8.0735E-07	1.7413E-07 to 8.4354E-07
^{235}U	3.4593E-05	3.4500E-05 to 3.4893E-05
^{236}U	4.6979E-06	4.4215E-06 to 4.6370E-06
^{238}U	2.0896E-02	2.0910E-02 to 2.0927E-02
^{238}Pu	3.9782E-05	3.5013E-05 to 3.9340E-05
^{239}Pu	6.3728E-04	6.2980E-04 to 6.5524E-04
^{240}Pu	4.4837E-04	4.4499E-04 to 4.6350E-04
^{241}Pu	2.3731E-04	2.3210E-04 to 2.3979E-04
^{242}Pu	1.7027E-04	1.4147E-04 to 1.4982E-04
^{237}Np	3.1341E-06	3.6114E-07 to 3.2139E-06
^{241}Am	1.5907E-05	1.4680E-05 to 1.5982E-05
^{243}Am	2.9191E-05	2.7797E-05 to 3.1620E-05
^{242}Cm	2.5536E-06	2.3253E-06 to 2.6204E-06
^{243}Cm	7.2443E-08	5.8709E-08 to 7.0660E-08
^{244}Cm	1.7168E-05	9.2778E-06 to 1.3050E-05
^{245}Cm	1.7035E-06	8.1985E-07 to 1.2348E-06
^{95}Mo	2.9454E-05	2.8330E-05 to 3.4297E-05
^{99}Tc	4.1886E-05	4.1811E-05 to 4.4400E-05
^{101}Ru	4.3865E-05	4.2320E-05 to 4.5186E-05
^{103}Rh	4.0075E-05	3.7469E-05 to 4.0914E-05
^{109}Ag	9.0959E-06	8.0989E-06 to 1.0640E-05
^{133}Cs	4.6303E-05	4.4403E-05 to 4.6602E-05
^{143}Nd	3.0328E-05	2.9970E-05 to 3.1809E-05
^{145}Nd	2.1678E-05	2.1322E-05 to 2.2191E-05
^{147}Sm	2.1430E-06	2.4130E-06 to 2.4742E-06
^{149}Sm	4.0373E-07	3.5930E-07 to 4.1990E-07
^{150}Sm	1.0296E-05	1.0197E-05 to 1.1350E-05
^{151}Sm	1.5541E-06	1.5306E-06 to 1.8870E-06
^{152}Sm	4.9712E-06	5.0468E-06 to 5.9850E-06
^{153}Eu	4.9325E-06	5.0480E-06 to 5.4745E-06
^{155}Gd	1.6016E-08	7.9700E-09 to 2.8935E-08

Table 5-29. EOC 3 results for Case A of the Phase IVB Benchmark.

Nuclide	MCNPX (atoms/b-cm)	Range of Values from Other Depletion Codes (atoms/b-cm)
^{234}U	9.4561E-07	1.4169E-07 to 1.0509E-06
^{235}U	2.6715E-05	2.6596E-05 to 2.7129E-05
^{236}U	6.2239E-06	5.8461E-06 to 6.1140E-06
^{238}U	2.0648E-02	2.0657E-02 to 2.0678E-02
^{238}Pu	4.0397E-05	2.9577E-05 to 3.9688E-05
^{239}Pu	5.0933E-04	5.0368E-04 to 5.3435E-04
^{240}Pu	4.1054E-04	4.0836E-04 to 4.2870E-04
^{241}Pu	2.3785E-04	2.3107E-04 to 2.4058E-04
^{242}Pu	1.8086E-04	1.5231E-04 to 1.6558E-04
^{237}Np	4.3966E-06	6.9348E-07 to 4.5652E-06
^{241}Am	1.8127E-05	1.7960E-05 to 2.0066E-05
^{243}Am	3.6401E-05	3.6793E-05 to 4.2000E-05
^{242}Cm	4.3963E-06	3.5650E-06 to 4.0436E-06
^{243}Cm	1.5834E-07	1.2551E-07 to 1.4820E-07
^{244}Cm	3.1800E-05	1.8435E-05 to 2.4950E-05
^{245}Cm	4.1506E-06	2.1928E-06 to 3.2335E-06
^{95}Mo	4.3988E-05	4.3990E-05 to 4.9929E-05
^{99}Tc	5.9641E-05	6.0068E-05 to 6.3850E-05
^{101}Ru	6.4487E-05	6.1990E-05 to 6.6364E-05
^{103}Rh	5.3043E-05	5.1041E-05 to 5.5357E-05
^{109}Ag	1.2395E-05	1.0524E-05 to 1.4480E-05
^{133}Cs	6.4706E-05	6.2829E-05 to 6.6172E-05
^{143}Nd	4.2327E-05	4.2830E-05 to 4.5385E-05
^{145}Nd	3.1270E-05	3.0386E-05 to 3.2104E-05
^{147}Sm	3.1679E-06	4.0280E-06 to 4.1579E-06
^{149}Sm	3.2126E-07	3.2302E-07 to 3.8520E-07
^{150}Sm	1.5873E-05	1.5410E-05 to 1.7660E-05
^{151}Sm	1.5666E-06	1.5340E-06 to 2.0110E-06
^{152}Sm	6.3075E-06	6.3335E-06 to 7.9580E-06
^{153}Eu	7.5412E-06	8.1310E-06 to 8.6655E-06
^{155}Gd	1.9499E-08	1.3920E-08 to 4.2299E-08

Table 5-30. Five year cooling time results for Case A of the Phase IVB Benchmark.

Nuclide	MCNPX (atoms/b-cm)	Range of Values from Other Depletion Codes (atoms/b-cm)
^{234}U	2.6607E-06	1.4169E-07 to 2.7220E-06
^{235}U	2.6785E-05	2.6668E-05 to 2.7206E-05
^{236}U	6.4390E-06	5.8461E-06 to 6.2030E-06
^{238}U	2.0648E-02	2.0657E-02 to 2.0678E-02
^{238}Pu	4.3111E-05	2.8432E-05 to 4.1989E-05
^{239}Pu	5.1081E-04	5.0542E-04 to 5.3613E-04
^{240}Pu	4.1585E-04	4.1217E-04 to 4.3260E-04
^{241}Pu	1.8680E-04	1.8167E-04 to 1.8891E-04
^{242}Pu	1.8086E-04	1.5231E-04 to 1.6558E-04
^{237}Np	4.8116E-06	7.0645E-07 to 4.9848E-06
^{241}Am	6.8783E-05	6.6320E-05 to 7.0845E-05
^{243}Am	3.6406E-05	3.6793E-05 to 3.9880E-05
^{242}Cm	2.5594E-09	1.6887E-09 to 5.0942E-09
^{243}Cm	1.4022E-07	1.1143E-07 to 1.2852E-07
^{244}Cm	2.6279E-05	1.5224E-05 to 1.9671E-05
^{245}Cm	4.1491E-06	2.1928E-06 to 3.2321E-06
^{95}Mo	4.9799E-05	4.9929E-05 to 5.0765E-05
^{99}Tc	5.9856E-05	6.0280E-05 to 6.4090E-05
^{101}Ru	6.4487E-05	6.3251E-05 to 6.6366E-05
^{103}Rh	5.6463E-05	5.1041E-05 to 5.8208E-05
^{109}Ag	1.2416E-05	1.0524E-05 to 1.4490E-05
^{133}Cs	6.5257E-05	6.2829E-05 to 6.6172E-05
^{143}Nd	4.3169E-05	4.4116E-05 to 4.5385E-05
^{145}Nd	3.1278E-05	3.0386E-05 to 3.2104E-05
^{147}Sm	7.8905E-06	9.9452E-06 to 1.0734E-05
^{149}Sm	3.6852E-07	3.7494E-07 to 4.2796E-07
^{150}Sm	1.5873E-05	1.5410E-05 to 1.6679E-05
^{151}Sm	1.5196E-06	1.4779E-06 to 1.8916E-06
^{152}Sm	6.3090E-06	6.3335E-06 to 7.9580E-06
^{153}Eu	7.5868E-06	8.1650E-06 to 8.6716E-06
^{155}Gd	3.6011E-07	3.3400E-07 to 1.0081E-06

Table 5-31. EOC 1 results for Case B of the Phase IVB Benchmark.

Nuclide	MCNPX (atoms/b-cm)	Range of Values from Other Depletion Codes (atoms/b-cm)
^{234}U	2.1859E-07	2.1683E-07 to 2.2681E-07
^{235}U	4.2074E-05	4.1730E-05 to 4.2085E-05
^{236}U	3.1619E-06	3.0287E-06 to 3.1900E-06
^{238}U	2.2041E-02	2.2000E-02 to 2.2049E-02
^{238}Pu	1.1757E-06	3.7913E-07 to 7.1826E-07
^{239}Pu	5.6960E-04	5.6280E-04 to 5.7659E-04
^{240}Pu	1.5241E-04	1.4600E-04 to 1.5008E-04
^{241}Pu	6.0895E-05	5.6781E-05 to 6.3800E-05
^{242}Pu	7.1572E-06	5.3572E-06 to 6.1170E-06
^{237}Np	1.5688E-06	1.3364E-07 to 1.6488E-06
^{241}Am	1.6417E-06	1.3107E-06 to 1.4360E-06
^{243}Am	9.6882E-07	6.2689E-07 to 8.0100E-07
^{242}Cm	1.8012E-07	1.5269E-07 to 1.7950E-07
^{243}Cm	2.0951E-09	1.6814E-09 to 2.0300E-09
^{244}Cm	2.4339E-07	9.3251E-08 to 1.3100E-07
^{245}Cm	1.1257E-08	3.4090E-09 to 4.6024E-09
^{95}Mo	1.3153E-05	1.2181E-05 to 1.8204E-05
^{99}Tc	2.1838E-05	2.1900E-05 to 2.2950E-05
^{101}Ru	2.1979E-05	2.1769E-05 to 2.3058E-05
^{103}Rh	2.0336E-05	1.8759E-05 to 2.1765E-05
^{109}Ag	4.3321E-06	3.6778E-06 to 5.5840E-06
^{133}Cs	2.4560E-05	2.3439E-05 to 2.4574E-05
^{143}Nd	1.5453E-05	1.5100E-05 to 1.6346E-05
^{145}Nd	1.0969E-05	1.1117E-05 to 1.1454E-05
^{147}Sm	7.6879E-07	7.6500E-07 to 7.8701E-07
^{149}Sm	2.3529E-07	1.9930E-07 to 2.2432E-07
^{150}Sm	4.7705E-06	4.9051E-06 to 5.2700E-06
^{151}Sm	8.6623E-07	8.8308E-07 to 1.0200E-06
^{152}Sm	2.8949E-06	2.9600E-06 to 3.3370E-06
^{153}Eu	2.0836E-06	2.0570E-06 to 2.2659E-06
^{155}Gd	4.5104E-09	1.8000E-09 to 7.6886E-09

Table 5-32. EOC 2 results for Case B of the Phase IVB Benchmark.

Nuclide	MCNPX (atoms/b-cm)	Range of Values from Other Depletion Codes (atoms/b-cm)
^{234}U	1.8049E-07	1.7098E-07 to 1.9333E-07
^{235}U	2.9106E-05	2.8760E-05 to 2.9257E-05
^{236}U	5.5884E-06	5.3234E-06 to 5.5600E-06
^{238}U	2.1773E-02	2.1767E-02 to 2.1800E-02
^{238}Pu	2.6720E-06	2.9817E-07 to 2.0587E-06
^{239}Pu	3.7031E-04	3.6608E-04 to 3.8300E-04
^{240}Pu	1.8694E-04	1.8070E-04 to 1.8624E-04
^{241}Pu	9.7981E-05	9.4093E-05 to 1.0080E-04
^{242}Pu	2.2218E-05	1.9550E-05 to 2.1840E-05
^{237}Np	3.0365E-06	4.5945E-07 to 3.1897E-06
^{241}Am	4.1152E-06	3.6692E-06 to 3.9280E-06
^{243}Am	4.3621E-06	3.6612E-06 to 4.7300E-06
^{242}Cm	8.9769E-07	7.7886E-07 to 8.9591E-07
^{243}Cm	4.3621E-06	1.6565E-08 to 2.0900E-08
^{244}Cm	1.8948E-06	1.0277E-06 to 1.4100E-06
^{245}Cm	1.4495E-07	6.0866E-08 to 8.6913E-08
^{95}Mo	2.9951E-05	2.9300E-05 to 3.5096E-05
^{99}Tc	4.1181E-05	4.1730E-05 to 4.3780E-05
^{101}Ru	4.3022E-05	4.2699E-05 to 4.5057E-05
^{103}Rh	3.5805E-05	3.3166E-05 to 3.7099E-05
^{109}Ag	7.7718E-06	6.5223E-06 to 9.7410E-06
^{133}Cs	4.5646E-05	4.3917E-05 to 4.6063E-05
^{143}Nd	2.8262E-05	2.8500E-05 to 3.0200E-05
^{145}Nd	2.0952E-05	2.1048E-05 to 2.1882E-05
^{147}Sm	1.9461E-06	2.2520E-06 to 2.2924E-06
^{149}Sm	2.0460E-07	1.7336E-07 to 1.9700E-07
^{150}Sm	1.0170E-05	1.0500E-05 to 1.1600E-05
^{151}Sm	8.4275E-07	8.4937E-07 to 1.0900E-06
^{152}Sm	4.7605E-06	4.8514E-06 to 5.9030E-06
^{153}Eu	4.8992E-06	5.1650E-06 to 5.5763E-06
^{155}Gd	9.7191E-09	3.8100E-09 to 1.1850E-08

Table 5-33. EOC 3 results for Case A of the Phase IVB Benchmark.

Nuclide	MCNPX (atoms/b-cm)	Range of Values from Other Depletion Codes (atoms/b-cm)
^{234}U	1.1520E-13	1.3174E-07 to 1.7954E-07
^{235}U	1.8445E-05	1.8119E-05 to 1.8791E-05
^{236}U	7.1794E-06	6.8091E-06 to 7.0700E-06
^{238}U	2.1481E-02	2.1467E-02 to 2.1500E-02
^{238}Pu	5.5067E-06	2.2123E-07 to 4.7927E-06
^{239}Pu	2.5259E-04	2.4767E-04 to 2.7200E-04
^{240}Pu	1.8124E-04	1.7470E-04 to 1.8437E-04
^{241}Pu	1.0690E-04	1.0323E-04 to 1.0850E-04
^{242}Pu	4.3597E-05	3.9815E-05 to 4.3080E-05
^{237}Np	4.1982E-06	8.5608E-07 to 4.4424E-06
^{241}Am	4.9089E-06	4.9773E-06 to 5.4746E-06
^{243}Am	1.0121E-05	9.3994E-06 to 1.1700E-05
^{242}Cm	1.9925E-06	1.5821E-06 to 1.8030E-06
^{243}Cm	6.2628E-08	4.8232E-08 to 5.9200E-08
^{244}Cm	6.7113E-06	4.1608E-06 to 5.4200E-06
^{245}Cm	6.6887E-07	3.2603E-07 to 4.7115E-07
^{95}Mo	4.4224E-05	4.5000E-05 to 5.0570E-05
^{99}Tc	5.7742E-05	5.9218E-05 to 6.2220E-05
^{101}Ru	6.2895E-05	6.2300E-05 to 6.5908E-05
^{103}Rh	4.3988E-05	4.2315E-05 to 4.7011E-05
^{109}Ag	1.0536E-05	8.5551E-06 to 1.2920E-05
^{133}Cs	6.2697E-05	6.1230E-05 to 6.4442E-05
^{143}Nd	3.7203E-05	3.8700E-05 to 4.0746E-05
^{145}Nd	2.9770E-05	2.9641E-05 to 3.1166E-05
^{147}Sm	2.7210E-06	3.5820E-06 to 3.6688E-06
^{149}Sm	1.2934E-07	1.4821E-07 to 1.6900E-07
^{150}Sm	1.5432E-05	1.5880E-05 to 1.7900E-05
^{151}Sm	7.8954E-07	8.0820E-07 to 1.1000E-06
^{152}Sm	5.6451E-06	5.7314E-06 to 7.4850E-06
^{153}Eu	7.1295E-06	7.9849E-06 to 8.6528E-06
^{155}Gd	8.0878E-09	6.3000E-09 to 1.5641E-08

Table 5-34. Five year cooling time results for Case B of the Phase IVB Benchmark.

Nuclide	MCNPX (atoms/b-cm)	Range of Values from Other Depletion Codes (atoms/b-cm)
^{234}U	4.4485E-07	1.3174E-07 to 4.1870E-07
^{235}U	1.8480E-05	1.8119E-05 to 1.8830E-05
^{236}U	7.2745E-06	6.9037E-06 to 7.0634E-06
^{238}U	2.1481E-02	2.1467E-02 to 2.1493E-02
^{238}Pu	7.2430E-06	2.1267E-07 to 6.3483E-06
^{239}Pu	2.5476E-04	2.4983E-04 to 2.7284E-04
^{240}Pu	1.8232E-04	1.7540E-04 to 1.8510E-04
^{241}Pu	8.3970E-05	8.1013E-05 to 8.5710E-05
^{242}Pu	4.3597E-05	3.9817E-05 to 4.3090E-05
^{237}Np	4.3965E-06	8.7398E-07 to 4.6418E-06
^{241}Am	2.7709E-05	2.6942E-05 to 2.8303E-05
^{243}Am	1.0125E-05	9.3994E-06 to 1.0616E-05
^{242}Cm	9.8698E-10	7.5522E-10 to 1.4676E-09
^{243}Cm	5.5486E-08	4.2821E-08 to 5.1277E-08
^{244}Cm	5.5500E-06	3.4362E-06 to 3.8927E-06
^{245}Cm	6.6887E-07	3.2603E-07 to 4.7096E-07
^{95}Mo	5.0010E-05	5.0570E-05 to 5.1528E-05
^{99}Tc	5.7945E-05	5.9428E-05 to 6.2460E-05
^{101}Ru	6.2895E-05	6.2654E-05 to 6.5909E-05
^{103}Rh	4.7293E-05	4.2315E-05 to 4.9970E-05
^{109}Ag	1.0552E-05	8.5551E-06 to 1.2940E-05
^{133}Cs	6.3248E-05	6.1230E-05 to 6.4442E-05
^{143}Nd	3.8029E-05	3.9608E-05 to 4.0746E-05
^{145}Nd	2.9778E-05	2.9642E-05 to 3.1176E-05
^{147}Sm	6.8077E-06	8.7798E-06 to 9.5399E-06
^{149}Sm	1.7692E-07	2.0516E-07 to 2.2260E-07
^{150}Sm	1.5432E-05	1.5880E-05 to 1.7344E-05
^{151}Sm	7.7139E-07	7.7864E-07 to 9.9180E-07
^{152}Sm	5.6451E-06	5.7314E-06 to 7.4860E-06
^{153}Eu	7.1797E-06	7.9849E-06 to 8.7110E-06
^{155}Gd	3.3990E-07	3.2182E-07 to 9.2307E-07

In both cases, for most actinides and fission products, values were predicted within the range of values of the other depletion codes available in the benchmark. General trends of buildup and depletion also fit the data from other depletion codes available in the benchmark. However, the buildup of Cm isotopes is larger in both Cases A and B as compared to other depletion codes. Since this benchmark is code-code comparison benchmark, deviation from

expected buildup must be the result of methodology or utilized data differences. First of all, though metastable isotope representation is available in MCNPX, for this benchmark, metastable isotopes were not tracked in particle transport. However, historically in the data releases for the MCNP codes, ^{242m}Am has been listed with a zaid of 95242 instead of the 95642 as expected from equations 3-9 and 3-10. As a result of the heritage of the data release, MCNPX depletion expects Am-242m to be listed as 95242; however, the cross sections for these calculations were generated by an external source that decided to generate ^{242}Am as 95242. The end result of this confusion is that in particle transport reaction rates were calculated for 95242 using the ^{242}Am cross sections; however, these reaction rates were converted into destruction and creation coefficients for ^{242m}Am, and the 63-group match approach was used to generate coefficients for ^{242}Am. The isomer and the ground state isotope do posses different reaction rate probabilities; ^{242m}Am has a long half life (141 years) and a larger resonance integral in the harder MOX spectrum as compared to the ground state ^{242}Am. ^{242m}Am either fissions, possessing a large fission cross section, or captures a neutron to become Am-243, which decays to Cm-243. The nuclide Am-242 decays quickly to Cm-242 which then decays to Pu-238. ^{242}Am has a higher capture-to-fission ratio than ^{242m}Am and a larger radiative capture resonance integral in the harder MOX spectrum; therefore, using the ^{242}Am cross section instead of ^{242m}Am will lead to more captures resulting in greater production of Cm-243 Cm-244 and Cm-245. This hypothesis seems to be validated by the fact that Cm-243, Cm -244 and Cm-245 seem to be predicted higher than the range of values. Other possible hypothesized differences in calculation may result from the CINDER90 depletion algorithm. Further working of the CINDER90 algorithm will be required in order to validate the latter hypothesis. The results do, however, suggest good

agreement with the other available depletion codes, and do show that MCNPX is capable of modeling MOX fuel assemblies.

Further Considerations

In the analyzed benchmarks either single pin or single assembly geometries were analyzed. Reflective boundary conditions were assumed for each boundary of the examined geometries. In a real reactor operating scenario, net current at the pin or assembly boundary is never zero. Therefore in order to truly test the validity of the methodology for a certain application, a full core analysis would be required. In order to preserve exact accuracy, a full core analysis involves detailed initial isotope and operation data. Most commercial data, at this level of detail, is proprietary and for the moment unavailable to the general public.

Another major issue to consider is that the NEA only has available accepted benchmark data for roughly 14 LWRs. The necessary measured data to test a depletion methodology versus more complicated reactor designs is not readily available or yet to be validated. Development of time-dependent nuclear reactor experiments and the radiochemical analysis involved in exacting isotope concentrations for analysis is expensive. Unfortunately, this concern has limited the amount of available benchmark data for advanced reactor designs. However, as the United States attempts to meet the initiatives of the GNEP program and develop further advanced reactor technologies, experiments should be developed, and valuable data should be extracted, leading to a plethora of new benchmarks to prove the viability of advanced methodologies.

CHAPTER 6
CONCLUSIONS AND SUMMARY

The MCNPX depletion capability offers complete, relatively easy-to-use depletion calculations in a single, well established, radiation transport Monte Carlo code. The capability links the well-established MCNPX steady-state reaction rate calculator to the CINDER90 temporal nuclide inventory calculator. MCNPX is not limited by typical approximations utilized in deterministic methodologies. The MCNPX steady-state reaction rate calculator implements 3-dimensional continuous energy Monte Carlo in order to determine true interaction rate behavior for any type of material and geometry combination. The use of CINDER90 allows for the most potential robustness in modeling capability because the Linear Markov Chain method does not rely upon parsing a matrix into a solvable form and approximating depletion behavior of certain nuclides. CINDER90 simply casts the set of coupled depletion equations into sets of linear transmutation chains, solving each chain for partial nuclide densities, and then summing those nuclide densities to determine total nuclide concentrations. This algorithm allows any type of depletion system, fast burning or slow burning, to be modeled exactly. This work differs from prior efforts in Monte Carlo linked depletion development in that the capability has been incorporated into a widely used and accepted radiation transport package. Each feature implemented in the methodology has been tested in order to provide adequate justification for implementation instead of simply arbitrarily incorporating methodologies for the sake of linking to independent code packages. This capability attempts to track as many nuclides as data permits while tracking all important reaction rates, and accounting for average interaction rate behavior in order to achieve a highly accurate depletion solution that attempts to account for true system physics behavior.

Accomplishments

Many features have been implemented into the methodology and tested in order to enhance the versatility of the capability as compared to other available code packages. The following features were accomplished as part of this work:

1. A comprehensive input structure that gives the user versatility in modeling capability was developed.

2. An organized easy to understand output structure that groups data in terms of average system parameters and individual burn material data was provided.

3. Isotope tracking was simplified by providing predefined fission product tier sets which contain all available fission products containing ENDF/B VII.0 transport cross sections as well as CINDER90 fission yield information. Testing demonstrated that implementing the maximum amount of fission products better mimics the results of the benchmarked MONTEBURNS depletion code.

4. A mechanism was developed for automatically determining and tracking all immediate daughter reaction isotopes.

5. A capability was created in order to allow the user to manually adjust the concentration of any nuclide at any time step by specifying the atom fraction, weight fraction, atom density or weight density of the nuclide to be changed.

6. A structure was engineered for including available metastable isotopes in continuous energy reaction rate tracking and transforming that the nuclide's information for use in the depletion calculation in CINDER90.

7. A methodology was established for tracking in continuous energy the (n, fission), (n,γ), (n,2n), (n,3n), (n,p), and (n,α) interaction rates for predefined nuclides. Testing has demonstrated that the inclusion of these reaction rates, for a simple pin cell calculation, demonstrates improvement in actinide predictability as compared to simply tracking (n, fission) and (n,γ).

8. A methodology was conceived for determining system averaged flux normalization parameters used in determining global neutron source, which is also used in calculating the total magnitude of the flux. This capability was further augmented to work with the repeated structures feature in MCNPX.

9. An algorithm was developed to automatically determin the proper energy dependent fission yield to be used in a given burn material by determining the energy band containing the majority of fission reactions and using that corresponding fission yield.

10. A technique for adjusting depletion coefficients was developed in order to account for average behavior over a given time step by incorporating a cross section averaging technique that utilizes spectra calculation at both the predictor and corrector steps. Two independent methods were tested, and the results demonstrate the MONTEBURNS "like" method achieved similar results to the CELL-2 "like" method, and because the MONTEBURNS "like" method achieved the result incorporating less memory usage, this method was chosen for implementation in MCNPX.

11. The default decay chain convergence criterion for use in CINDER90 was determined based on testing. A keyword value was implemented in order to allow user control of this criteria

Analysis of Benchmark Results

Three different benchmarks were also completed in order to validate the current methodology. The OECD/ NEA Phase IB benchmark results showed that the code was capable of modeling an adjusted fuel-to-moderator ratio pin cell and achieve results within the range of other depletion methodologies. Though the modeled geometry for this benchmark did not account for the true spatial behavior witnessed in the experiment, comparison to experiment did demonstrate ability to achieve adequate results. The H. B. Robinson benchmark demonstrated ability to model real core behavior, of a typical PWR assembly, and achieve accurate results if appropriate burnup steps were implemented. The OECD/ NEA Phase IVB benchmark results demonstrated the ability to model MOX assemblies and achieve the similar results to other depletion methodologies. Though these calculations only represent the ability to model a PWR assembly, uranium-dioxide or MOX fueled, placed in an operating scenario in which the assembly boundaries may be modeled as infinitely reflected, the results do suggest positive evidence that the capability can model depletion systems adequately.

Differences between measured and calculated values, or code-to-code differences, were a result of the following issues: accuracy of the applied nuclear data, treatment of normalization parameters, inadequacy of the implemented time steps, differences in neutron spectra as

compared to a critical spectrum calculation, spatial reactivity effects of the modeled geometry, and statistical variance of the reaction rates and rare events. ENDF/B VII.0 cross sections were utilized in particle transport. Due to the recent availability of this data, the pedigree of the data is not exactly known as it has not been widely tested. The cross sections implemented in the calculation were generated utilizing an automated subroutine with resonance reconstruction tolerances that may or may not be adequate for the applied application. The ENDF/B VII.0 data may also not be complete and therefore may not contain cross section information for every reaction of interest. However, MCNPX depletion assumes that if an isotope is used in particle transport and contains an accessible cross section file, then data must exist for each reaction type. Though the methodology only requires cross section information for (n, fission), (n,γ), (n,2n), (n,3n), (n,p), and (n,α) interactions, it may be possible that some of these reactions do not exist in the cross section data file. Unfortunately, such an instance would result in the code assuming a zero cross section for that reaction type even though a nonzero reaction rate might be available in the CINDER90 library file. Most of the "other depletion code" results were previously generated using ENDF/B IV, V, or VI data and therefore discrepancies in the ENDF/B VII.0 data as compared to these libraries also resulted in differences in calculated values. CINDER90 also contains transmutation cross sections for 3400 nuclides and over 3000 of those nuclides do not contain available ENDF data. Therefore cross section determination codes were used to calculate the data implemented in CINDER90 library file. Unfortunately, the pedigree of the cross section determination code is version dependent and has evolved in accuracy as better models have become available. Therefore the CINDER90 data for these nuclides may have also differed from what is used by other codes leading to further error in calculation when comparing to other tools. Pedigree of this implemented data will only be proven with further benchmarking

and testing. The buildup of Cm isotopes, in the Phase IVB Benchark, was larger for both cases when compared to other depletion codes. Though metastable isotope representation was available in MCNPX, for this benchmark, metastable isotopes were not tracked in particle transport. The confusion in utilizing the ^{242}Am cross section as opposed to the ^{242m}Am resulted in further calculation error. The isomer and the ground state isotope do posses very different reaction rate probabilities. Ground state ^{242}Am has a larger resonance integral over the harder MOX spectrum than ^{242}Am. ^{242}Am also decays into ^{242}Cm which then decays to ^{238}Pu, or fissions. The 1st excited state isomer ^{242m}Am absorbs a neutron and either fissions or becomes ^{243}Am which later becomes other Cm isotopes. Due to the differences in capture-to-fission ratio between the ground and excited states, and the difference in resonance integral over the harder MOX spectrum, the mix up in isomer representation caused more buildup of ^{244}Cm and thus more buildup of ^{245}Cm. The discrepancies in ^{238}Pu production were also probably a function of the misrepresentation of this isomer.

MCNPX determines the global neutron source, for use as a flux normalization constant, by calculating system averaged parameters. Unfortunately, these system average parameters only exist for certain actinides. One example is recoverable energy per fission. Though an energy dependent fission cross section exists for almost every actinide, prompt fission release energy information only exists for 1/3 of all fissionable actinides. For all other actinides, ^{235}U based parameters are assumed in MCNPX depletion. MCNPX depletion currently does account for the true recoverable energy per fission. An approximation is made in order to try and determine the delayed energy contribution by multiplying the prompt fission release energy by a constant that is assumed to account for delayed energy. The delayed energy contribution is unfortunately system dependent. For these benchmarks, however, the geometry modeled was not the actual

experimental geometry, the full core was not modeled, and therefore accounting for the true recoverable energy per fission in the adjusted geometry would not be possible. Also understanding how the delayed energy is deposited involves knowing the emission spectra of that energy and transporting that energy to where it is deposited. As mentioned previously, even for the majority of nuclides containing ENDF/B VII.0 transport cross sections, capture gamma photon emission spectra is unknown. An initial calculation was performed to determine the mass defect integral energy contribution. However, a photon containing the integral energy from the mass defect transports differently than the actual photons spectra generated from the reaction. Therefore due to lack of photon spectra information, the applied constant was deemed most acceptable for accounting for delayed energy contribution, and this constant ultimately affected the solution outcome. For full core modeling at critical, the delayed energy contribution only scales as a function of neutrons emitted per fission therefore this value only changes between 2.43-3 neutrons per fission as function of building up higher actinides, and therefore the delayed energy contribution change should not be very significant as function of burnup for these types of systems.

For each calculation, common time durations using varied powers were implemented in order to burn each of the benchmarks to the required burnups. Unfortunately, this type of burning led to burning the system with varied burnup steps. If reactivity contributing isotope changes density too significantly during a burn step, then it is possible that the constant creation and destruction coefficient approximation is not valid for that time step. The most probable reason for the benchmark calculations achieving poorer predictability for higher burnups was related to the fact that the burnup steps for the higher burnup cases may have been too long in

order to assume the constant coefficient approximation. However, the results for the lower burnup cases did show excellent agreement in code-to-code and experimental comparison.

Each of the modeled geometries did not incorporate an approximation to account for critical spectrum. When the pin or assembly is in the reactor core, the geometry is burned assuming the geometry is in a critical configuration. Therefore the true leakage in and out of the modeled benchmark geometries varies as function of burnup and is not a true reflective boundary condition. In deterministic based codes, critical spectrum is approximated by adjusting the flux by a normalization parameter generated from a buckling adjustment calculation. Not modeling a geometry utilizing the critical spectra will cause the propagation of nuclide generation and depletion to be different from what is expected from the actual geometry because the captures, fissions, and scatters will be different than what is expected from the critical spectrum. Because the system is not modeled accounting for the true operating behavior, the spatial reactivity behavior will also be affected. For the Phase IB Benchmark, the adjusted-fuel-to-moderator ratio pin cell calculation does not account for the true spatial behavior of the reactions because the pin dimensions have been augmented in order to achieve similar global reactivity behavior. However, the actual interaction rate behavior within the pin for each reaction type is not preserved. Therefore the evolution of the temporal nuclide inventory will be in error as the true reaction rates differ from the calculation. Even in the H. B. Robinson and Phase IVB benchmarks, where a full assembly was modeled, true interaction rate behavior is not preserved because the reflective boundary condition is not indicative of the expected leakage condition for those assemblies during actual reactor operation. Only modeling the full reactor, with the actual operating conditions will achieve the most accurate result.

Most codes, deterministic/Monte Carlo based, have historically had issues in calculated ^{237}Np concentration as well as other downstream nuclides produced from the ^{237}Np transmutation path. As determined from the previous testing, ^{237}Np and therefore ^{238}Pu predictability is improved by accounting for the energy integrated collision rate of (n,2n) reactions (i. e. $^{238}U + n \rightarrow 2n + ^{237}U$; $^{237}U \rightarrow ^{237}Np$; $^{237}Np + n \rightarrow ^{238}Np \rightarrow ^{238}Pu$ (rare event!) or $^{239}Pu + n \rightarrow ^{238}Pu + 2n$ (very rare event!). It also possible to form ^{237}Np from either $^{235}U + n \rightarrow$ no fission $\rightarrow ^{236}U$; $^{236}U + n \rightarrow ^{237}U \rightarrow ^{237}Np$ (only account for 10-20% of reactions with ^{235}U) or alpha decay from ^{241}Am (rare event due to long half life). ^{238}Pu is also formed from decay of $^{242m}Am \rightarrow ^{242}Cm \rightarrow ^{238}Pu$. Where ^{242m}Am is formed from multiple Pu isotope captures. The common theme in the miscalculation of these isotopes is related to properly sampling rare events. Therefore why not try a type of forced reaction type sample? In "Nonanalog Implementations of Monte Carlo Isotope Inventory Analysis," the authors tried to develop a method of stochastically solving the actual depletion equations (instead of just stochastically solving for coefficients to be applied for a deterministic temporal nuclide inventory solution).[99] They tried a forced collision method for sampling rare events (rare interactions), and found that forced collision sampling of rare events for a finite amount of histories decreased the amount of sampled non-rare events leading to an inadequate sampling of non-rare events and ultimately affecting the transmutation path outcome. Forced collision sampling may affect some part of the analyzed problem when an artificial bias is introduced. They found that the only way to really cure this issue was to use more histories. Therefore this evidence suggests that running more histories may fix the problem of sampling rare events and therefore lead to better prediction of rare event isotopes. Further testing of a variety of benchmarks will be required in order to truly validate this hypothesis.

Future Work

Further enhancements to the MCNPX depletion methodology will be required in order to enhance the usefulness of the technology. The current MCNPX 2.6.F depletion method does not currently account for critical spectrum adjustments or posses a method to incorporate thermo hydraulic feedback, which is essential for modeling true system physics.[32] Critical spectrum may be calculated by weighting the impinging reflected leakage flux with the mean free path and continuing to adjust the impinging flux until criticality is reached. More or less weight would be given to a reflected neutron depending upon if the system was initially sub or super critical. This type of calculation would involve tagging and tracking all reflected neutrons that contribute to reactivity. However, this approximation must be thoroughly tested versus a wide variety of benchmarks in order to prove validity of the method. Thermohydraulic feedback may be incorporated into MCNPX by linking MCNPX to a code that takes power distribution data in order to generate temperature distributions. Unfortunately, the calculation of thermohydraulic feedback is an iterative process, because the effects are nonlinear and dependent upon each other, and therefore a computationally expensive process when using Monte Carlo. However, this type calculation is required in order to preserve true system physics. The depletion methodology also does not propagate number density error, or possess functionality to alter the geometry during the burnup.[98] The relative error associated with the isotope concentration calculations are a function of the relative error of the flux used to calculate the collision densities, as well as the isotopes' relative error from the previous calculation. Knowledge of the propagation of the number density error is required in order to understand the precision of the calculated result and therefore must be incorporated in further versions of the capability. The evidence of the benchmark calculations does suggest that further investigation is also required in the passby calculation in the CINDER90 algorithm. Many tests exist for determining progeny generation

and it is possible that the ordering of these tests may affect the solution outcome. However, these issues along with other functionality concerns will be addressed in further development of the capability.

This capability does set up a significant foundation, in a well established and supported radiation transport code, for further development of a Monte Carlo-linked depletion methodology. Such a capability will be essential to the future development of advanced reactor technologies, and detector systems to monitor those reactor technologies, that violate the limitations of current deterministic based methods.

APPENDIX A
SAMPLE INPUT

In the following example, a 4 X 4 fuel pin array is modeled in order to demonstrate the necessary keyword implementation for burning a repeated structure while also utilizing manual concentration changes at specific time steps:

```
...
1   1  6.87812e-2  -1        u=2  imp:n=1 vol=192.287          $ fuel
3   2  4.5854e-2    1 -2     u=2  imp:n=1 vol=66.43    $ clad
4   3  7.1594e-2    2        u=2  imp:n=1 vol=370.82           $ water
6   4  6.87812e-2  -1        u=3  imp:n=1 vol=192.287          $ fuel
7   5  4.5854e-2    1 -2     u=3  imp:n=1 vol=66.43    $ clad
8   6  7.1594e-2     2        u=3  imp:n=1 vol=370.82           $ water
10  0          -3 4 -5 6                u=1  imp:n=1 lat=1 fill=0:1 0:1 0:0
                                        2 3
                                        2 3
...

...
BURN  TIME=50,10,500
     MAT=           1 4
     POWER=      1.0
     PFRAC=       1.0 0 0.2
     OMIT= 1,8,6014,7016,8018,9018,90234,91232,95240,95244
                    4,8,6014,7016,8018,9018,90234,91232,95240,95244
     BOPT= 1.0, -4
     AFMIN= 1e-32
     MATVOL= 384.57 384.57
     MATMOD= 2
                                  1
                                                  1 -4 1 94238 1e-6
                                 2
                                                  2 -1 2 94238 1e-6 94241 1e-6
                                                    -4 1 94238 1e-6
...
```

The following example utilizes a lattice containing universes 2 and 3 which are both repeated twice in the lattice. Universe 2 is comprised of cells 1, 3 and 4, where cell 1 contains material 1, and universe 3 is comprised of cells 6, 7 and 8, where cell 6 contains material 4. The MAT keyword specifies that both materials 1 and 4 will be burned. The combination of the TIME, POWER and PFRAC keywords specify that these materials will be burned first for 50 days at 100% of 1MW, then decayed for 10 days, and then finally burned for 500 days at 20% of 1 MW.

The BOPT keyword specifies that the following options will be invoked: Q-value multiplier = 1.0, tier 1 fission products, output ordered by zaid, the output is printed at the end of each kcode run and only tabular transport cross sections are utilized. Because tabular transport cross sections do not exist for every isotope generated, and OMIT card is required in order to omit these isotopes from the transport process. The transmutation of these isotopes is accounted for by sending a 63-group flux from MCNPX to be matched to a 63-group cross section set within CINDER90 which will be energy integrated to determine a total collision rate. The OMIT card in the example omits 8 isotopes from material 1 and 8 isotopes from material 4. The AFMIN card states that only isotopes possessing an atom fraction below 1e-32 will be omitted from the transport calculation.

Since repeated structures are utilized in the example, a MATVOL keyword is required in order to calculate the track length estimated reaction rates in each repeated structure. In this example, since material 1 and 4 are repeated twice and each material possesses a volume of 192.287, MATVOL keyword entries of 384.57 (192.287*2) were required for each material being burned.

A MATMOD keyword is used in order to manually change the concentration of certain isotopes at specified time steps. In this example, manual isotope concentration changes are to be completed at 2 time steps. At time step 1, material 4 will have the atom density of 1 isotope changed: 94238 will be set to 1e-6 atoms/barn-cm. At time step 2, material 1 will have the atom densities of 2 isotopes changed: material 1 will have isotope 94238 changed to 1e-6 atoms/barn-cm and isotope 94241 will be changed to 1e-6 atoms/barn-cm, material 4 will have the atom density of 1 isotope changed: 94238 will be set to 1e-6 atoms/barn-cm.

LIST OF REFERENCES

1. U.S. Department of Energy Office of Civilian Radioactive Waste Management, *Oklo: Natural Nuclear Reactors,* November 2004, <http://www.ocrwm.doe.gov/factsheets/doeymp0010.shtml> (December 2007).

2. J. J. DUDERSTADT and L. J. HAMILTON, *Nuclear Reactor Analysis*, John Wiley & Sons, Inc., New York, NY (1976).

3. E. M. BAUM, H. D. KNOX, and T. R. MILLER, "Nuclides and Isotopes: Chart of Nuclides, Sixteenth Edition," Knolls Atomic Power Laboratory and Lockheed and Martin Corporation , Schenectady, NY (2006).

4. E. FERMI, "The Future of Atomic Energy," Technical Information Division, Oak Ridge Directed Operation of the Atomic Energy Commission Report: 10-11-48-850-11425, Oak Ridge, TN (1946).

5. S. GLASSTONE and W. H. JORDAN, *Nuclear Power and its Environmental Effects*, American Nuclear Society, La Grange Park, IL (1980).

6. R.T. LAHEY and F.J. MOODY, *The Thermal Hydraulics of a Boiling Water Nuclear Reactor*, American Nuclear Society, La Grange Park, IL(1979).

7. J. R. LAMARSH, *Introduction to Nuclear Engineering*, Addison-Wesley Publishing Company, Inc., Melano Park, CA (1983).

8. K. O. OTT, C. W. TERREL, R. C. BORG, and P. J. MAUDLIN, "Integrated Fuel-Cycle Models for Fast Breeder Reactors," *Annuls of Nuclear Engineering*, **8**, pg. 371-392 (1981).

9. R. G. COCHRAN and N. TSOULFANIDIS, *The Nuclear Fuel Cycle: Analysis and Management*, American Nuclear Society, Inc., La Grange Park, IL (1999).

10. A. ROMANO, P. HEJZLAR, and N. E. TODREAS, "Fertile-Free Fast Lead-Cooled Incinerators for Efficient Actinide Buruning," *Journal of Nuclear Technology*, **147**, pg. 368-386 (2004).

11. G. S. CHANG, "Neutronic and Burnup Characteristics of an Actinide-Reduced Plutonium Fuel with Tungsten," *Journal of Nuclear Technology*, **122**, pg. 43-51 (1998).

12. T. A. TAIWO, T. K. KIM, J. A. STILLMAN, R. N. HILL, M. SALVATORES, "Assessment of a Heterogeneous PWR Assembly for Plutonium and Minor Actinide Recycle," *Journal of Nuclear Technology*, **155**, pg. 43-51 (1998).

13. X. JIANG and Z. XIE, "Transport-burnup Code Systems and Their Applications for IAEA ADS Benchmark," *Annuls of Nuclear Energy*, **31**, pg. 213-225 (2004).

14. N. MESSAOUDI and J. TOMMASI, "Fast Burner Reactor Devoted to Minor Actinide Incineration," *Journal of Nuclear Technology*, 137, pg. 89-96 (2002).

15. M. DELPECH, H. GOLFIER, A. VASILE, F. VARAINE, L. BOUCHER, "Minor Actinides in PWRs," *International Congress on Advances in Nuclear Power Plants Embedded International Topical Meeting at the 2006 ANS Annual Meeting*, Reno, NV, (2006).

16. United States Department of Energy, Office of Nuclear Energy, Science and Technology "Advanced Fuel Cycle Initiative: Status Report for FY 2005", Report to congress (2006).

17. G. W. MCKINNEY and H. R. TRELLUE, "Transmutation Feature within MCNPX," Los Alamos National Laboratory Report: LA-UR-04-1572, Los Alamos, NM (2004).

18. United States Department of Energy, Office of Nuclear Energy, Office of Fuel Cycle Management "Global Nuclear Energy Partnership Strategic Plan", Report to congress: GNEP-167312 (2007).

19. M. D. LOWENTHAL, "Transmutation in the Nuclear Fuel Cycle: Approaches and Impacts," *Journal of Nuclear Technology*, **138**, pg. 284-299 (2002).

20. M. VISOSKY, P. HEJZLAR, M. KAZIMI, "Actinide Transmutation Using Pressurized Water Reactors," *International Congress on Advances in Nuclear Power Plants Embedded International Topical Meeting at the 2006 ANS Annual Meeting*, Reno, NV, (2006).

21. T. TAKEDA, T. YAMAMOTO, M. MIYAUCHI, "Interpretation of Actinide Transmutation," *Progress in Nuclear Energy*, 40, pg. 449-456 (2002).

22. M. SALVATORES, "Nuclear Fuel Cycle Strategies Including Partitioning and Transmutation," Nuclear Engineering and Design, 235, pg. 805-816 (2005).

23. United States Department of Energy, *Global Nuclear Energy Partnership: Improved Nuclear Safeguards,* December 2006, <http://www.gnep.energy.gov/gnepNuclearSafeguards.html> (December 2007).

24. G. F. KNOLL, Radiation Detection and Measurement, John Wiley and Sons, Inc., New York, NY (1999).

25. H. C. HURIA and R. J. BUECHEL, "Recent Improvements and New Features in the Westinghouse Lattice Physics Codes," Transactions of the American Nuclear Society, 72, pp. 369–371 (1995).

26. T. P. SHANNON, J. K. WHEELER, and G. TOUVANNAS, "TGBLA/PANACEA and CASMO/MICROBURN analyses of GE9B/GE10 Fuel in the Quad Cities," Transactions of the American Nuclear Society, 74, pp. 287–290 (1996).

27. C. V. PARKS, "Summary Description of the SCALE Modular Code System," Martin Marietta Energy Systems, Inc. and Oak Ridge National Laboratory Report: NUREG/CR-5033 ORNL/CSD/TM-252, Oak Ridge, TN (1987).

28. M. J. KHAN, N. AHMAD, "Proliferation Resistance Potential and Burnup Characteristics of an Equalibrium Core of Novel Natural Uranium Fueled Nuclear Research Reactor," *Annuls of Nuclear Energy*, **32**, pg. 612-620 (2005).

29. K. SUYAMA, H. MOCKIZUKI, T. KIYOSUMI, "Revised Burnup Code System SWAT: Description and Validation Using Postirradiation Examination Data," *Nuclear Technology*, **138**, pp. 97-108.

30. M. EDENIUS, K. EKBERG, B. H. FORSSEN, and D. KNOTT, "Casmo-4, A Fuel Assembly Burnup Program, User's Manual," Studsvik Report: SOA-95/15, Studsvik of America, Inc., Kjeller, Norway (1995).

31. N. SUGIMURA, A. YAMAMOTO, T. USHIO, M. MORI, M. TABUCHI, and T. ENDO, "Neutron Transport Models of AEGIS: An Advanced Next-Generation Neutronics Design System," *Nuclear Science and Engineering*, **155**, pp. 276-289 (2007).

32. D. KNOTT, E. WEHLAGE, "Description of the LANCER02 Lattice Physics Code for Single-Assembly and Multibundle Analysis," *Nuclear Science and Engineering*, **155**, pp. 331-354 (2007).

33. K. LASSMANN, C. T. WALKER, J. VAN DE LAAR, "Extensions of the TRANSURANUS Burnup Model to Heavy Water Reactor Conditions," *Journal of Nuclear Materials*, **255**, pg. 222-233 (1998).

34. A. NUNEZ-CARRERA, J. L. FRANCOIS, G. ESPINOSA-PAREDES, "Comparison between HELIOS Critical-Depletion Calculations and a PWR Thorium Cell Burnup Benchmark," *Annuls of Nuclear Energy*, **31**, pg. 713-722 (2004).

35. M. L. FENSIN and S. ANGHAIE, "Current Methods of Depletion Analysis," Los Alamos National Laboratory Report LA-UR-06-3933, *American Nuclear Society's 2006 Winter Meeting,* Albuquerque, NM (2006).

36. G. S. CHANG, J. M. RYSKAMP, "Depletion Analysis of Mixed-Oxide Fuel Pins in Light Water Reactors and the Advanced Test Reactor**",** *Nuclear Technology*, **129**, pp. 326-337 (2000).

37. W. HAECK, "An Optimum Approach to Monte Carlo Burn-Up," PhD thesis, Ghent University, Belgium (2007).

38. E. J. PARMA, "BURNCAL: A Nuclear Reactor Burnup Code Using MCNP Tallies," Sandia National Laboratory Report: SAND2002-3868, Albuquerque, NM (2002).

39. Z. XU, "Design Strategies for Optimizing High Burnup Fuel in Pressurized Water Reactors", PhD thesis, Massachusetts Institute of Technology, Cambridge, MA (2003).

40. N. A. HANAN, A. P. OLSON, R. B. POND, J. E. MATOS, "A Monte Carlo Burnup Code Linking MCNP and REBUS", *1998 International Meeting on Reduced Enrichment for Research and Test Reactors*, Sao Paulo, Brazil (1998).

41. G. S. CHANG, "MCWO-Linking MCNP and ORIGEN2 For Fuel Burnup Analysis," *American Nuclear Society's Topical Meeting on Monte Carlo*, Chattanooga, TN (2005).

42. J. CETNAR, W. GUDOWSKI, and J. WALLENIUS, "User Manual for Monte-Carlo Continuous Energy Burnup (MCB) Code—Version 1," draft report, Department of Nuclear and Reactor Physics, Royal Institute of Technology, Stockholm, Sweden (2005).

43. D. LI, X. ZHONGSHENG, L. SHU, "Monte Carlo Transport and Burnup Calculation," *Annuls of Nuclear Energy*, **30**, pg. 127-132 (2003).

44. R. L. MOORE, B. G. SCHNITZLER, C. A. WEMPLE, R. S. BABCOCK, D. E. WESSOL, "MOCUP: MCNP-ORIGEN2 Coupled Utility Program", Idaho National Engineering Laboratory Report: INEL-95/0523, Idaho Falls, ID (1995).

45. H. R. TRELLUE and D. I. POSTON, "User's Maunual, Version 2.0 for MONTEBURNS, Version 5B," Los Alamos National Laboratory report LA-UR-99-4999, Los Alamos, NM (1999).

46. M. AOYAMA, S. UCHIKAWA, K. MIKI, K. HIRAMOTO, and R. TAKEDA, "A Conceptual Design of a Fuel Bundle for Extended Bunup in Boiling Water Reactors," *Journal of Nuclear Technology*, **64**, pg. 19-25 (July 1993).

47. N. A HANAN, A. P. OLSON, R. B. POND, and J. E. MATOS, "A Monte Carlo Burnup Code Linking MCNP and REBUS," Argonne National Laboratory Report: ANL-TD-CP-97492, Agonne, IL (no date specified).

48. D. J. KELLY, "Depletion of a BWR Lattice Using the RACER Continuous Energy Monte Carlo Code," *International Conference of Mathematics and Computation, Reactor Physics, and Environmental Analysis*, Portland, OR, (1995).

49. M. DEHART, "High-Fidelity Depletion Capabilities of the SCALE Code System Using Triton," *American Nuclear Society's 2007 Winter Meeting*, Washington, D. C. (2007).

50. D. B. PELOWITZ, "MCNPXTM User's Manual Version 2.5.0," Los Alamos National Laboratory Report LA-CP-05-0369, Los Alamos, NM (2005).

51. W. B. WILSON, T. R. ENGLAND, E. D. ARTHUR, C. A. BEARD, C. D. BOWMAN, L. N. ENGEL, A. GAVRON, D. C. GEORGE, L. L. DAEMEN, H. G. HIGHES, III, W. W. KINNISON, R. J. LABAUVE, D. M. LEE, H. LICHTENSTEIN, P. W. LISOWSKI, D. W.

MUIR, A. P. MUIR, A. P. PALOUNEK, R. T. PERRY, E. J. PITCHER, R. E. PRAEL, R. J. RUSSEL, G. SANDERS, L. S. WATERS, P. G. YOUNG and J. J. ZIOCK, "Accelerator Transmutation Studies at Los Alamos with LAHET, MCNPX and CINDER90," Los Alamos National Laboratory Report LA-UR-93-3080, *Workshop on Simulation of Accelerator Radiation Environments*, Sante Fe, NM (1993).

52. M. D. DEHART, M. C. BRADY, C. V. PARKS, "OECD/NEA Burnup Credit Calculation Criticality Benchmark Phase I-B Results," Oak Ridge National Laboratory Report: ORNL-6901, Oak Ridge, TN (1996).

53. O. W. HERMANN, S. M. BOWMAN, M. C. BRADY, C. V. PARKS, "Validation of the Scale System for PWR Spent Fuel Isotopic Composition Analysis," Oak Ridge National Laboratory Report: ORNL/TM-12667, Oak Ridge, TN, USA (1995).

54. G. J. O'CONNOR and P. H. LIEM "Burn-up Credit Criticality Benchmark PHASE IV-B: Results and Analysis of MOX Fuel Depletion Calculations," Nuclear Energy Agency Report: NEA/NSC/DOC(2003)4 (2003).

55. G. F. THOMAS and D. H. BARBER, "Numerical Solution of Bateman Systems," *Annuls of Nuclear Energy*, **20**, pg. 407-414 (1993).

56. M. YAMAMOTO, "Coarse Time-Step Integration Method for Burnup Calculation of LWR Lattice Containing Gadolinium-Poisoned Rods," *Journal of Nuclear Science and Technology*, **22**, pg.1-15 (1985).

57. G. ILAS, B. D. MURPHY, and I. C. GAULD, "Overview of Origen-ARP and its Applications VVER and RBMK," *American Nuclear Society's 2007 Winter Meeting*, Washington, D. C. (2007).

58. A. G. CROFF, "ORIGEN2: A Versatile Computer Code for Calculating the Nuclide Compositions and Characteristics of Nuclear Materials," *Journal of Nuclear Technology*, **62**, pg. 335-352 (1983).

59. G. F. THOMAS and D. H. BARBER, "Stiffness in Radioactive Decay Chains," *Annuls of Nuclear Energy*, **21**, pg 309-320 (1994).

60. A. G. CROFF, "ORIGEN2 - A Revised and Updated Version of the Oak Ridge Isotope Generation and Depletion Code", Oak Ridge National Laboratory Report: ORNL-5621, Oak Ridge, TN (1980).

61. W. B. WILSON, V. DYADECHKO, T. R. ENGLAND, P. MOLLER, H. R. TRELLUE, "A Manual for CINDER90 Version 06.1 Codes and Data," Los Alamos National Laboratory Draft Report, Los Alamos, NM (2006).

62. M. L. FENSIN, "Optimum Boiling Water Reactor Fuel Design Strategies to Enhance Shutdown by the Standby Liquid Control System" Masters Thesis, University of Florida, Gainesville, FL (2004).

63. E. E. LEWIS and W. F. MILLER, Jr., *Computational Methods of Neutron Transport*, Ch. 7, American Nuclear Society, Inc., La Grange Park, IL (1993).

64. H. GREENSPAN. C. N. KELBER, D. OKRENT, *Computing Methods in Reactor Physics*, Gordon and Breach Science Publishers, Inc. New York, NY (1968).

65. M. CLARK, K. F. HANSEN, *Numerical Methods of Reactor Analysis*, Academic Press, Inc., New York, NY (1964).

66. I. M. SOBOL, *The Monte Carlo Method*, Mir Publishers, Moscow, Russia (1984).

67. A. PAUTZ, "Fuel Assembly Calculations Using the Method of Discrete Ordinates," *Nuclear Science and Engineering*, **149**, pg. 197-210 (2005).

68. D. S. LUCAS, "Attila Modeling with Comparison to Data, MCNP and MCNPX for the Advanced Test Reactor," *International Congress on Advances in Nuclear Power Plants Embedded International Topical Meeting at the 2006 ANS Annual Meeting*, Reno, NV, (2006).

69. S. G. HONG and N. Z. CHO, "Method of Characteristic Direction Probabilities for Heterogeneous Lattice Calculation," *Nuclear Science and Engineering*, **132**, pg. 65-77 (1999).

70. H. HERMAN, "ENDF-6 FORMATS MANUAL," Brookhaven National Laboratory Report: BNL-NCS-44945-05-Rev., Long Island, NY (2005).

71. M. L. FENSIN and D. I. POSTON, "Optimum Reflector Configurations for Minimizing Fission Power Peaking in a Lithium-Cooled, Liquid-Metal Reactor with Sliding Reflectors," Los Alamos National Laboratory Report LA-UR-7154, *Space Technology and Applications International Forum 2005*, Albuquerque, NM (2005).

72. M. L. FENSIN, J. O. ELLIOTT, R. J. LIPINSKI, D. I. POSTON, "Radiation Shielding Design and Orientation Considerations for a 1 kWe Heat Pipe Cooled Reactor Utilized to Bored Through the Ice Caps of Mars," Los Alamos National Laboratory Report LA-UR-05-8018, *Space Technology and Applications International Forum 2006*, Albuquerque, NM (2006).

73. J. L. DEVORE, Probability and Statistics for Engineers and Scientists, Brooks/Cole, Pacific Grove, CA (2000).

74. J. F. BRIESMEISTER, "MCNP-A General Monte Carlo N-Particle Transport Code," Los Alamos National Laboratory Report: LA-13709-M, Los Alamos, NM (2000).

75. H. R. TRELLUE, “Development of Monteburns: A Code That Links MCNP and ORIGEN2 in a Automated Fashion for Burnup Calculations” Los Alamos National Laboratory Report LA-13514-T, Los Alamos, NM (1998).

76. S. M. BOWMAN, M. D. DEHART, and L. M. PETRIE, “Integrated Keno Monte Carlo Transport for 3-Depletion with SCALE,” *The American Nuclear Society’s Monte Carlo 2005 Topical Meeting*, Chattanooga, TN (2005).

77. S. M. BOWMAN, D. F. HOLLENBACH, M. D. DEHART, B. T. REARDEN, I. C. GAULD, and S. GOLUOGLU, “SCALE 5: Powerful New Criticality Safety Analysis Tools,” *7th International Conference on Nuclear Criticality Safety*, Tokai-mura, Japan (2003).

78. A. S. GERASIMOV, T. S. Zaritskaya, G. V. Kiselev, and L. A. Myrtsymova, “The Cost of Transmutation of Fission Products in Nuclear Reactors,” *Atomic Energy*, **94**, pg. 154-157 (2003).

79. J. S. HENDRICKS, G. W. MCKINNEY, H. R. TRELLUE, J. W. DURKEE, T. L. ROBERTS, H. W. EGDORF, J. P. FINCH, M. L. FENSIN, M. R. JAMES, D. B. PELOWITZ, and L. S. WATERS, “MCNPX, Version 2.6.A,” Los Alamos National Laboratory Report: LA-UR-05-8225, Los Alamos, NM (2005).

80. M. B. CHADWICK, P. OBLOZINSKY, M. HERMAN, N. M. GREENE, R. D. MCKNIGHT, D. L. SMITH, P. G. YOUNG, R. E. MACFARLANE, G. M. HALE, S. C. FRANKLE, A. C. KAHLER, T. KAWANO, R. C. LITTLE, D. G. MADLAND, P. MOLLER, R. D. MOSTELLER, P. R. PAGE, P. TALOU, H. TRELLUE, M. C. WHITE, W. B. WILSON, R. ARCILLA, C. L. DUNFORD, S. F. MUGHABGHHAB, B. PRITYCHENKO, D. ROCHMAN, A. A. SONZOGNI, C. R. LUBITZ, T. H. TRUMBULL, J. P. WEINMAN, D. A. BROWN, D. E. CULLEN, D. P. HEINRICHS, D. P. MCNABB, H. DERRIEN, M. E. DUNN, N. M. LARSON, L. C. LEAL, A. D. CARLSON, R. C. BLOCK, J. B. BRIGGS, E. T. CHENG, H. C. HURIA, M. L. ZERKLE, K. S. KOZIER, A. COURCELLE, V. PRONYAEV and S. C. VAN DER MARCK,"ENDF/B-VII.0: Next Generation Evaluated Nuclear Data Library for Nuclear Science and Technology", *Nuclear Data Sheets*, **107**, pg. 2931-3060 (2006).

81. T. R. ENGLAND, B. F. RIDER, “ENDF-349 evaluation and compilation of fission product yields,” Los Alamos National Laboratory Report: LA-UR-94-3106, Los Alamos, NM (1994).

82. M. L. FENSIN, J. S. HENDRICKS, G. W. MCKINNEY, H. R. TRELLUE, "Advances in Monte Carlo Depletion Capabilities for MCNPX," Los Alamos National Laboratory Report LA-UR-05-7895, *American Nuclear Society 14th Biennial Topical Meeting of the Radiation Protection and Shielding Division*, Carlsbad, NM, (2006).

83. H. R. TRELLUE, “Reduction of the Radiotoxicity of Spent Nuclear Fuel Using a Two-Tiered System Comprising Light Water Reactors and Accelerator-Driven Systems,”Los Alamos National Laboratory Report: LA-14052-T, Los Alamos, NM (2003).

84. J. S. HENDRICKS, G. W. MCKINNEY, J. W. DURKEE, J. P. FINCH, M. L. FENSIN, M. R. JAMES, R. C. JOHNS, D. B. PELOWITZ, L. S. WATERS, F. X. GALLMEIER, "MCNPX, Version 2.6.C," Los Alamos National Laboratory Report: LA-UR-06-7991, Los Alamos, NM (2006).

85. M. L. FENSIN, J .S. HENDRICKS, S. ANGHAIE, "Enhanced Monte Carlo Linked Depletion Capabilities in MCNPX," Los Alamos National Laboratory Report LA-UR-06-0363, 2006 *International Congress on Advances in Nuclear Power Plants Embedded International Topical Meeting at the 2006 ANS Annual Meeting*, Reno, NV, (2006).

86. J. S. HENDRICKS, G. W. MCKINNEY, M. L. FENSIN, M. R. JAMES, R. C. JOHNS, J. W. DURKEE, J. P. FINCH, D. B. PELOWITZ, L. S. WATERS, F. X. GALLMEIER, "MCNPX Version 2.6.E," Los Alamos National Laboratory Report: LA-UR-07-6632, Los Alamos, NM (2007).

87. J. S. HENDRICKS, G. W. MCKINNEY, M. L. FENSIN, M. R. JAMES, R. C. JOHNS, J. W. DURKEE, J. P. FINCH, D. B. PELOWITZ, L. S. WATERS, F. X. GALLMEIER, "MCNPX Version 2.6.F," Los Alamos National Laboratory Report: Draft Report, Los Alamos, NM (2007).

88. G. AUDI, A.H. WAPSTRA, C. THIBAULT, J. BLACHOT and O. BERSILLON "Ame2003: Atomic Mass Evaluation," November 2003, <http://www.nndc.bnl.gov/amdc/web/masseval.html> (November 2007).

89. S. K. GHOSHAL, M. GUPTA, and V. RAJARAMAN, "A Parallel Multistep Predictor-Corrector Algorithm for Solving Ordinary Differential Equations," *Journal of Parallel and Distributed Computing*, **6** , pg. 636-648 (1989).

90. A. E. ABOANBER, "Numerical Solution of the chain model of fission product nuclides. Effect on the reactivity of the reactor," *Annuls of Nuclear Energy*, **28**, pg 923-933 (2001).

91. C. M. KANG, R. O. MOSTELLER, and S. LEVY, "Incorporation of a Predictor-Corrector Depletion Capability into the CELL-2 Code," *Transaction of the American Nuclear Society*, **45**, pp. 729–731 (1983).

92. M. L. FENSIN, J. S. HENDRICKS, H. R. TRELLUE, S. ANGHAIE "Incorporation of a Predictor-Corrector Methodology and 1-GroupReaction Rate Reporting Scheme for the MCNPX Depletion Capability," Los Alamos National Laboratory Report LA-UR-06-3925, *American Nuclear Society's 2006 Winter Meeting*, Albuquerque, NM (2006).

93. Z. XU, J. RHODES III, K. SMITH, N. GHEORGHIU, "MCNPX-5/ORIGEN-2.2/MCODE-2.2 versus CASMO-5 Depletion for a Heavy Gd-Poisoned BWR Fuel Assembly," *American Nuclear Society's 2007 Summer Meeting*, Boston, MA (2007).

94. J. S. HENDRICKS, G. W. MCKINNEY, H. R. TRELLUE, J. W. DURKEE, J. P. FINCH, M. L. FENSIN, M. R. JAMES, D. B. PELOWITZ, L. S. WATERS, F. X. GALLMEIER J. S. HENDRICKS, J. C. DAVID, "MCNPX, Version 2.6.B," Los Alamos National Laboratory Report: LA-UR-06-3248, Los Alamos, NM (2006).

95. J. S. HENDRICKS, G. W. MCKINNEY, M. L. FENSIN, M. R. JAMES, R. C. JOHNS, J. W. DURKEE, J. P. FINCH, D. B. PELOWITZ, L. S. WATERS, F. X. GALLMEIER "MCNPX, Version 2.6.D," Los Alamos National Laboratory Report: LA-UR-07-4137, Los Alamos, NM (2007).

96. M. L. FENSIN, J. S. HENDRICKS, S. ANGHAIE, "The Enhancements and Testing of the MCNPX Depletion Capability," Los Alamos National Laboratory Report: LA-UR-08-0305, To be presented at: *International Congress on Advances in Nuclear Power Plants Embedded International Topical Meeting at the 2008 ANS Annual Meeting*, Anaheim, CA, (2008).

97. Organisation for Economic Co-operation and Development: Nuclear Energy Agency, "NEA Expert Group on Burn-up Credit Criticality Safety," September 2003, <http://www.nea.fr/html/science/wpncs/buc/index.html> (December 2007).

98. T. TAKEDA, N. HIROKAWA, and T. NODA, "Estimate of Error Propagation in Monte-Carlo Burnup Calculations," *Journal of Nuclear Science and Technology,* **36**, *No. 9*, pp. 738–745 (1999).

99. P. PHRUKASAROJANAKUN and P. WILSON, "Nonanalog Implementations of Monte Carlo Isotope Inventory Analysis," *Nuclear Science and Engineering*, **156**, pp. 164-179 (2007).

BIOGRAPHICAL SKETCH

Michael Fensin was born on February 2 1980, to Dr. Matthew and Dr. Sheryl Fensin. Michael has one brother, Jeffrey Fensin. During his career as a student at the University of Florida's Nuclear and Radiological Engineering Department, Michael has completed various internships. Michael got his first start, from Dr. William Vernetson, as a laboratory technician for the University of Florida's radiochemistry laboratory and training reactor facility. Michael then moved on to complete a summer internship in reactor engineering with Southern Nuclear Company at the plant Vogtle site. During this internship Michael, participated in daily reactor operation and monitoring tasks. After his summer internship, Michael returned to the University of Florida to complete his Master of Engineering degree. During this degree, Michael also completed a six month internship with Global Nuclear Fuels (GNF), a General Electric Company, where he collaborated his master's degree research efforts with work completed at GNF. At GNF, Michael developed optimum fuel bundle design strategies in order to meet the limiting constraints of shutdown reactivity management. Michael then moved on to Los Alamos National Laboratory where he completed research in the area of compact reactor design for space applications. Michael then moved to the, MCNPX code development group, where he completed the work for this dissertation. After graduation, Michael will stay at Los Alamos National Laboratory and continue his work on advanced Monte Carlo linked depletion strategies for applied reactor safeguards efforts.